RADC-TR-88-215
Final Technical Report
October 1988

THE EFFECTS OF DIELECTRIC AND METAL LOADING ON THE DISPERSION CHARACTERISTICS FOR CONTRAWOUND HELIX CIRCUITS USED IN HIGH POWER TRAVELING-WAVE TUBES

University of Utah

William N. Cain

ROME AIR DEVELOPMENT CENTER
Air Force Systems Command
Griffiss Air Force Base, NY 13441-5700

This report has been reviewed by the RADC Public Affairs Division (PA) and is releasable to the National Technical Information Service (NTIS). At NTIS it will be releasable to the general public, including foreign nations.

RADC-TR-88-215 has been reviewed and is approved for publication.

APPROVED: Andrew E Chrostowski

ANDREW E. CHROSTOWSKI, Capt, USAF
Project Engineer

APPROVED:

FRED J. DEMMA
Acting Director
Directorate of Surveillance

FOR THE COMMANDER:

BILLY G. OAKS
Directorate of Plans & Programs

If your address has changed or if you wish to be removed from the RADC mailing list, or if the addressee is no longer employed by your organization, please notify RADC (OCTP) Griffiss AFB NY 13441-5700. This will assist us in maintaining a current mailing list.

Do not return copies of this report unless contractual obligations or notices on a specific doucment require that it be returned.

UNCLASSIFIED

SECURITY CLASSIFICATION OF THIS PAGE

REPORT DOCUMENTATION PAGE

Form Approved OMB No. 0704-0188

1a. REPORT SECURITY CLASSIFICATION UNCLASSIFIED	1b. RESTRICTIVE MARKINGS N/A
2a. SECURITY CLASSIFICATION AUTHORITY N/A	3. DISTRIBUTION/AVAILABILITY OF REPORT Approved for public release; distribution unlimited.
2b. DECLASSIFICATION/DOWNGRADING SCHEDULE N/A	
4. PERFORMING ORGANIZATION REPORT NUMBER(S) UTEC MD-88-050	5. MONITORING ORGANIZATION REPORT NUMBER(S) RADC-TR-88-215
6a. NAME OF PERFORMING ORGANIZATION University of Utah 6b. OFFICE SYMBOL (If applicable)	7a. NAME OF MONITORING ORGANIZATION Rome Air Development Center (OCTP)
6c. ADDRESS (City, State, and ZIP Code) Department of Electrical Engineering Salt Lake City UT 84112	7b. ADDRESS (City, State, and ZIP Code) Griffiss AFB NY 13441-5700
8a. NAME OF FUNDING/SPONSORING ORGANIZATION AFOSR 8b. OFFICE SYMBOL (If applicable) NE	9. PROCUREMENT INSTRUMENT IDENTIFICATION NUMBER F30602-84-C-0153
8c. ADDRESS (City, State, and ZIP Code) Bolling AFB Wash DC 20332	10. SOURCE OF FUNDING NUMBERS PROGRAM ELEMENT NO. 61102F; PROJECT NO. 2305; TASK NO J9; WORK UNIT ACCESSION NO. 17

11. TITLE (Include Security Classification)
THE EFFECTS OF DIELECTRIC AND METAL LOADING ON THE DISPERSION CHARACTERISTICS FOR CONTRAWOUND HELIX CIRCUITS USED IN HIGH POWER TRAVELING-WAVE TUBES

12. PERSONAL AUTHOR(S)
William N. Cain

13a. TYPE OF REPORT	13b. TIME COVERED	14. DATE OF REPORT (Year, Month, Day)	15. PAGE COUNT
Final	FROM Sep 85 TO Sep 87	October 1988	146

16. SUPPLEMENTARY NOTATION Research was accomplished in conjunction with the Air Force Thermionics Engineering Research Program (AFTER) AFTER-30. William N. Cain was an AFTER student from (over)

17. COSATI CODES			18. SUBJECT TERMS (Continue on reverse if necessary and identify by block number)
FIELD	GROUP	SUB-GROUP	Helix Tubes, Numerical Analysis, Contrawound Helix, Metal Loading, Dielectric Loading
09	01		

19. ABSTRACT (Continue on reverse if necessary and identify by block number)

The dispersion characteristics for countrawound helix structures are examined to determine the effects of dielectric and metal loading. The theory developed by Chodorow and Chu is expanded to include the problem of a countrawound helix interposed between two dielectric regions, symmetrically oriented inside a conducting cylinder. Simultaneously analyzed is the single helix oriented in an identical fashion. Numerical results are presented in the form of dispersion diagrams over a wide range of parameters. Interesting behavior found within these diagrams is discussed and, whenever possible, compared to experimental results.

20. DISTRIBUTION/AVAILABILITY OF ABSTRACT	21. ABSTRACT SECURITY CLASSIFICATION
☑ UNCLASSIFIED/UNLIMITED ☐ SAME AS RPT. ☐ DTIC USERS	UNCLASSIFIED
22a. NAME OF RESPONSIBLE INDIVIDUAL Andrew E. Chrostowski, Capt, USAF	22b. TELEPHONE (Include Area Code) (315) 330-4381 22c. OFFICE SYMBOL RADC (OCTP)

DD Form 1473, JUN 86 Previous editions are obsolete.

SECURITY CLASSIFICATION OF THIS PAGE

UNCLASSIFIED

Block 16. Supplementary Notation (Cont'd)

Hughes Aircraft Company. This report was submitted in partial fulfillment of the requirements for the degree of Electrical Engineer.

ACKNOWLEDGMENTS

The author would like to express his sincere and heartfelt gratitude to his adviser, Professor Richard W. Grow, for his patience, understanding, and the effort he invested in the course of this research. No less an appreciation of Professor J. Mark Baird could ever suffice.

A special note of thanks is extended to Dr. Kyle J. Bunch for his insightful assistance.

The author is also indebted to Walter Howard for his continuing help with the technical problems associated with numerical analysis.

Grateful appreciation to the author's parents for their love, understanding, and support. It is doubtful that this work could have been undertaken by the author without the motivation provided by his wife, Jae.

Appreciation is also extended to Ruth Eichers for technical assistance provided in the preparation of this manuscript.

The author acknowledges partial support from a development fund of the Microwave Device and Physical Electronics Laboratory of the University of Utah.

TABLE OF CONTENTS

Page

LIST OF FIGURES vi

LIST OF TABLES ix

GLOSSARY OF SYMBOLS x

SECTION

I. INTRODUCTION 1

1.1 History 1

1.2 Purpose of the Report 6

1.3 Organization 7

1.4 Mathematical Preliminaries 8

1.4.1 Symmetry and Periodicity 9

1.4.2 Boundary Conditions and Space Harmonics 13

1.4.3 Dispersion Equations and Solution by Variational Calculus 14

II. THE CONTRAWOUND HELIX IN FREE SPACE 16

2.1 The Boundary Value Problem 16

2.1.1 Field Functions 18

2.1.2 Boundary Conditions 21

2.1.3 The Field Components in Terms of the Surface Current Densities 21

2.1.4 The Surface Current Densities on the Helices . 26

2.1.5 The Determinantal Equation from the Exact Solution to the Boundary Value Problem 31

Page

2.1.6 Using the Variational Method to Derive an Approximation to the Determinantal Equation . . 36

2.1.7 The Single Helix Determinantal Equation 41

2.2 Results for the Free Space Problem 43

III. ANALYTICAL CONSIDERATIONS OF METAL AND DIELECTRIC LOADING ON THE CONTRAWOUND HELIX 52

3.1 The Boundary Value Problem 52

3.1.1 The Field Functions 52

3.1.2 Approximating the Determinantal Equation . . . 60

3.2 Results for Dielectric and Metal Loading 63

3.2.1 Dielectric Loading 63

3.2.2 Metal Loading 68

3.2.3 Simultaneous Metal and Dielectric Loading . . . 79

IV. SUMMARY AND CONCLUSIONS 89

APPENDIX A. THE FOURIER DECOMPOSITION OF THE E AND H FIELDS . . . 91

APPENDIX B. FLOQUET'S THEOREM AND STEP-TURN PERIODICITY 105

APPENDIX C. DERIVATION OF THE LAGRANGIAN USED IN CONJUNCTION WITH THE VARIATIONAL METHOD OF SOLUTION 113

APPENDIX D. RELATIONSHIPS BETWEEN THE COEFFICIENTS OF THE FOURIER DECOMPOSITION OF THE SURFACE CURRENT DENSITIES FOR THE SYMMETRICAL MODE 119

APPENDIX E. NUMERICAL CONSIDERATIONS 123

REFERENCES 127

LIST OF FIGURES

Figure No.		Page
1.1	The two tape contrawound helix (a) and the ring-bar version of the contrawound helix (b)	2
1.2	The single helix	12
2.1	The countrawound helix in free space	17
2.2	The contrawound helix showing the positive directions of the parallel and perpendicular components of the current densities on the helix tapes	28
2.3	Theoretical dispersion characteristics for both a contrawound helix and single helix in free space with $\xi = 1$, showing the effect of varying cot θ	45
2.4	Theoretical dispersion characteristics for both a contrawound helix and single helix in free space with $\xi = 2$, showing the effect of varying cot θ	46
2.5	Theoretical dispersion characteristics for both a contrawound helix and single helix in free space with cot $\theta = 10$, showing the effect of varying ξ . . .	47
2.6	Theoretical dispersion characteristics for both a contrawound helix and single helix in free space with cot $\theta = 5$, showing the effect of varying ξ	48
2.7	Theoretically and experimentally derived dispersion characteristics for a contrawound helix of cot θ = 4.4 in free space, showing the effect of varying ξ . .	49
2.8	Experimentally derived dispersion characteristics for a contrawound helix in free space, showing the effect of varying the tape thickness, are compared to theoretical results which assume infinitely thin tapes. Cot $\theta = 4.4$, $\xi = \pi/4$	50
2.9	Experimentally derived dispersion characteristics for a contrawound helix in free space, showing the effect of varying the tape thickness, are compared to theoretical results which assume infinitely thin tapes. Cot $\theta = 4.4$, $\xi = 3\pi/4$	51
3.1	The contrawound helix interposed between two dielectric regions	53

Figure No.		Page
3.2	The contrawound helix interposed between two dielectric regions at r = a and bounded by a conducting cylinder at r = b	54
3.3	Theoretical dispersion characteristics for both a contrawound helix and a single helix, showing the effect of dielectric loading. Cot θ = 10, ξ = 1 . . .	64
3.4	Experimentally derived dispersion characteristics for a contrawound helix, showing the effect of dielectric loading. Cot θ = 4.4, ξ = π/2	65
3.5	Comparison between theoretically and experimentally derived dispersion characteristics for a contrawound helix, showing the effect of dielectric loading. Cot θ = 4.4, ξ = π/2	66
3.6	Theoretical dispersion characteristics for a contrawound helix, showing the effect of dielectric loading. Cot θ = 5, ξ = 1	69
3.7	Theoretical dispersion characteristics for a contrawound helix, showing the effect of dielectric loading. Cot θ = 2.5, ξ = 1	70
3.8	Theoretical dispersion characteristics for a contrawound helix of ξ = 1 interposed between two dielectric regions with relative constitutive properties of $\varepsilon_2/\varepsilon_1$ = 1.5 and k_2/k_1 = 1.225, showing the effect of varying cot θ	71
3.9	Theoretical dispersion characteristics for a contrawound helix of ξ = 1 interposed between two dielectric regions with relative constitutive properties of $\varepsilon_2/\varepsilon_1$ = 9 and k_2/k_1 = 3, showing the effect of varying cot θ	72
3.10	Theoretical dispersion characteristics for a contrawound helix of cot θ = 10 and ξ = 1, showing the effect of metal loading	73
3.11	Comparison of Fig. 3.10 with the dispersion for a single helix in free space. Refer to Fig. 3.10 for details	75
3.12	Enlarged portion of Fig. 3.11. Refer to Figs. 3.11 and 3.10 for details	76

Figure No.		Page
3.13	Enlarged portion of Fig. 3.11. Refer to Figs. 3.10 and 3.11 for details	77
3.14	Theoretical dispersion characteristics for a single helix of cot θ = 10 and ξ = 1 , showing the effects of metal loading	78
3.15	Enlarged portion of Fig. 3.14. Refer to Fig. 3.14 for details	80
3.16	Theoretical dispersion characteristics for a contrawound helix of cot θ = 2.5 and ξ = 1 , showing the effect of metal loading	81
3.17	Comparison of Fig. 3.16 with the dispersion for a single helix in free space. Refer to Fig. 3.16 for details	82
3.18	Comparison between theoretically and experimentally derived dispersion characteristics for a contrawound helix of cot θ = 4.4 and $\xi = \pi/2$, showing the effect of metal loading	83
3.19	Theoretical dispersion characteristics for a contrawound helix of cot θ = 10 and ξ = 1, showing the effects of simultaneous dielectric and metal loading. $\varepsilon_2/\varepsilon_1 = 1.5$, $k_2/k_1 = 1.225$	85
3.20	Theoretical dispersion characteristics for a single helix of cot θ = 10 and ξ = 1, showing the effects of simultaneous dielectric and metal loading. $\varepsilon_2/\varepsilon_1 = 1.5$, $k_2/k_1 = 1.225$	86
3.21	Theoretical dispersion characteristics for a contrawound helix of cot θ = 10 and ξ = 1, showing the effects of simultaneous dielectric and metal loading. $\varepsilon_2/\varepsilon_1 = 9$, $k_2/k_1 = 3$	87
3.22	Comparison of Fig. 3.21 with the dispersion for a single helix in free space and with the dispersion for a single helix dielectrically loaded. Refer to Fig. 3.21 for details	88

LIST OF TABLES

Table No.		Page
1.1	Symmetry of the field components for the symmetic and antisymmetric modes	10
A.1	TE and TM Fourier coefficients, used in conjunction with the formulation of Appendix A	95

GLOSSARY OF SYMBOLS

a	Radius of the slow-wave structure, assumed to be infinitely thin; arbitrary constant
a_i, a_o	Inner and outer radii of the slow-wave structure of finite thickness
A	Shorthand notation for $A_{\ell,n}$
$A_{\ell,n}$	Fourier decomposition amplitude coefficients for the TM fields in Region 1
b	Radius of the outer cylindrical boundary of Region 2; radius of the outer conducting cylinder; arbitrary constant
b_i, b_o	Inner and outer radii of the dielectric cylinder of finite thickness
B	Shorthand notation for $B_{\ell,n}$
$B_{\ell,n}$	Fourier decomposition amplitude coefficients for the TM fields in Region 2
c	Velocity of light in free space
C	Shorthand notation for $C_{\ell,n}$
$C_{\ell,n}$	Fourier decomposition amplitude coefficients for the TE fields in Region 1
D	Shorthand notation for $D_{\ell,n}$
$D_{\ell,n}$	Fourier decomposition amplitude coefficients for the TE fields in Region 2
$\underline{E}$, $_i\underline{E}$	Electric field vector and electric field vector in Region i
$_iE_{r,\phi,z}$	Components of $\underline{E}$ in circular cylindrical coordinates and in Region i
$\tilde{E}(z)$	Functional form of the E-fields periodic in z with period p, as defined in Eq. B.8
f_i	Sum of the first i terms of a converging series
f_∞	Extrapolated sum of a converging series as defined in Eq. E.12

$F(z)$, F_ℓ	General function as defined in Eq. 3.6
$g^{\pm}_{\mu,\nu}$	Orthonormal functions defined on helix tapes only
$G^{\pm}_{\ell,n;\mu,\nu}$	Function resulting from the application of orthogonality to $g^{\pm}_{\mu,\nu}$
$\underline{H}$, $_i\underline{H}$	Magnetic field vector and magnetic field vector in Region i
$_iH_{r,\phi,z}$	Components of $\underline{H}$ in circular cylindrical coordinates and in Region i
$^zH_{\ell,n}$	Fourier decomposition amplitude coefficients for H_z as defined in Eq. D.8
i	Integer index
I	Shorthand notation for $I_\ell(z)$; a constrained form of the Lagrangian for Maxwell's equations
I'	Shorthand notation for $I'_\ell(z)$
$I_\ell(z)$	Modified cylindrical Bessel function of the first kind of order ℓ and argument z
$I'_\ell(z)$	The derivative of $I_\ell(z)$ with respect to z
j	$\sqrt{-1}$
$\underline{J}^{\pm}$	The surface current density vectors
$^{\phi}\underline{J}^{\pm}$, $^{z}\underline{J}^{\pm}$	Vector components of $\underline{J}^{\pm}$ in the ϕ and z directions
$\underline{J}^{\pm}_{\parallel}$, $\underline{J}^{\pm}_{\perp}$	Vector components of $\underline{J}^{\pm}$ parallel and perpendicular to the helix tapes
$J^{\pm}_{\phi}$, $J^{\pm}_{z}$	Magnitude of $^{\phi}\underline{J}^{\pm}$, $^{z}\underline{J}^{\pm}$; shorthand notation for $J^{\pm}_{\phi,\ell,n}$, $J^{\pm}_{z,\ell,n}$
$J^{\pm}_{\parallel}$, $J^{\pm}_{\perp}$	Magnitude of $\underline{J}^{\pm}_{\parallel}$, $\underline{J}^{\pm}_{\perp}$
$^{\phi}J^{\pm}_{\ell,n}$, $^{z}J^{\pm}_{\ell,n}$	Fourier decomposition amplitude coefficients for $^{\phi}J^{\pm}$, $^{z}J^{\pm}$
$J^{\pm}_{\parallel,\ell,n}$, $J^{\pm}_{\perp,\ell,n}$	Fourier decomposition amplitude coefficients for $J^{\pm}_{\parallel}$, $J^{\pm}_{\perp}$
k	Wave number, ω/c, propagation constant of a plane wave in free space; a (complex) constant
k_i	Wave number in Region i, $\omega\sqrt{\mu_i\varepsilon_i}$, propagation constant of a plane wave in Region i

K_e, K_h, K'_e, K'_h	Shorthand notation for (grouped) Bessel functions as defined in Eqs. 3.16 and 3.17
$K_\ell(z)$	Modified cylindrical Bessel function of the second kind of order ℓ and argument z
$K'_\ell(z)$	The derivative of $K_\ell(z)$ with respect to z
ℓ	Integer index
L	The Lagrangian for Maxwell's equations; also used to denote half the axial period: $L = p/2$
M	A function defined in Eq. 3.24
n	Integer index
$\hat{n}$	Unit vector normal to a surface
N	A function defined in Eq. 3.25
O(x)	"On the order of x"
p	The length of one axial period for a periodic structure
Q	A function defined in Eq. 3.23
$Q_{\ell,n}$	A function defined in Eq. 2.30
r,ϕ,z	Circular cylindrical coordinate variables
R	A function defined in Eq. 3.21
$\underline{s}$	The general boundary condition on S
S	The surface enclosing the volume V; a function defined in Eq. 3.22
T	A function defined in Eq. 3.27
U_o	The form of $U_{o,n}$ with $n = 0$
$U_{o,n}$	A function defined in Eqs. 2.58 and 3.33
v_g	Group velocity, $d(k)/d(\beta)$
v_p	Phase velocity, k/β
V	Volume enclosed by the closed surface S
V_o	A function defined in Eqs. 2.74 and 3.36

W	The only letter not used in this report
x	Independent variable
X	A function defined in Eq. 3.28
y	Dependent variable
y"	Second derivative of y with respect to x
$Y_{\ell,n}$	A function defined in Eqs. 2.59 and 3.34
$\hat{z}$	Unit vector in the z direction
$Z_{\ell,n}$	A function defined in Eqs. 2.60 and 3.35
α_{ℓ}	A sinc function as defined in Eq. 2.69
β	Axial propagation constant; shorthand notation for $\beta_{\ell,n}$
β_o, $\beta_{o,o}$	Axial propagation constant of the fundamental space harmonic
β_n, $\beta_{\ell,n}$	Axial propagation constant of the n^{th} of ℓ,n^{th} space harmonic
γ, γ_o, $\gamma_{o,o}$, γ_{ℓ}, $\gamma_{\ell,n}$	Radial propagation constants defined analagously to β, β_o, $\beta_{o,o}$, β_n, $\beta_{\ell,n}$
γ_i	Shorthand notation for $\left(\gamma_{\ell,n}\right)_i$
$\left(\gamma_{\ell,n}\right)_i$	$\gamma_{\ell,n}$ in Region i as defined in Eq. 3.2
Γ	Phase constant
δ	Tape width; differential length
$\delta(n)$	Delta function as defined in Eq. 2.70
Δ	Differential length
ϵ	Permittivity
ϵ_i	Permittivity of Region i
η_i	The intrinsic wave impedance, Eq. 3.3
θ	Pitch angle; $\cot\theta = 2\pi a/p$

λ	Wavelength
Λ_3	A series summation defined in Eq. E.3
μ	Permeability; integer index
μ_1	Permeability in Region i
μ_o	Permeability of free space
μ'	Integer index
ν, ν'	Integer index
ξ	Angular tape width, $\xi = 2\pi\delta/p$
$\hat{\phi}$	Unit vector in the ϕ direction
Φ	Dependent variable
ω	Angular frequency
$\times$	Cross product of two vectors
$\cdot$	Dot product of two vectors
$*$	Sign denoting multiplication; superscript denoting complex conjugate

I. INTRODUCTION

1.1 History

With the invention of the traveling-wave tube (TWT) by Rudolf Kompfner [1] in 1942, the helix structure was established as the delay mechanism used to slow down the forward propagation of the electromagnetic waves. It was this same helical geometry with its differential screw symmetry which ultimately proved to yield the least dispersion and widest bandwidth. However, a problem was encountered for high voltage operation: backward-wave oscillation (BWO). At high voltages, the axial focusing of the electron beam became difficult, which resulted in the beam interacting with field components other than the fundamental. At a certain voltage, interaction with the space harmonics became strong enough to induce backward-wave oscillation. To compound the problem, the impedance for the electron interaction with the fundamental component of the fields was reduced because of the increased energy content of the noninteracting space harmonics. Though advanced focusing methods helped to resolve these problems, a better solution was a device which had a larger interaction impedance of the fundamental component relative to the space harmonics, while maintaining the wide band characteristics of the helix. The contrawound helix proved to be such a device.

The contrawound helix shown in Fig. 1.1a was first investigated by Chodorow and Chu [2] in 1954. They observed that such a structure, consisting of two tape helices wound in opposite directions, could be qualitatively analyzed by considering the simple superposition of the two single-helix fields. In one situation, the fields were thought of

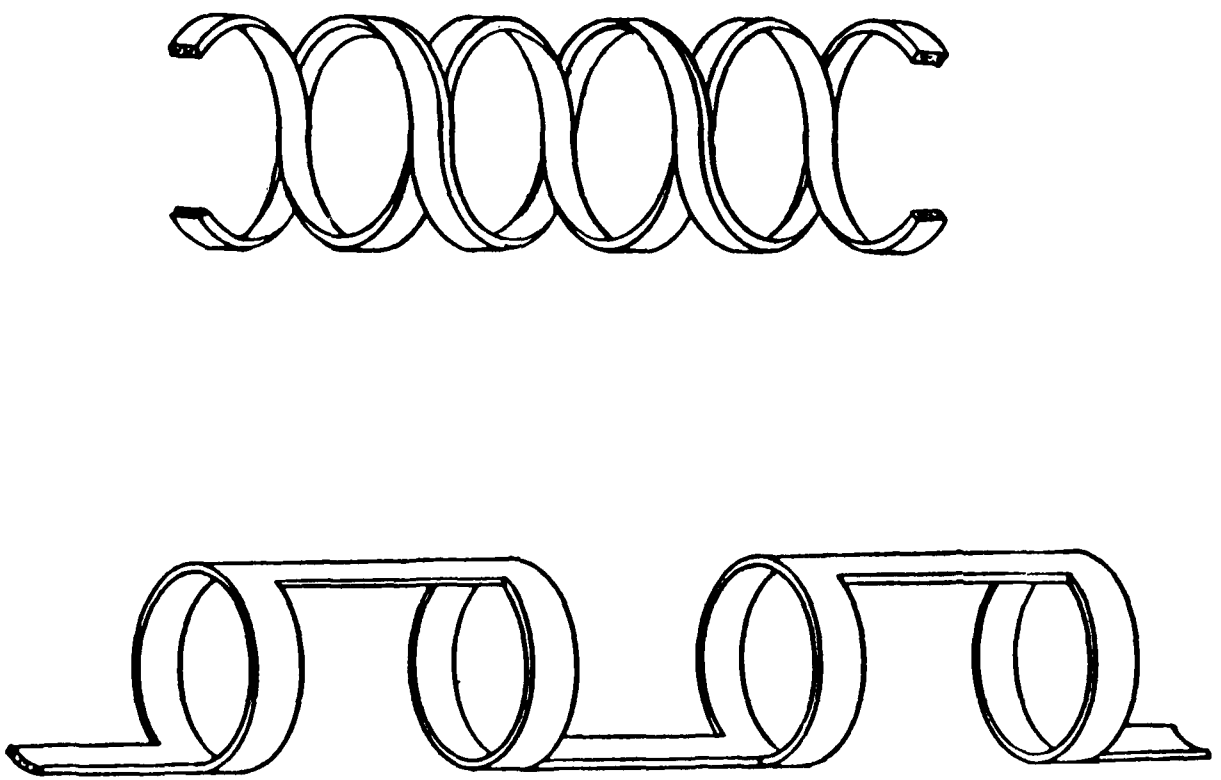

Fig. 1.1. The two tape contrawound helix (a) and the ring-bar version of the contrawound helix (b).

as being superimposed 180° out of phase. This yielded a field configuration, labeled the antisymmetric mode, with a decreased axial field and an increased radial field relative to the usual single helix fields. A second mode, the symmetric mode, resulted when the two single-helix modes were considered superimposed in phase. For such a mode, the axial electric fields of the fundamental component added rather than subtracted, giving a stronger axial field, while at the same time reducing the radial field. Furthermore, the stored energy associated with the fundamental component of the magnetic field -- energy which is useless for electron beam interaction -- was found to approach zero. The implication was that the fundamental component of the symmetric mode primarly carried electric energy and that the space harmonics carried principally magnetic energy. This was in contrast to the single helix in which the electric and magnetic energy were roughly equal in the fundamental component of the operating mode. However, such qualitative analysis ignored completely the interaction between the two helices.

The quantitative analysis of the contrawound helix performed by Chodorow and Chu was simply that of solving Maxwell's equations under the appropriate boundary conditions, i.e., a boundary value problem. The difficulty arose in defining adequately these boundary conditions and describing correctly the field configuration for the particular mode under investigation. To accomplish this, the electric and magnetic fields were expressed in terms of the surface current density on the helices. Together with a technique involving variational calculus, these expressions were used to obtain a determinantal equation in which the propagation constant in free space was written as a function of the

axial propagation constant of the fundamental space harmonic. The variational method was chosen because it had the great advantage that it permitted the use of successive approximations, which in the final form converge to the exact solution. The result was a determinantal equation which was both compact and numerically economical.

Building on the work of Chodorow and Chu, Ayers and Kirstein [3] examined the ring-bar circuit, an easy-to-make version of the contrawound helix. The ring-bar structure illustrated in Fig. 1.1b consisted of a series of rings connected one to another by bars at alternate ends of a diameter. To manufacture, it was simply a matter of making a number of saw cuts in a tube. Numerical analysis was done based on an unpublished determinantal equation for the ring-bar structure derived by Chodorow and Chu. This determinantal equation was completely unlike that for the contrawound helix. Rather than describing the fields in terms of the surface currents, assumptions were made about the form of the fields themselves. These were then manipulated by a variational technique into a determinantal equation. Furthermore, Floquet's theorem was applied to the step screw symmetry of the problem so that mathematical orthogonality was defined over only half of the normal period, rather than the usual full period.† Useful results were obtained using this model, which matched experimental data quite well over the first portion of the dispersion diagram.

† Refer to Appendix B for more details.

Ayers and Kirstein's work was not strictly numerical, however. Mostly, they dealt with the experimental aspect of the problem as did others at that time.

Concurrently, similar experimental work was being performed on the contrawound helix as well as its related circuits. Birdsall and Everhard [4] analyzed various forms of these circuits and how they were affected by such things as dielectric loading, helix-to-waveguide transitions, and periodic support stubs. Nevins [5] considered the effects of altering various geometric parameters along with examining the electron beam interaction. However, after the initial flurry of work in this area, interest in contrawound helix structures declined.

1.2 Purpose of the Report

In spite of their many excellent properties, contrawound helix type circuits have been neglected in the years since their initial development. This is mainly because they have been difficult to manufacture to the high tolerances necessary, but also because single-helix technology is well established. However, with today's manufacturing capability, renewed investigation into these structures is warranted.

It is the purpose of this report to reanalyze the work first carried out by Chodorow and Chu [2] on an unloaded contrawound helix. This mathematical model is then extended to include both the effects of a surrounding conducting sheath as well as dielectric loading. The results obtained are then compared to previously published experimental results.

1.3 Organization

This report deals primarily with Chodorow and Chu's [2] contrawound helix circuit in free space and the more general problem in which shielding and dielectric loading are considered.

Chapter Two investigates the free space problem. It begins with a discussion of the mathematical formulation used to derive the dispersion equation. It then proceeds to comment on the numerical results and how they compare to experimental results for similar cases.

Chapter Three is concerned with the general problem of a contrawound helix surrounded by a conducting sheath and dielectrically loaded. It is shown how these new boundary conditions effectively alter the dispersion equation and how this alteration affects the numerical solution. Furthermore, these results are compared with the appropriate experimental results so as to determine the effectiveness of the changes to the determinantal equation.

Finally, several topics related to the solution of the contrawound helix boundary value problem are covered in the appendices: the general form of Floquet's theorem for step-screw periodicity, the general Fourier expansion of the electromagnetic field functions in circular cylindrical coordinates, and a discussion of the associated Lagrangian which is used in conjunction with a variational method to obtain a solution.

1.4 Mathematical Preliminaries

The mathematical problem is simply to solve Maxwell's equations under the appropriate boundary conditions, i.e., a boundary value problem. The problem is constrained to be source free, so that for the electric field (E),

$$\nabla \cdot \underline{E} = 0 \tag{1.1}$$

everywhere in space. Further conditions are that the structure is lossless and that the solutions are restricted to the time harmonic form $e^{-j\omega t}$. These restrictions allow Maxwell's equations to be manipulated into wave equations for the electric field,

$$\nabla^2 \underline{E} + k^2 \underline{E} = 0 \tag{1.2}$$

and for the magnetic field (H),

$$\nabla^2 \underline{H} + k^2 \underline{H} = 0 \tag{1.3}$$

where

$$k = \omega\sqrt{\mu\varepsilon} \tag{1.4}$$

in which μ and ε are the permeability and permittivity, respectively, of the medium under consideration, and ω is the radian frequency. Though Eqs. 1.2 and 1.3 are vector equations, they reduce to the scalar

Helmholtz equation as one considers separately transverse electric (TE) and transverse magnetic (TM) polarizations of the fields. However, unlike the traditional waveguide in which the boundary conditions can be fulfilled by either a transverse electric or a transverse magnetic field, the geometry of any slow-wave structure is such that a superposition of these two fields is necessary to satisfy the boundary conditions.

1.4.1 Symmetry and Periodicity

The contrawound helix has several symmetry characteristics uniquely associated with this class of structures. There are two planes of reflective symmetry, the (r, θ) plane and the (r, z) plane, each intersecting at the crossover point of the two helices. Considered together with Maxwell's equations, these reflection symmetries require that any solution must be either even or odd in z and ϕ, excluding degeneracy. Such solutions are standing waves which can be combined to give running waves. Each plane of reflective symmetry yields two types of solutions, depending on whether a conducting or magnetic wall is considered. The result is a total of four types of field configurations (Table 1.1). Of interest is the scenario in which the (r, z) plane of reflective symmetry is replaced by a magnetic wall. The result is that the vector component of the electric field in the z direction, E_z, is even in ϕ, while that for the magnetic field, H_z, is odd in ϕ. Because H_z is odd in ϕ, it must vanish on the axis. In particular, the fundamental Fourier component of H_z is identically zero and the energy associated with the fundamental space harmonic for the system is stored

Table 1.1. Symmetry of the field components for the the symmetric and antisymmetric modes.

	TYPE	EVEN IN ϕ		ODD IN ϕ	
		EVEN IN Z	ODD IN Z	EVEN IN ϕ	ODD IN ϕ
SYMMETRIC MODE ⇨	1	E_z H_ϕ	E_r	H_r	E_ϕ H_z
	2	E_r	E_z H_ϕ	H_z E_ϕ	H_r
ANTISYMMETRIC MODE ⇨	3	H_r	H_z E_ϕ	E_z H_ϕ	E_r
	4	H_z E_ϕ	H_r	E_r	E_z H_ϕ

principally in the electric field. The combination of solution types 1 and 2 produces a wave traveling in the z direction with these desirable properties and is called the symmetric mode.

The antisymmetric mode is a combination of the basic field types 3 and 4. This yields another traveling wave, but one in which the electric field is shorted out along the z axis. Because the (r, z) plane of symmetry is now a conducting wall, the energy associated with the fundamental component is stored primarily in the magnetic field, a characteristic detrimental for TWT operation.

Like all periodic structures, the contrawound helix is invariant under the transformation,

$$(r, \phi, z) \rightarrow (r, \phi, z \pm p) \tag{1.5}$$

where p is the period. This relationship requires a certain functional dependence in the description of the fields for the structure. Known as Floquet's theorem, this requirement states that under a translation of an integral number of periods, the fields can differ at most by a constant. The result is that the axial propagation characteristics are limited to a particular form.

Floquet's theorem is also applicable to step-turn periodicity, also known as screw symmetry.[†] For the case of the single helix (Fig. 1.2), the step-turn periodicity is described by the differential screw

[†] See Appendix B.

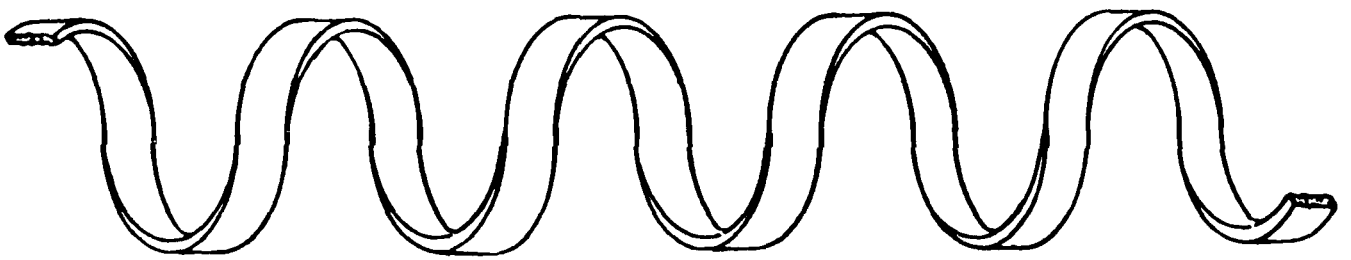

Fig. 1.2. The single helix.

transformation,

$$(r, \phi, z) \rightarrow \left(r, \phi \pm \frac{2\pi}{p} \delta z, z + \delta z\right) \tag{1.6}$$

where the choice of sign depends on whether the helix is right- or left-handed. The form of the fields remains invariant, again to within a constant, for a differential step in the z direction coupled with the appropriate amount of differential twist. The situation with the contrawound helix is that this "differential" step is uniquely half of the axial period, $\delta z = p/2$, such that transformation of Eq. 1.6 becomes

$$(r, \phi, z) \rightarrow \left(r, \phi \pm \pi, z + \frac{p}{2}\right) \tag{1.7}$$

As with the traditional application of Floquet's theorem, the step-turn symmetry imposes further restrictions on the propagation characteristics. As one might expect, these particular restrictions are an aspect of coupling between the z and ϕ coordinates.†

1.4.2 Boundary Conditions and Space Harmonics

It is no simple matter to satisfy the boundary conditions for the contrawound helix. A comparison with the circular cylindrical waveguide shows the inherent difficulties of matching the boundary conditions for a slow wave structure. The functional form of the field intensities for

† See Appendix B.

a perfectly conducting waveguide consists of regular cylindrical Bessel's functions, each having an infinite number of zeros. This property enables each mode to individually satisfy the boundary conditions and to therefore exist independently of all the other modes. It is the closed nature of the waveguide boundary which allows this type of separation among the modes.

In the mathematical description of the field configurations for the slow wave structure, the regular Bessel's functions are replaced by modified Bessel's functions which have no zeros. Thus, it is not possible to satisfy the boundary conditions uniquely for each mode, but rather the solution is found in an aggregate of these modes. The distinction is then made that these "modes" are not really modes in the sense that they can exist independently of each other, but are instead waves, termed space harmonics, which must exist in unison to satisfy the boundary conditions. These space harmonics are related by the periodicity of the structure, and each is orthogonal to the rest, in r, ϕ, and z. For the contrawound helix, the ϕ dependence of each harmonic either has the form cos ($n\phi$) or sin ($n\phi$). The component with $n = 0$ is labeled the fundamental space harmonic.

1.4.3 Dispersion Equations and Solution by Variational Calculus

With Maxwell's equations satisfied and the boundary conditions correctly accounted for, a determinantal equation can be found for the slow wave structure. The dispersive characteristics -- how frequency varies as a function of the phase constant (phase velocity over

frequency) -- are described by this equation. It is obtained formally by the usual technique of analysis in terms of orthogonal functions which yield four infinite sets of homogeneous simultaneous equations. The overall system is then solved by well known matrix methods.

This formal method of solution, however, is especially inconvenient in the case of the contrawound helix. For unlike the helix, the simultaneous equations describing the contrawound helix are doubly infinite over two indices. Thus, a variational technique is used for deriving approximate solutions to yield numerical results. Though this technique also leads to the same infinite set of equations just described, its advantage is that it allows one to systematically approximate the solution to the eigenvalue problem.

II. THE CONTRAWOUND HELIX IN FREE SPACE

2.1 The Boundary Value Problem

The analysis of the contrawound helix in free space is initiated by separating the problem into two regions, one inside and one outside the cylindrical surface r = a, Region 1 and Region 2, respectively, as shown in Fig. 2.1. The helices are assumed to be infinitely long, of equal radii (r = a), and wound with an infinitely thin perfectly conducting tape. The dimensional quantities that describe the structure are the pitch, the tape width, and the radius. These quantities are related as follows:

$$\frac{2\pi a}{p} = \cot \theta \tag{2.1}$$

$$\frac{2\pi\delta}{p} = \xi \tag{2.2}$$

where

a = helix radius

p = period of helix

δ = tape width

θ = pitch angle

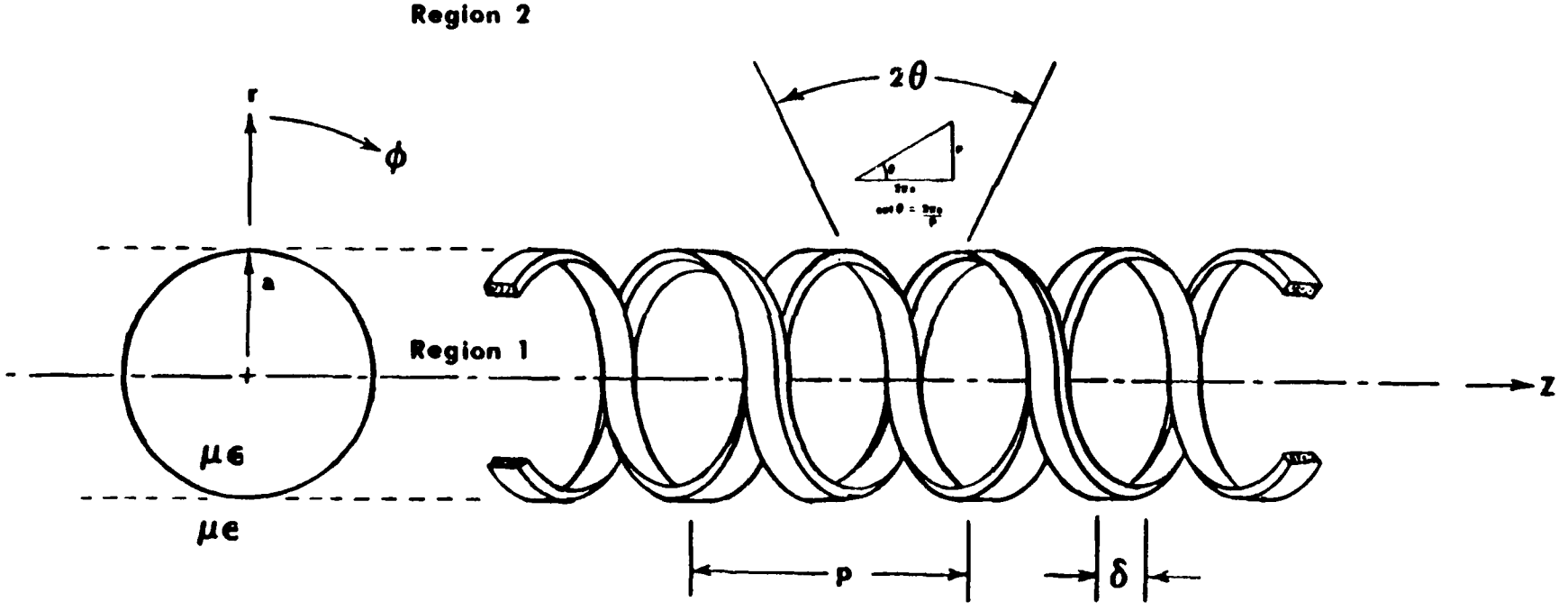

Fig. 2.1. The countrawound helix in free space.

2.1.1 The Field Functions

To satisfy Maxwell's equations in the form of the Helmholtz equation as well as the complicated boundary conditions, it is necessary to construct a solution using the usual technique of Fourier decomposition. Thus, each field component is written as an infinite sum of elementary waves in which each wave satisfies the differential equation and some of the symmetry conditions. By superimposing the total set of waves, all other restricting conditions can be satisfied.

Any arbitarary field in a homogeneous source-free region can be expressed as the sum of a TM field and a TE field. The skew boundary conditions of the contrawound helix make it necessary to have both TE and TM fields present in any given mode. Thus, the Fourier decompositions describing E_z and H_z in the two regions are

$$\begin{Bmatrix} {}_1E_z \\ {}_2E_z \end{Bmatrix} \sum_{\ell=-\infty}^{\infty} \sum_{n=-\infty}^{\infty} \begin{Bmatrix} A_{\ell,n} I_\ell(\gamma_n r) \\ B_{\ell,n} K_\ell(\gamma_n r) \end{Bmatrix} e^{-j\beta_n z} e^{j\ell\phi} \qquad \begin{cases} 0 < r < a & (2.3) \\ a < r & (2.4) \end{cases}$$

and

$$\begin{Bmatrix} {}_1H_z \\ {}_2H_z \end{Bmatrix} = \sum_{\ell=-\infty}^{\infty} \sum_{n=-\infty}^{\infty} \begin{Bmatrix} C_{\ell,n} I_\ell(\gamma_n r) \\ D_{\ell,n} K_\ell(\gamma_n r) \end{Bmatrix} e^{-j\beta_n z} e^{j\ell\phi} \qquad \begin{cases} 0 < r < a & (2.5) \\ a < r & (2.6) \end{cases}$$

From Maxwell's equations, the other field components are written in each region in terms of E_z and H_z.† These are in Region 1,

$(0 < r < a)$

$$ {}_1E_\phi = \sum_{\ell=-\infty}^{\infty} \sum_{n=-\infty}^{\infty} \left[\frac{-\ell\beta_n r}{(\gamma_n r)^2} A_{\ell,n} I_\ell(\gamma_n r) - \frac{j\omega\mu r}{\gamma_n r} C_{\ell,n} I'_\ell(\gamma_n r) \right] e^{-j\beta_n z} e^{j\ell\phi} \tag{2.7} $$

$$ {}_1H_\phi = \sum_{\ell=-\infty}^{\infty} \sum_{n=-\infty}^{\infty} \left[\frac{j\omega\epsilon}{\gamma_n} A_{\ell,n} I'(\gamma_n r) - \frac{\ell\beta_n r}{(\gamma_n r)^2} C_{\ell,n} I_\ell(\gamma_n r) \right] e^{-j\beta_n z} e^{j\ell\phi} \tag{2.8} $$

and in Region 2

$(a < r)$

$$ {}_2E_\phi = \sum_{\ell=-\infty}^{\infty} \sum_{n=-\infty}^{\infty} \left[\frac{-\ell\beta_n r}{(\gamma_n r)^2} B_{\ell,n} K_\ell(\gamma_n r) - \frac{j\omega\mu r}{\gamma_n r} D_{\ell,n} K'_\ell(\gamma_n r) \right] e^{-j\beta_n z} e^{j\ell\phi} \tag{2.9} $$

$$ {}_2H_\phi = \sum_{\ell=-\infty}^{\infty} \sum_{n=-\infty}^{\infty} \left[\frac{j\omega\epsilon}{\gamma_n} B_{\ell,n} K'_\ell(\gamma_n r) - \frac{\ell\beta_n r}{(\gamma_n r)^2} D_{\ell,n} K_\ell(\gamma_n r) \right] e^{-j\beta_n z} e^{j\ell\phi} \tag{2.10} $$

In Eqs. 2.3 through 2.10, $I_\ell(\gamma_n r)$ and $K_\ell(\gamma_n r)$ are modified cylindrical Bessel functions. These are necessary for slow waves (phase velocity

† Refer to Appendix A.

less than c, the speed of light) and are chosen to give nonradiating solutions. Any derivative of these functions is with respect to r. The relationship between β_n and γ_n is provided by Maxwell's equations (again for slow waves) and is

$$\gamma_n^2 = \beta_n^2 - k^2 \tag{2.11}$$

where k is the wave number as defined in Eq. 1.4. From periodicity and Floquet's theorem, β_n has the property,

$$\beta_n = \beta_o + \frac{2\pi n}{p} \tag{2.12}$$

such that $\beta_o p$ is the phase shift per period along the structure.† However, the screw-symmetry or step-turn periodicity provides an additional relationship between the two summation indices ℓ and n, whereby the axial propagation constant can be redefined to be†

$$\beta_n = \beta_{\ell,n} = \beta_{o,o} + (\ell + 2n)\frac{2\pi}{p} \tag{2.12'}$$

$$\beta_{o,o} \equiv \beta_o$$

In light of Eq. 2.12, Eq. 2.11 is then reformed as

† Refer to Appendix B for details.

$$\gamma_n^2 = \gamma_{\ell,n}^2 = \beta_{\ell,n}^2 - k^2 \tag{2.13}$$

2.1.2 Boundary Conditions

The boundary conditions to be satisfied are that

$$\hat{n} \times \underline{E} \quad \text{is continuous everywhere on the the cylindrical surface } r = a \tag{2.14a}$$

except on the helices where it is zero,

$$\hat{n} \times \underline{E} = 0 \text{ on helices} \tag{2.14b}$$

and that

$$\hat{n} \times \underline{H} \quad \text{is continuous on } r = a, \text{ except on the helices} \tag{2.15}$$

where it is proportional to the surface current density. In the above conditions, $\hat{n}$ is the unit vector normal to the surface $r = a$.

2.1.3 The Field Components in Terms of the Surface Current Densities

Separating condition 2.14a into its orthogonal components yields the equations:

$$_1E_z = {}_2E_z , \qquad r = a \tag{2.16}$$

and

$$_1E_\phi = {}_2E_\phi , \qquad r = a \tag{2.17}$$

From Eq. 2.16, the Eqs. 2.3 and 2.4 are equated. After applying the principle of orthogonality over one period on the cylindrical surface r = a, the relationship between the two sets of Fourier coefficients is obtained:

$$A_{\ell,n} = B_{\ell,n} \frac{K_\ell}{I_\ell} \tag{2.18}$$

where $I_\ell \equiv I_\ell(\gamma_n a)$, etc. Proceeding similarly from Eq. 2.17, Eqs. 2.7 and 2.9 are employed to yield the relationship

$$C_{\ell,n} = D_{\ell,n} \frac{K'_\ell}{I'_\ell} \tag{2.19}$$

Examined next is the boundary condition for the $\underline{H}$ fields, Eq. 2.15. Like the fields, the surface current density on the helices can be expanded in a convenient form for algebraic manipulation. Its ϕ and z directed components are decomposed as

$$\phi_J^- = \sum_{\ell,n} \phi_{J\ell,n}^- e^{-j\beta_{\ell,n} z} e^{j\ell\phi} \tag{2.20}$$

$$\phi_J^+ = \sum_{\ell,n} \phi_{J\ell,n}^+ e^{-j\beta_{\ell,n} z} e^{j\ell\phi} \tag{2.21}$$

$$z_J^- = \sum_{\ell,n} z_{J\ell,n}^- e^{-j\beta_{\ell,n} z} e^{j\ell\phi} \tag{2.22}$$

and

$$z_{J^+} = \sum_{\ell,n} z_{J^+_{\ell,n}} e^{-j\beta_{\ell,n} z} e^{j\ell\phi} \tag{2.23}$$

in which the "+" and "-" superscripts designate the left-handed and right-handed helices, respectively, and in which ℓ and n are allowed to range from minus infinity to plus infinity. In terms of the $\underline{H}$ field components, the condition of Eq. 2.15 yields the boundary equations:

$$_1H_z - {}_2H_z = \phi_{J^-} + \phi_{J^+}, \quad r = a \tag{2.24}$$

and

$$_2H_\phi - {}_1H_\phi = z_{J^-} + z_{J^+}, \quad r = a \tag{2.25}$$

by writing Eq. 2.24 in terms of the appropriate Fourier expansions (Eqs. 2.5, 2.6, 2.20, and 2.21), orthogonality is used to express the two sets of field expansion coefficients ($C_{\ell,n}$ and $D_{\ell,n}$) in terms of the current density coefficients. This gives, after making use of the relationship in Eq. 2.19,

$$C_{\ell,n} = \frac{K'_\ell \left(\phi_{J^-_{\ell,n}} + \phi_{J^+_{\ell,n}} \right)}{K'_\ell I_\ell - K_\ell I'_\ell} \tag{2.26}$$

and

$$D_{\ell,n} = \frac{I'_\ell \left(z_{J^-_{\ell,n}} + z_{J^+_{\ell,n}} \right)}{K'_\ell I_\ell - K_\ell I'_\ell} \tag{2.27}$$

Finally, considerations of Eq. 2.25 in which the appropriate expansions (Eqs. 2.8, 2.10, 2.22, and 2.23) are substituted yields, after some algebra, the result that

$$A_{\ell,n} = Q_{\ell,n} K_\ell \tag{2.28}$$

and

$$B_{\ell,n} = Q_{\ell,n} I_\ell \tag{2.29}$$

where

$$Q_{\ell,n} = \frac{\gamma_{\ell,n}}{j\omega\varepsilon} * \left[\left(z_{J^-_{\ell,n}} + z_{J^+_{\ell,n}}\right) - \frac{\ell\beta_{\ell,n}}{\gamma^2_{\ell,n}}\left(\phi_{J^-_{\ell,n}} + \phi_{J^+_{\ell,n}}\right)\right] / \left[I_\ell K'_\ell - I'_\ell K_\ell\right] \tag{2.30}$$

Again note that the modified Bessel functions have the argument $\gamma_{\ell,n}a$. The denominator in Eq. 2.30 is the wronskian of (I_ℓ, K_ℓ) and can be replaced by $-1/(\gamma_{\ell,n}a)$:

$$I_\ell K'_\ell - I'_\ell K_\ell = -\frac{1}{\gamma_{\ell,n}a} \tag{2.31}$$

Having written the Fourier coefficients for the fields in terms of the current density coefficients, Eqs. 2.26 through 2.29, the field intensities are at last expressed in terms of the surface current density. And since all field quantities are defined to within a constant, the summations can be multiplied by the quantity $-\sqrt{\varepsilon}/\sqrt{\mu}$ so as to express the field components in the following form:

$$E_z(r = a, \phi, z) = \frac{1}{jka} \sum_{\ell,n} (\gamma_{\ell,n}a)^2 \left\{\left(z_{J^-_{\ell,n}} + z_{J^+_{\ell,n}}\right) - \frac{\ell\beta_{\ell,n}a}{(\gamma_{\ell,n}a)^2} * \left(\phi_{J^-_{\ell,n}} + \phi_{J^+_{\ell,n}}\right)\right\} I_\ell K_\ell \, e^{-j\beta_{\ell,n}z} \, e^{j\ell\phi} \tag{2.32}$$

$$E_\phi(r = a,\ \phi,\ z) = \frac{1}{ka} \sum_{\ell,n} \left\{ \ell\beta_{\ell,n}a\ K_\ell I_\ell \left({}^{z}J^{-}_{\ell,n} + {}^{z}J^{+}_{\ell,n} \right) \right.$$

$$\left. - \left[\left(\frac{\ell\beta_{\ell,n}a}{\gamma_{\ell,n}a} \right)^2 K_\ell I_\ell + (ka)^2\ K'_\ell I'_\ell \right] \left({}^{\phi}J^{-}_{\ell,n} + {}^{\phi}J^{+}_{\ell,n} \right) \right\} e^{-j\beta_{\ell,n}z}\ e^{j\ell\phi} \tag{2.33}$$

$$H_z(r \le a,\ \phi,\ z) = -\sum_{\ell,n} (\gamma_{\ell,n}a) \left({}^{\phi}J^{-}_{\ell,n} + {}^{\phi}J^{+}_{\ell,n} \right)$$

$$* K'_\ell(\gamma_{\ell,n}a)\ I_\ell(\gamma_{\ell,n}r)\ e^{-j\beta_{\ell,n}z}\ e^{j\ell\phi} \tag{2.34a}$$

$$H_z(r \ge a,\ \phi,\ z) = -\sum_{\ell,n} (\gamma_{\ell,n}a) \left({}^{\phi}J^{-}_{\ell,n} + {}^{\phi}J^{+}_{\ell,n} \right)$$

$$* I'_\ell\ (\gamma_{\ell,n}a)\ K_\ell(\gamma_{\ell,n}r)\ e^{-j\beta_{\ell,n}z}\ e^{j\ell\phi} \tag{2.34b}$$

$$H_\phi(r \le a,\ \phi,\ z) = \sum_{\ell,n} \left\{ \frac{\ell\beta_{\ell,n}a}{\gamma_{\ell,n}a} \left({}^{\phi}J^{-}_{\ell,n} + {}^{\phi}J^{+}_{\ell,n} \right) \right.$$

$$* \frac{a}{r} K'_\ell\ (\gamma_{\ell,n}a)\ I_\ell\ (\gamma_{\ell,n}r) - \gamma_{\ell,n}a$$

$$* \left({}^{z}J^{-}_{\ell,n} + {}^{z}J^{+}_{\ell,n} \right) - \frac{\ell\beta_{\ell,n}a}{\gamma_{\ell,n}a} \left({}^{\phi}J^{-}_{\ell,n} + {}^{\phi}J^{+}_{\ell,n} \right)$$

$$\left. * K_\ell\ (\gamma_{\ell,n}a)\ I'_\ell(\gamma_{\ell,n}r) \right\} e^{-j\beta_{\ell,n}z}\ e^{j\ell\phi} \tag{2.35a}$$

$$H_\phi(r \geq a,\ \phi,\ z) = \sum_{\ell,n} \left\{ \frac{\ell\beta_{\ell,n}a}{\gamma_{\ell,n}a} \left({}^{\phi}J^{-}_{\ell,n} \; {}^{\phi}J^{+}_{\ell,n} \right) \right.$$

$$* \frac{a}{r} I'_\ell (\gamma_{\ell,n}a)\, K_\ell(\gamma_{\ell,n}r) - \gamma_{\ell,n}a$$

$$* \left({}^{z}J^{-}_{\ell,n} + {}^{z}J^{+}_{\ell,n} \right) - \frac{\ell\beta_{\ell,n}a}{\gamma_{\ell,n}a} \left({}^{\phi}J^{-}_{\ell,n} + {}^{\phi}J^{+}_{\ell,n} \right)$$

$$\left. * I_\ell (\gamma_{\ell,n}a)\, K'_\ell (\gamma_{\ell,n}r) \right\} e^{-j\beta_{\ell,n}z}\, e^{j\ell\phi} \qquad (2.35b)$$

In Eqs. 2.32 and 2.33, the modified Bessel functions have for their arguments $\gamma_{\ell,n}a$, and throughout Eqs. 2.32 through 2.35, the indices ℓ and n range from minus infinity to infinity.

2.1.4 The Surface Current Densities on the Helices

With the field components written in terms of ${}^{\phi}J^{\pm}_{\ell,n}$ and ${}^{z}J^{\pm}_{\ell,n}$, it is important to analyze in some detail the characteristics of the surface current densities.

From the boundary condition of Eq. 2.15, H_ϕ and H_z are continuous at $r = a$, except on the helices. To meet this condition, the surface current densities must be constrained as

$$\underline{J}^{-} \equiv 0 \quad \text{off helix } (-) \qquad (2.36a)$$

$$\underline{J}^{+} \equiv 0 \quad \text{off helix } (+) \qquad (2.36b)$$

In other words, there can be no current off the helix tapes. A constraint such as this is somewhat of a novelty in boundary value problems. In this case (as well as other open structures), the boundary at r = a must be explicitly defined to satisfy the geometrical considerations. Similarly, the current amplitudes are chosen to satisfy the symmetry properties and the particular mode of operation.

To obtain the symmetric mode as defined in Section 1.4.1, it is necessary for $\underline{E}_r$, $\underline{E}_z$, and $\underline{H}_\phi$ to be even in ϕ, while $\underline{H}_r$, $\underline{H}_z$, and $\underline{E}_\phi$ are odd in ϕ. From Eqs. 2.24 and 2.25, it follows that the current densities must satisfy the same symmetry conditions as the fields. Thus,

$$^{z}\underline{J}^{+}(a, \phi\ z) = {}^{z}\underline{J}^{-}(a, -\phi, z) \tag{2.37a}$$

and

$$^{\phi}\underline{J}^{+}(a, \phi, z) = - \ {}^{\phi}\underline{J}^{-}(a, -\phi, z) \tag{2.37b}$$

To facilitate the narrow tape approximation in which it is assumed current flow is primarily in a direction parallel to the helices, it is advantageous to express $^{z}\underline{J}^{\pm}$ and $^{\phi}\underline{J}^{\pm}$ in terms of components parallel and perpendicular to the appropriate helix tape. Referring to Fig. 2.2 and noting that each pair of currents $(\underline{I}_J^{-}, \underline{I}_J^{+})$ and $(\underline{\perp}_J^{-}, \underline{\perp}_J^{+})$ is oriented symmetrically with respect to the $\underline{z}$ axis, the following expressions may be formed:

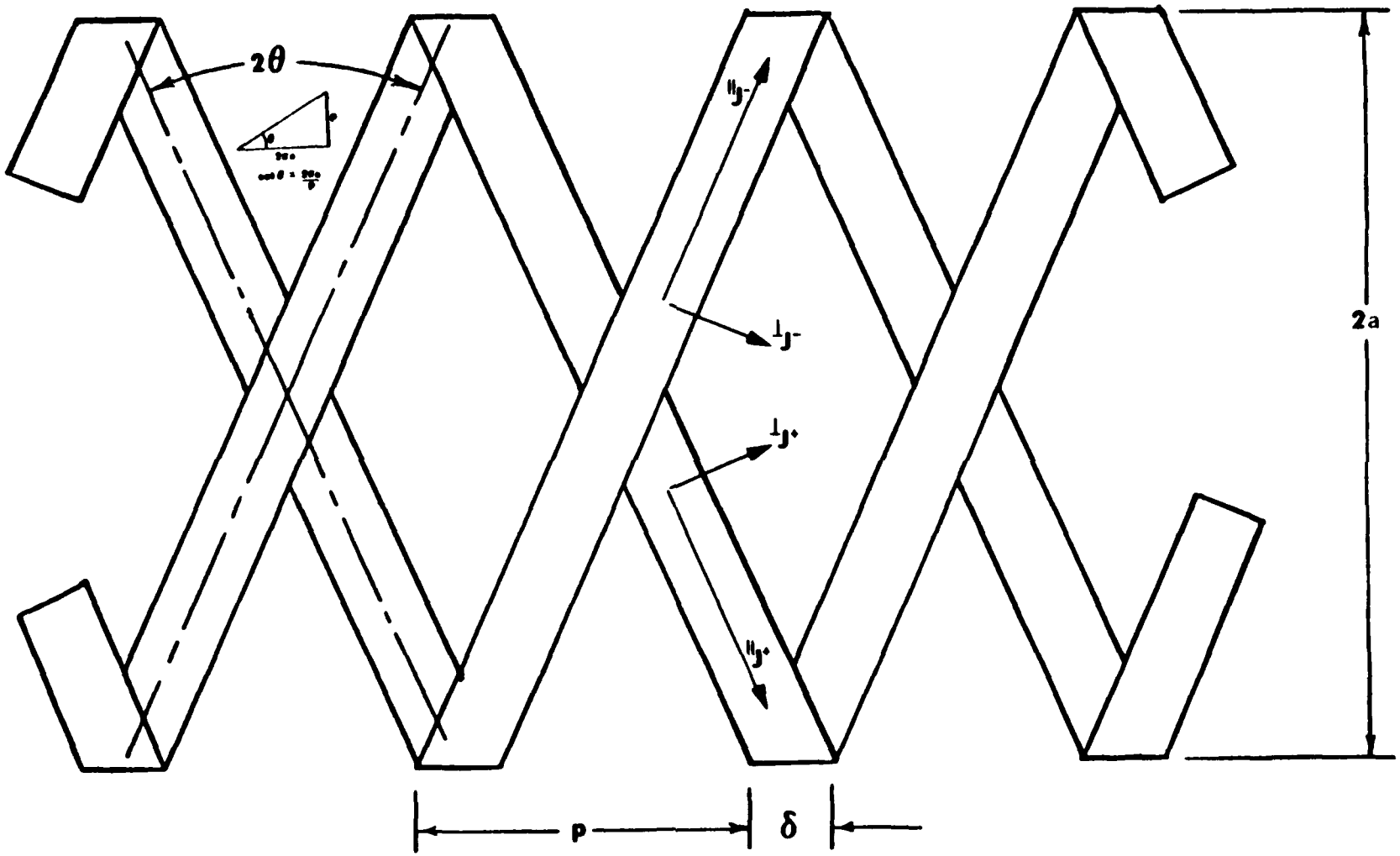

Fig. 2.2. The contrawound helix showing the positive directions of the parallel and perpendicular components of the current densities on the helix tapes.

$$\begin{matrix} {}^{z}\underline{J}^{-}(a,\phi,z) & & \sin\theta & & \cos\theta \\ = {}^{\parallel}\underline{J}^{-}(a,\phi,z) & & \pm & {}^{\perp}\underline{J}^{-}(a,\phi,z) & \end{matrix} \qquad (2.38a)$$

$$\begin{matrix} {}^{\phi}\underline{J}^{-}(a,\phi,z) & & \cos\theta & & \sin\theta \end{matrix} \qquad (2.38b)$$

$$\begin{matrix} {}^{z}\underline{J}^{+}(a,\phi,z) & & \sin\theta & & \cos\theta \\ = \pm {}^{\parallel}\underline{J}^{+}(a,\phi,z) & & + & {}^{\perp}\underline{J}^{+}(a,\phi,z) & \end{matrix} \qquad (2.39a)$$

$$\begin{matrix} {}^{\phi}\underline{J}^{+}(a,\phi,z) & & \cos\theta & & \sin\theta \end{matrix} \qquad (2.39b)$$

Condition 2.37 then becomes

$${}^{\parallel}\underline{J}^{+}(a,\phi,z) = {}^{\parallel}\underline{J}^{-}(a,-\phi,z) \qquad (2.40a)$$

$${}^{\perp}\underline{J}^{+}(a,\phi,z) = {}^{\perp}\underline{J}^{-}(a,-\phi,z) \qquad (2.40b)$$

With the Fourier coefficients for ${}^{\parallel}\underline{J}^{\pm}$ and ${}^{\perp}\underline{J}^{\pm}$ defined in the usual way,

$${}^{\parallel}\underline{J}^{\pm}(a,\phi,z) = \sum_{\ell,n} {}^{\parallel}J^{\pm}_{\ell,n}\, e^{-j\beta_{\ell,n}z}\, e^{j\ell\phi} \qquad (2.41a)$$

$${}^{\perp}\underline{J}^{\pm}(a,\phi,z) = \sum_{\ell,n} {}^{\perp}J^{\pm}_{\ell,n}\, e^{-j\beta_{\ell,n}z}\, e^{j\ell\phi} \qquad (2.41b)$$

the field expansions can be written in terms of these coefficients. However, by making the assumption of narrow helix tapes, the resulting expressions for the fields are greatly simplified. Mathematically, this assumption translates to

$$\perp_J \cot\theta << |_J \quad \text{and} \quad \perp_J \tan\theta << |_J$$

from which the set of Fourier coefficients

$$I_{J^{\pm}_{\ell,n}}$$

is seen to dominate. Thus, Eqs. 2.38 and 2.39 can be reformed as

$$z_{\underline{J}}^{-}(a, \phi, z) \qquad \sin\theta \qquad (2.42a)$$

$$\simeq I_{\underline{J}}^{-}(a,\phi,z)$$

$$\phi_{\underline{J}}^{-}(a, \phi, z) \qquad \cos\theta \qquad (2.42b)$$

and

$$z_{\underline{J}}^{+}(a, \phi, z) \qquad \sin\theta \qquad (2.42c)$$

$$\simeq \pm I_{\underline{J}}^{+}(a,\phi,z)$$

$$\phi_{\underline{J}}^{+}(a, \phi, z) \qquad \cos\theta \qquad (2.42d)$$

Finally, since

$$\beta_{\ell,n} = \beta_{-\ell,n+\ell} \qquad (2.43a)$$

$$\beta_{-\ell,n} = \beta_{\ell,n-\ell} \qquad (2.43b)$$

the symmetrical relationships between the Fourier coefficients for $I_{\underline{J}^+}$ and $I_{\underline{J}^-}$ can be established.† Making use of Eqs. 2.40a and 2.41a, these become

$$I_{J^+_{\ell,n}} = I_{J^-_{-\ell,n+\ell}} \tag{2.44a}$$

$$I_{J^+_{-\ell,n+\ell}} = I_{J^-_{\ell,n}} \tag{2.44b}$$

2.1.5 The Determinantal Equation from the Exact Solution to the Boundary Value Problem

As mentioned in the previous section, because of the nonhomogeneous character of the boundary at r = a, the geometry of the structure must be reflected in the nature of the surface current densities. Specifically, each surface current density, $\underline{J}^+$ and $\underline{J}^-$, cannot exist off its respective helix (Eq. 2.36). And from the relation between $\underline{H}$ and $\underline{J}$, it follows that this is also a restriction on the H fields at r = a. There is a similar condition for the E fields; namely, that

$$E_z(r = a) = 0 \quad \text{on helices} \tag{2.45a}$$

$$E_\phi(r = a) = 0 \quad \text{on helices} \tag{2.45b}$$

which is, in fact, the boundary condition 2.14b.

To satisfy Eq. 2.36, the constraint on the surface current densities, the usual technique of analysis in terms of orthonormal functions

† See Appendix D for details.

is used.† Needed are two complete sets of orthonormal functions (labeled $g^{+}_{\mu,\nu}$ and $g^{-}_{\mu,\nu}$), one for each helix tape, defined on the tapes only. Making use of orthogonality allows ${}^{z}J^{\pm}_{\ell,n}$ and ${}^{\phi}J^{\pm}_{\ell,n}$ to be written in terms of these functions so that each of these current coefficients will be compatible with the constraint of Eq. 2.36.

The result is that the E_z and E_ϕ expressions are now summed over four indices rather than just two, and Eqs. 2.45a and 2.45b take the form

$$E_z(r=a) = \sum_{\ell,n}\left[\left(\gamma_{\ell,n}a\right)^2 K_\ell I_\ell \left\{\sum_{\mu,\nu} {}^{z}J^{-}_{\mu,\nu}\, G^{-}_{\ell,n;\mu,\nu} + \sum_{\mu,\nu} {}^{z}J^{+}_{\mu,\nu}\, G^{+}_{\ell,n;\mu,\nu} - (\ell\beta_{\ell,n}a)\, K_\ell I_\ell \right.\right.$$

$$\left.\left. * \sum_{\mu,\nu} {}^{\phi}J^{-}_{\mu,\nu}\, G^{-}_{\ell,n;\mu,\nu} + \sum_{\mu,\nu} {}^{\phi}J^{+}_{\mu,\nu}\, G^{+}_{\ell,n;\mu,\nu} \right\}\right]$$

$$* e^{-j\beta_{\ell,n}z}\, e^{j\ell\phi} = 0 \quad \text{on helices} \qquad (2.46a)$$

† Refer to Reference 2 for detailed discussion, pp. 38-46.

$$E_{\phi}(r = a) = \sum_{\ell,n} \left[(\ell\beta_{\ell,n}a)K_{\ell}I_{\ell} \left\{ \sum_{\mu,\nu} {}^{z}J^{-}_{\mu,\nu} G^{-}_{\ell,n;\mu,\nu} + \sum_{\mu,\nu} {}^{z}J^{+}_{\mu,\nu} G^{+}_{\ell,n;\mu,\nu} \right\} - \left\{ \left(\frac{\ell\beta_{\ell,n}a}{\gamma_{\ell,n}a} \right)^2 K_{\ell}I_{\ell} + (ka)^2 K'_{\ell}I'_{\ell} \right\} \left\{ \sum_{\mu,\nu} {}^{\phi}J^{-}_{\mu,\nu} G^{-}_{\ell,n;\mu,\nu} + \sum_{\mu,\nu} {}^{\phi}J^{+}_{\mu,\nu} G^{+}_{\ell,n;\mu,\nu} \right\} \right] e^{-j\beta_{\ell,n}z} e^{j\ell\phi} = 0 \quad \text{on helices} \tag{2.46b}$$

In Eqs. 2.46a and 2.46b, the functions $G^{+}_{\ell,n;\mu,\nu}$ and $G^{-}_{\ell,n;\mu,\nu}$ are the result of applying orthogonality to the two sets of orthonormal functions $g^{+}_{\mu,\nu}$ and $g^{-}_{\mu,\nu}$.

Finally, one can operate E_z and E_{ϕ} with the orthonormal functions $g^{+}_{\mu,\nu}$ and $g^{-}_{\mu,\nu}$ to obtain

$$\sum_{\mu',\nu'} E_z(r = a)\, g^{\mp}_{\mu',\nu'} = 0 \tag{2.47^{a}_{b}}$$

and

$$\sum_{\mu',\nu'} E_{\phi}(r = a)\, g^{\mp}_{\mu',\nu'} = 0 \tag{2.48^{a}_{b}}$$

Equations 2.47 and 2.48 are zero over the entire cylindrical surface r = a, a result of $g^{-}_{\mu,\nu}$ and $g^{+}_{\mu,\nu}$ being defined only on the helix tapes, while E_z and E_{ϕ} are zero on these same tapes. Applying orthogonality to

Eqs. 2.47 and 2.48 over the cylindrical surface r = a eliminates the double summation over the indices μ' and ν'; and if the expressions in Eqs. 2.46a and 2.46b are substituted for $E_z(r = a)$ and $E_\phi(r = a)$, the result is four doubly infinite sets of linear homogeneous simultaneous equations having the same number of unknowns. By such manipulations and subsequent interchanging the order of the two summation signs $\sum_{\ell,n}$ and $\sum_{\mu,\nu}$, one finally obtains from Eq. 2.47,

$$\sum_{\mu,\nu} {}^{z}J^{-}_{\mu,\nu} \left\{ \sum_{\ell,n} G^{-}_{\ell,n;\mu,\nu} \left(\gamma_{\ell,n} a\right)^2 K_\ell I_\ell \, G^{\mp}_{\ell,n;\mu',\nu'} \right\}$$

$$+ \sum_{\mu,\nu} {}^{z}J^{+}_{\mu,\nu} \left\{ \sum_{\ell,n} G^{+}_{\ell,n;\mu,\nu} \left(\gamma_{\ell,n} a\right)^2 K_\ell I_\ell \, G^{\mp}_{\ell,n;\mu',\nu'} \right\}$$

$$- \sum_{\mu,\nu} {}^{\phi}J^{-}_{\mu,\nu} \left\{ \sum_{\ell,n} G^{-}_{\ell,n;\mu,\nu} \left(\ell\beta_{\ell,n} a\right) K_\ell I_\ell \, G^{\mp}_{\ell,n;\mu',\nu'} \right\}$$

$$- \sum_{\mu,\nu} {}^{\phi}J^{+}_{\mu,\nu} \left\{ \sum_{\ell,n} G^{+}_{\ell,n;\mu,\nu} \left(\ell\beta_{\ell,n} a\right) K_\ell I_\ell \, G^{\mp}_{\ell,n;\mu',\nu'} \right\} = 0 \qquad (2.49^{a}_{b})$$

and from Eq. 2.48,

$$\sum_{\mu,\nu} {}^{z}J^{-}_{\mu,\nu} \left\{ \sum_{\ell,n} G^{-}_{\ell,n;\mu,\nu} \left(\ell\beta_{\ell,n}a\right) K_\ell I_\ell \, G^{\mp}_{\ell,n;\mu',\nu'} \right\}$$

$$+ \sum_{\mu,\nu} {}^{z}J^{+}_{\mu,\nu} \left\{ \sum_{\ell,n} G^{+}_{\ell,n;\mu,\nu} \left(\ell\beta_{\ell,n}a\right) K_\ell I_\ell \, G^{\mp}_{\ell,n;\mu',\nu'} \right\}$$

$$- \sum_{\mu,\nu} {}^{\phi}J^{-}_{\mu,\nu} \left[\sum_{\ell,n} G^{-}_{\ell,n;\mu,\nu} \left\{ \left(\frac{\ell\beta_{\ell,n}a}{\gamma_{\ell,n}a} \right)^2 K_\ell I_\ell + (ka)^2 K'_\ell I'_\ell \right\} G^{\mp}_{\ell,n;\mu',\nu'} \right]$$

$$- \sum_{\mu,\nu} {}^{\phi}J^{+}_{\mu,\nu} \left[\sum_{\ell,n} G^{+}_{\ell,n;\mu,\nu} \left\{ \left(\frac{\ell\beta_{\ell,n}a}{\gamma_{\ell,n}a} \right)^2 K_\ell I_\ell + (ka)^2 K'_\ell I'_\ell \right\} G^{\mp}_{\ell,n;\mu',\nu'} \right] = 0 \qquad (2.50^{a}_{b})$$

A solution exists only if the determinant of the coefficients of these equations vanishes. Thus, formally at least, a determinantal equation can be obatained in which $\beta_{o,o}a$ is calculated as a function of ka. The problem is simplified by noting that the symmetry of the structure allows $\underline{J}^{+}$ to be determined from $\underline{J}^{-}$ or vice versa. The four sets of equations then degenerate into two sets of independent equations: either Eqs. 2.49a and 2.50a or Eqs. 2.49b and 2.50b.

However, the difficulty involved in the calculation of numerical results is clear, and a more convenient form for deriving approximate solutions is desired.

2.1.6. Using the Variational Method to Derive an Approximation to the Determinantal Equation

As mentioned in Section 1.4.3, a variational technique is useful for deriving approximate solutions to yield numerical results. Beginning with one of the standard forms of the Lagrangian for an electromagnetic field, a variational expression is found for the present problem in terms of field intensities, which satisfy Maxwell's equations as well as the symmetry and periodicity conditions, but not the boundary conditions on the cylindrical surface $r = a$.[†] The result is an expression for the complex power, I, which might be generated or absorbed by the cylindrical surface $r = a$:

$$I = \int_0^p dz \int_0^{2\pi} a\, d\phi\, \hat{n} \cdot \left[{}_1\underline{E}^*(r = a) \times {}_1\underline{H}(r = a) - {}_2\underline{E}^*(r = a) \times {}_2\underline{H}(r = a) \right] \tag{2.51}$$

Because the terms within the bracket are dotted with $\hat{n}$, the unit vector perpendicular to the surface $r = a$, one needs only to consider the tangential components of $\underline{E}$ and $\underline{H}$. In light of Eqs. 2.16 and 2.17, Eq. 2.51 is rewritten as

$$I = \int_0^p dz \int_0^{2\pi} a\, d\phi\, \hat{n} \cdot \underline{E}^*(r = a) \times \left[{}_1\underline{H}(r = a) - {}_2\underline{H}(r = a) \right] \tag{2.52}$$

[†] See Appendix C.

$$I = \int_0^p dz \int_0^{2\pi} a\, d\phi \left\{ E_\phi^*(r = a)\hat{\phi} + E_z^*(r = a)\hat{z} \right\}$$

$$\times \left\{ \left[{}_1H_\phi(r = a) - {}_2H_\phi(r = a) \right] \hat{\phi} + \left[{}_1H_z(r = a) - {}_2H_z(r = a) \right] \hat{z} \right\} \quad (2.53)$$

Writing the tangential components of the H field in terms of the surface current density (Eqs. 2.24 and 2.25) allows Eq. 2.53 to be expressed as

$$I = \int_0^p dz \int_0^{2\pi} a\, d\phi \left\{ E_\phi(r = a)^* \left[{}^{\phi}J^- + {}^{\phi}J^+ \right] + {}^*E_z(r = a) \left[{}^{z}J^- + {}^{z}J^+ \right] \right\} \quad (2.54)$$

By employing the usual Fourier expansion for E_ϕ, E_z, ${}^{\phi}J^{\mp}$, and ${}^{z}J^{\mp}$ and performing the integration (equivalent to an orthogonality integration whereby all the cross terms of the multiplied summations are eliminated), the following form for the variational expression results:

$$I = \sum_{\ell,n} \left\{ E_\phi(r = a)^*_{\ell,n} \left[{}^{\phi}J^-_{\ell,n} + {}^{\phi}J^+_{\ell,n} \right] + E_z(r = a)^*_{\ell,n} \left[{}^{z}J^-_{\ell,n} + {}^{z}J^+_{\ell,n} \right] \right\} \quad (2.55)$$

The solution to the problem is then given by

$$\left[\delta I \; \underline{J}^-_{\ell,n};\; \underline{J}^+_{\ell,n} \right] = 0 \quad (2.56)$$

but like $\underline{J}^-$ and $\underline{J}^+$, the small variations $\delta\underline{J}^-$ and $\delta\underline{J}^+$ must themselves vanish off their respective helices. Once this is taken care of, the four doubly infinite set of simultaneous equations which result are

identical to Eqs. 2.49 and 2.50.†

However, the goal here is to find a simplified version of the determinantal equation. Using the narrow tape approximation, Eq. 2.42, the variational expression

$$I\left[\underline{J}^{-}_{\ell,n},\ \underline{J}^{+}_{\ell,n}\right]$$

is written out in terms of the E field expansions given in Eqs. 2.32 and 2.33. After simplifying and making use of the relations in Eqs. 2.44a and 2.44b, this becomes

$$I = 2\sum_{n=-\infty}^{\infty} U_{o,n}\left(I_{J^{-},o,n}^{*}\right)\left(I_{J^{-}_{o,n}}\right) + \sum_{\ell=1}^{\infty}\sum_{n=-\infty}^{\infty}\left[Y_{\ell,n}\left(I_{J^{-},\ell,n}^{*}\right)\left(I_{J^{-}_{\ell,n}}\right)\right.$$
$$\left. + Y_{-\ell,n}\left(I_{J^{-},-\ell,n}^{*}\right)\left(I_{J^{-}_{-\ell,n}}\right)\right] + \sum_{\ell=1}^{\infty}\sum_{n=-\infty}^{\infty} Z_{\ell,n}\left[\left(I_{J^{-},\ell,n}^{*}\right)\left(I_{J^{-}_{-\ell,n+\ell}}\right) + \text{c.c.}\right] \tag{2.57}$$

where

$$U_{o,n} \equiv \left(\gamma_{o,n}a\right)^2 K_o\left(\gamma_{o,n}a\right) I_o\left(\gamma_{o,n}a\right) \sin^2\theta \tag{2.58}$$

$$Y_{\ell,n} \equiv \left(\gamma_{\ell,n}a\right)^2 K_\ell I_\ell \sin^2\theta + \left[\left(\frac{\ell\beta_{\ell,n}a}{\gamma_{\ell,n}a}\right)^2 K_\ell I_\ell + (ka)^2 K'_\ell I'_\ell\right]\cos^2\theta$$
$$- (\ell\beta_{\ell,n}a)\, K_\ell I_\ell \sin^2\theta \tag{2.59}$$

---

† See reference 2 for details, pp. 47-54.

and

$$Z_{\ell,n} = \left(\gamma_{\ell,n}a\right)^2 K_\ell I_\ell \sin^2\theta - \left[\left(\frac{\ell\beta_{\ell,n}a}{\gamma_{\ell,n}a}\right)^2 K_\ell I_\ell + (ka)^2 K'_\ell I'_\ell\right] \cos^2\theta \quad (2.60)$$

As in Section 2.1.5, the surface current densities can be made to conform to the constraint given in Eq. 2.36 by writing $I_{J^-_{\ell,n}}$ in terms of a complete set of orthonormal functions which are themselves defined only on the helix tapes. However, for an approximate solution, $I_{\underline{J}^-}$ may be given by a <u>finite</u> number of terms of certain convenient functions, each having an unknown coefficient and each defined only on the helix tapes. Though the degree of accuracy increases as the number of terms in the sequence increases, it has been found that a one-term approximation provides good results, while greatly simplifying the variational expression. For the one-term approximation, there is no variational problem, and the determinantal equation is simply

$$I = 0 \quad (2.61)$$

Thus, $I_{\underline{J}^-}$ is approximated by

$$I_{\underline{J}^-} = \begin{cases} A\, e^{j\beta_{o,o}z}, \; 0 \le z \le p \text{ and } \frac{2\pi z}{p} - \frac{\xi}{2} \le \phi \le \frac{2\pi z}{p} + \frac{\xi}{2} & \text{(on helix)} \\ 0, \text{ otherwise} & \text{(off helix)} \end{cases} \quad (2.62)$$

The Fourier coefficients $I_{J^-_{\ell,n}}$ are then found by setting the Fourier expansion for $I_{\underline{J}^-}$ (Eq. 2.41a) equal to Eq. 2.62 and applying orthogonality,

$$I_{J^-_{\ell,n}} = \frac{A}{2\pi p} \int_o^p dz \int_{2\pi z/p-\xi/2}^{2\pi z/p+\xi/2} d\phi \; e^{j\beta_{o,o} z} \; d^{-j\beta_{\ell,n}} \; e^{j\ell\phi} \qquad (2.63)$$

The integral over ϕ reduces to

$$\int_{2\pi z/p-\xi/2}^{2\pi z/p+\xi/2} d\phi \; e^{j\ell\phi} = e^{j\ell \frac{2\pi z}{p}} \left[\frac{\sin\left(\ell \frac{\xi}{2}\right)}{\ell} \right] \qquad (2.64)$$

and the integral over z then takes the form

$$\int_o^p dz \; e^{j\beta_{o,o} z} \; e^{-j\beta_{\ell,n} z} \; e^{j\ell \frac{2\pi z}{p}} = \frac{e^{jp\left(\beta_{o,o} - \beta_{\ell,n} + \frac{\ell 2\pi}{p}\right)} - 1}{\beta_{o,o} - \beta_{\ell,n} + \frac{\ell 2\pi}{p}} \qquad (2.65)$$

Since

$$\beta_{\ell,n} = \beta_{o,o} + (\ell + 2n) \frac{2\pi}{p} \qquad (2.12')$$

Eq. 2.65 reduces to

$$-\frac{p}{j4\pi n} \left(e^{-j4\pi n} - 1 \right) = \frac{2p}{2\pi n} \sin(2\pi n) \qquad (2.66)$$

$$= \begin{cases} 2p \;, & n = 0 \\ 0 \;, & n \neq 0 \end{cases} \qquad (2.67)$$

Considering Eq. 2.63 in its entirety yields the result that

$$I_{J^-_{\ell,n}} = A \frac{\xi}{2\pi} \alpha_\ell \; \delta(n) \qquad (2.68)$$

where

$$\alpha_\ell = \frac{\sin(\ell\xi/2)}{(\ell\xi/2)} \tag{2.69}$$

and

$$\delta(n) = \begin{cases} 1 , & n = 0 \\ 0 , & n \neq 0 \end{cases} \tag{2.70}$$

From Eq. 2.57, the determinantal equation becomes

$$2U_{o,o} + \sum_{\ell=1}^{\infty} \alpha_\ell^2 \left(Y_{\ell,o} - Y_{-\ell,o} \right) = 0 \tag{2.71}$$

The reason there is no $Z_{\ell,n}$ term in Eq. 2.71 is because of the delta function in the expression for $I_{J^-_{\ell,n}}$ (Eq. 2.68). In the original expression for the variation, Eq. 2.57, $Z_{\ell,n}$ is multiplied by $I_{J^-_{\ell,n+\ell}}$. While n can only be zero, the quantity $(n + \ell)$ is never zero since $\ell \geq 1$. This implies that

$$I_{J^-_{\ell,n+\ell}} = A \frac{\xi}{2\pi} \alpha_\ell \, \delta(n + \ell) \tag{2.72}$$

will always be zero, as the delta function will never take the form $\delta(0)$.

2.1.7 The Single Helix Determinantal Equation

The corresponding determinantal equation for the single helix is presented here for completeness. It is also helpful to have it in a form which is easily adaptable to the more general boundary value problem described in Chapter Three.

Instead of Eq. 2.71, the determinantal equation for the single helix is

$$U_o + V_o + \sum_{\ell=1}^{\infty} \alpha_\ell^2 \left(Y_\ell + Y_{-\ell}\right) = 0 \tag{2.73}$$

Noting that $Y_{\ell,o}$ for the contrawound helix is identical to Y_ℓ for the single helix, the terms U_o, Y_ℓ, and $Y_{-\ell}$ are simply $U_{o,o}$, $Y_{\ell,o}$, and $Y_{-\ell,o}$, respectively. The V_o term results from the fundamental component of the TE fields, which is of course not present in the symmetric mode of the contrawound helix,† and has the form

$$V_o = (ka)^2 K_o'(\gamma_o a) I_o'(\gamma_o a) \cos^2\theta \tag{2.74}$$

It should be of no surprise that the determinantal equation for the single helix differs only slightly from that of the twin helices. However, this difference is enough to significantly alter the dispersion characteristics, as will be seen in Section 2.2.

---

† This property is demonstrated analytically in Appendix D.

2.2 Results for the Free Space Problem

The formulation of Sections 2.1.6 and 2.1.7 for the free space problem is implemented with a HP 1000 minicomputer.†

Fixing the values of θ and ξ, the determinantal equation is solved numerically to obtain $\beta_{o,o}a$ as a function if ka, for the contrawound helix, and $\beta_o a$ as a function of ka for the single helix. Since $\beta_{o,o}a = \beta_o a$, all dispersion plots are made with respect to $\beta_o a$. Furthermore, the ordinate and abcissa are normalized in the conventional manner by the relations

$$ka/\cot\theta = p/\lambda_{freespace}$$

$$\beta a/\cot\theta = p/\lambda_{helix}$$

where λ is the wavelength.

Before proceeding, it is important to note that the numerical results compare well to experimental only for narrow helix tapes ($\xi < 1$) such that the overlap region between the two "touching" tapes is kept to a minimum. Nevins [12] demonstrates that the discrepancy between the theoretical predictions and experimental results is due to the currents deviating from their respective helical paths. When current flow from one tape to the other is prevented -- i.e., the two helix tapes are not allowed to touch -- the predicted and experimental results compare closely and are not dependent on ξ.

---

† Refer to Appendix E.

Figures 2.3 and 2.4 show how varying the pitch angle affects the dispersion, for $\xi = 1$ and $\xi = 2$, respectively. The pitch angle is reduced as cot θ is increased from 2.5 to 10, resulting in a decrease in the group velocity, v_g $(v_g = d(ka)/d(\beta a))$, along with a decrease in the phase velocity, v_p $(v_p = ka/\beta a)$.

Figures 2.5 and 2.6 show the effects of varying ξ, while cot θ is fixed at 10 and 5, respectively. In both cases, changing the tape width has a negligible affect on the dispersion characteristics for the single helix, while those for the contrawound structure are altered considerably. The reason the contrawound circuit is so affected is due to the interaction between the two helices, which becomes stronger as the tape width is increased.

Experimental results of Birdsall and Everhart [4] are plotted along with numerical results in Fig. 2.7. In both cases, the dispersion increases with increased tape width. The deviation between the theoretical and experimental results is due almost entirely to the foreshortened current paths which result when the two helix tapes are allowed to touch. However, the effects of finite tape thickness must also be considered.

Experimental results [4] for several tape thicknesses are plotted in Fig.s 2.8 and 2.9. Correlation with theory improves as the tape thickness is reduced; furthermore, a comparison between the two figures reveals that there is better agreement between theory and experiment for the smaller tape width, $\xi = \pi/4$.

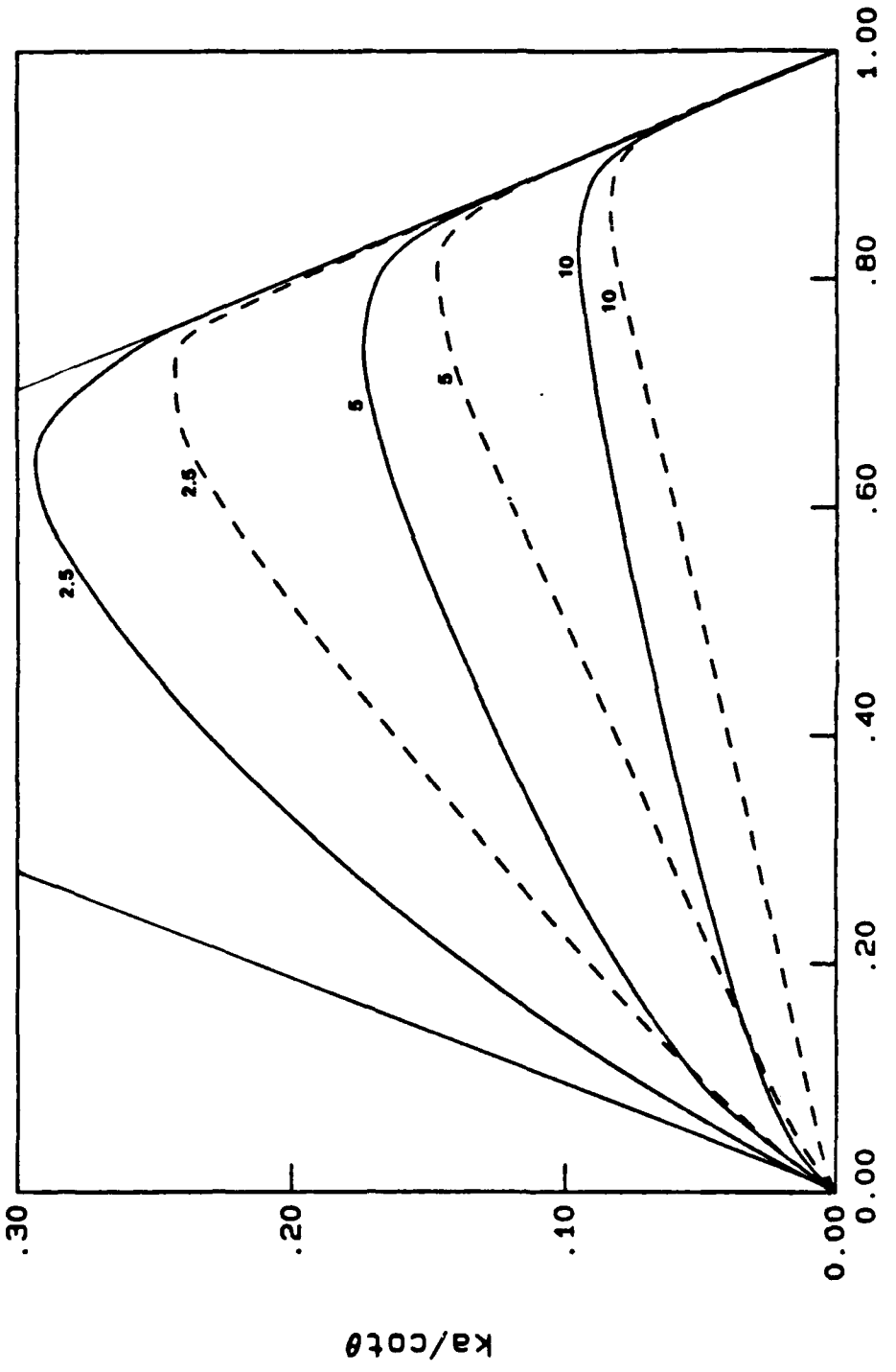

Fig. 2.3. Theoretical dispersion characteristics for both a contrawound helix (solid line) and for a single helix (dashed line) in free space showing the effects of varying cot θ: cot θ = 2.5, 5, 10. The tape width is described by ξ = 1 and is assumed to be infinitely thin.

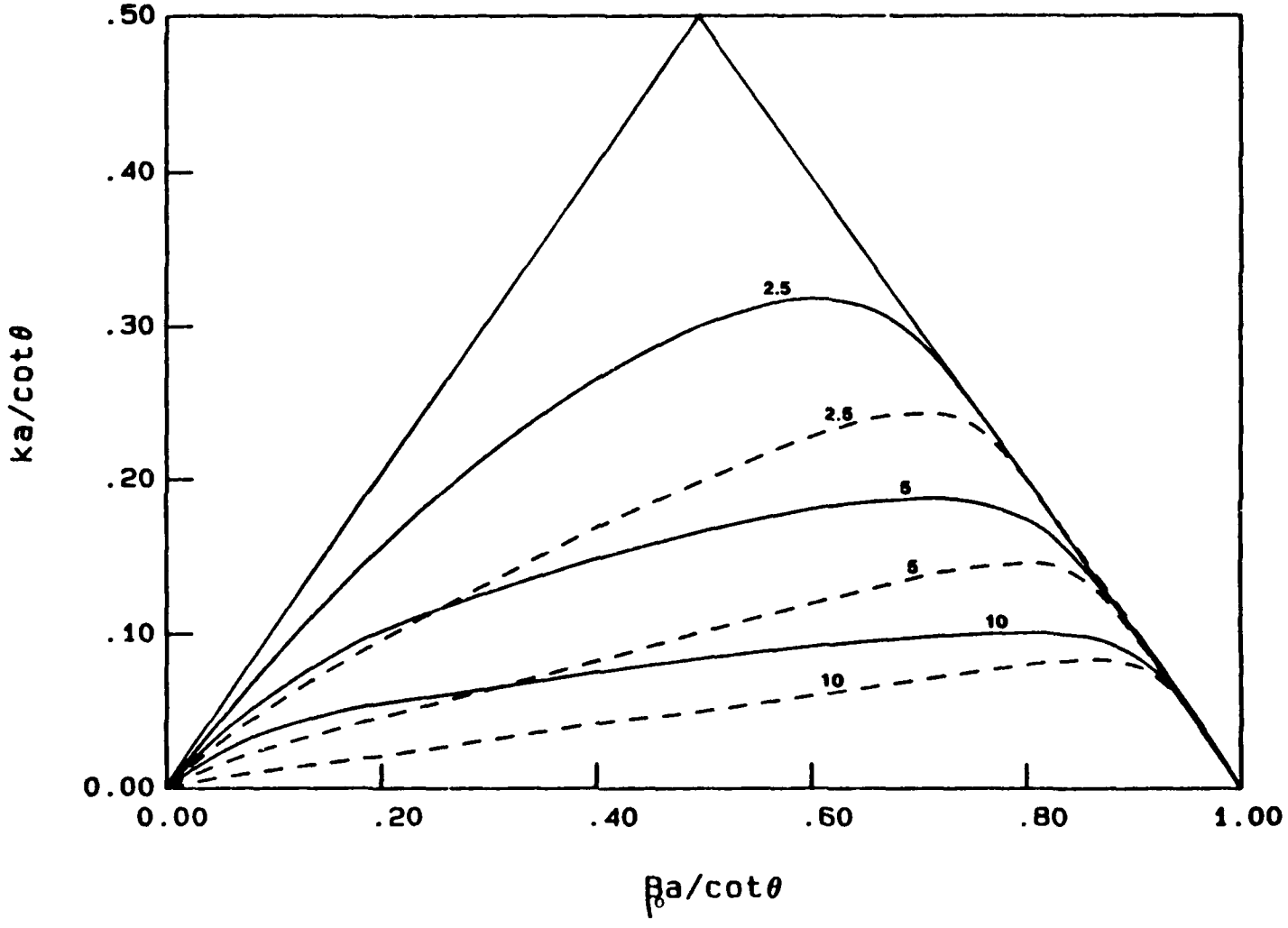

Fig. 2.4. Theoretical dispersion characteristics for a contrawound helix (solid line) and a single helix (dashed line) of $\xi = 2$ in free space, showing the effects of varying cot θ: cot θ = 2.5, 5, 10.

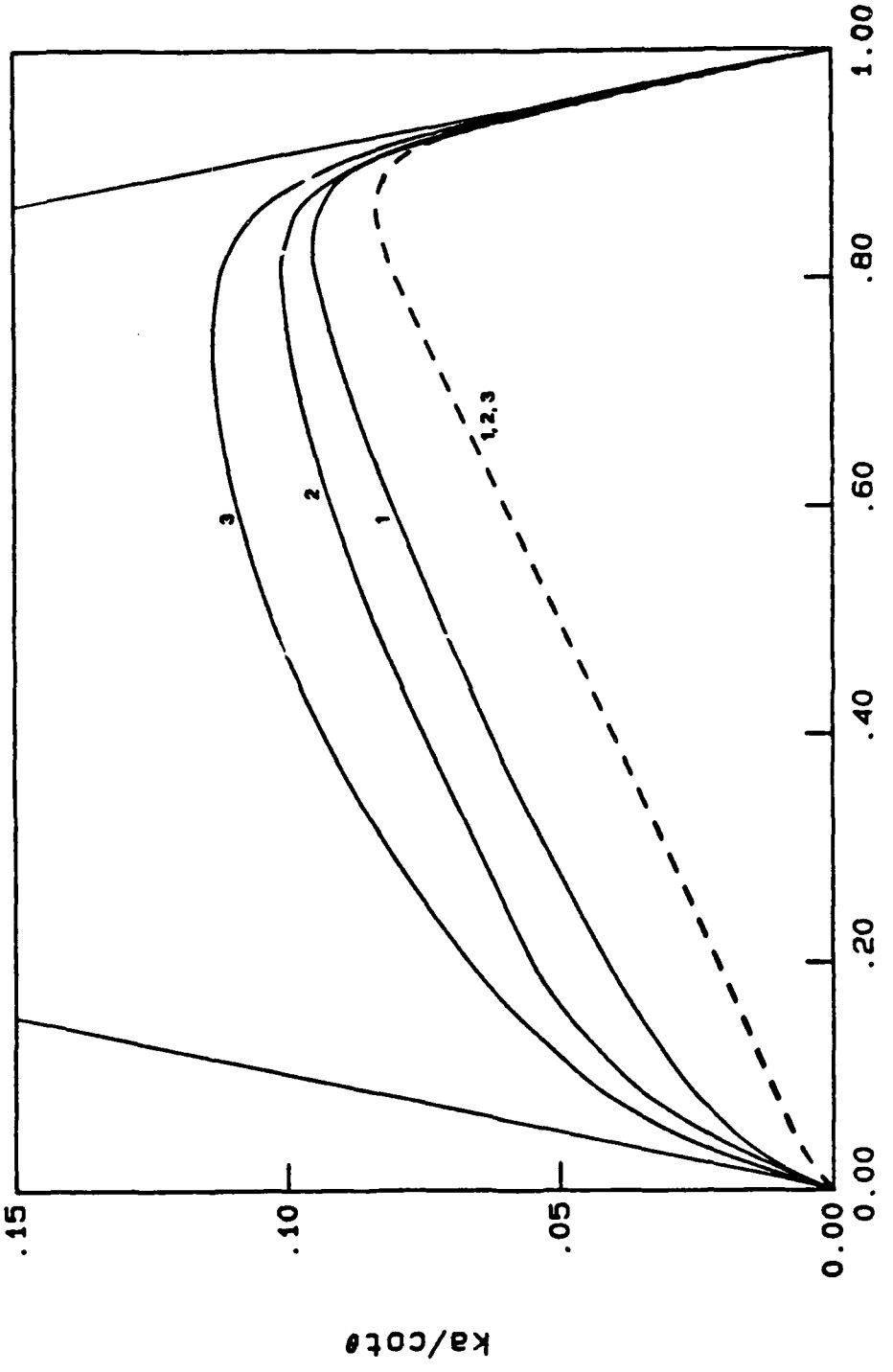

Fig. 2.5. Theoretical dispersion characteristics for a contrawound helix (solid line) and a single helix (dashed line) of cot = 10 in free space, showing the effects of varying ξ: ξ = 1, 2, 3.

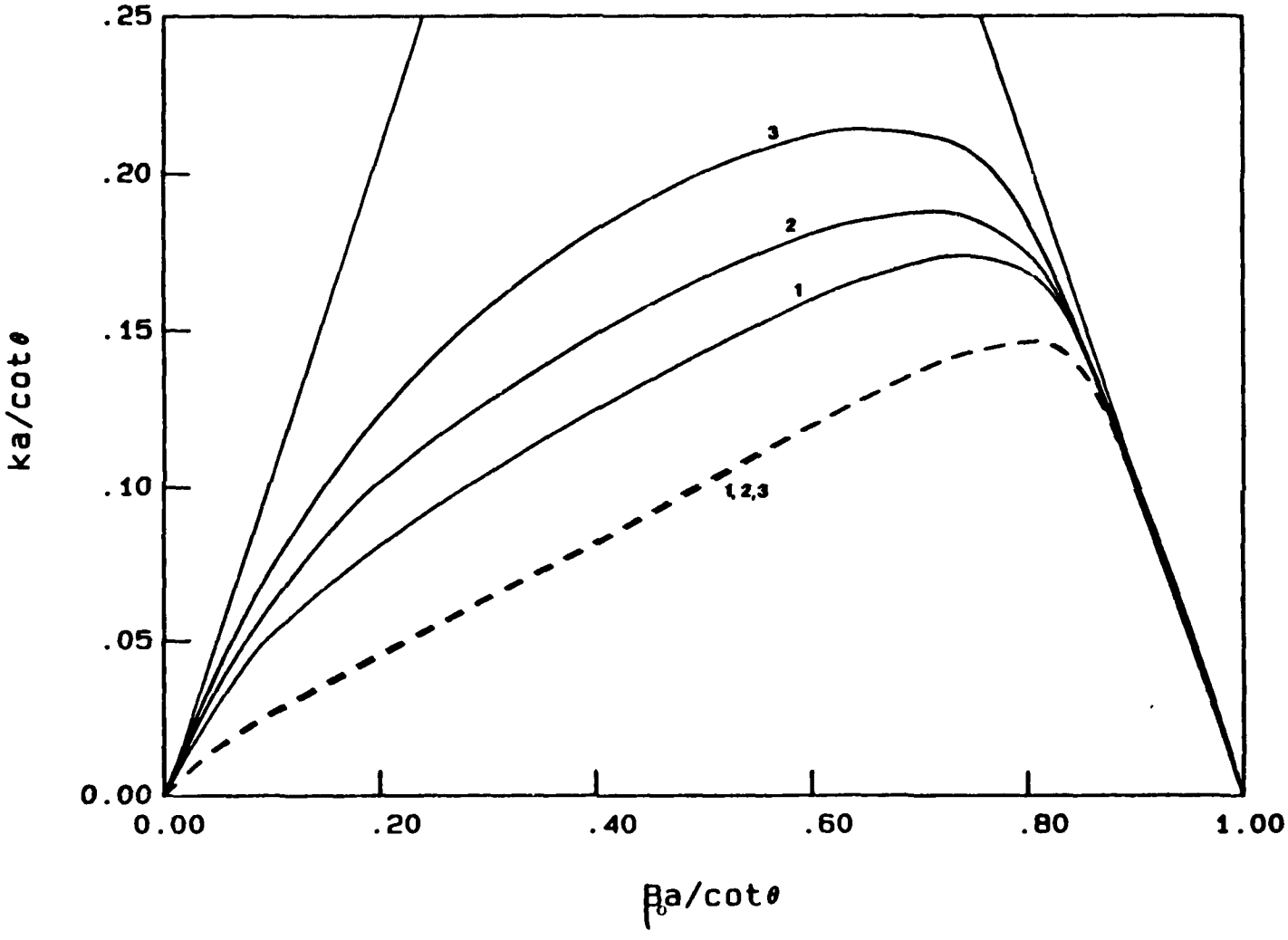

Fig. 2.6. Theoretical dispersion characteristics for a contrawound helix (solid line) and a single helix (dashed line) of cot θ = 5 in free space showing the effects of varying ξ: ξ = 1, 2, 3.

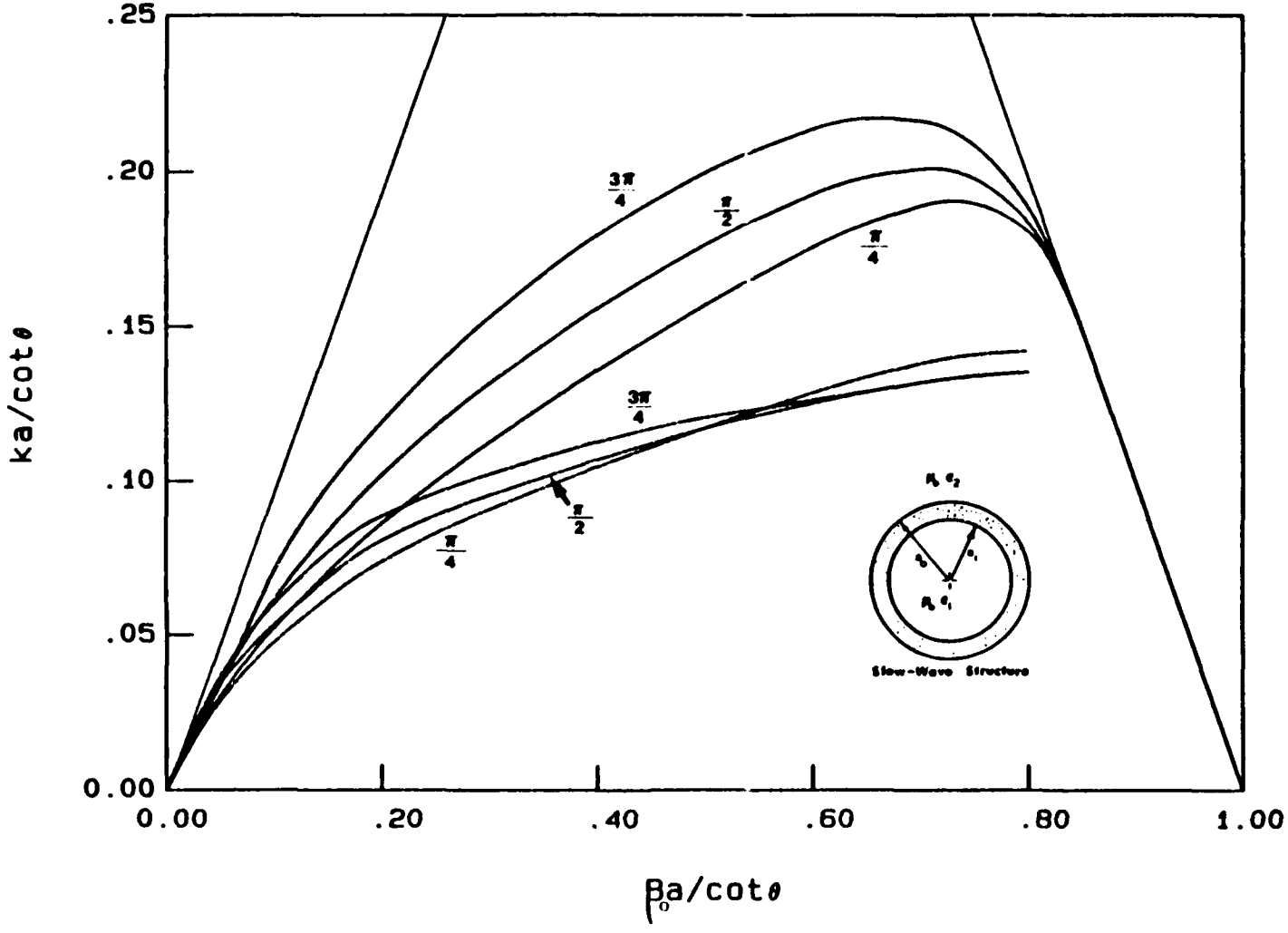

Fig. 2.7. Theoretically (solid line) and experimentally (dot-dashed line) derived dispersion characteristics for a contrawound helix of cot θ = 4.4 in free space, showing the effects of varying ξ: ξ = π/4, π/2, 3π/4. In the experiment a_1/a_o = 0.9, while a_1/a_o = 1 is assumed in the theory.

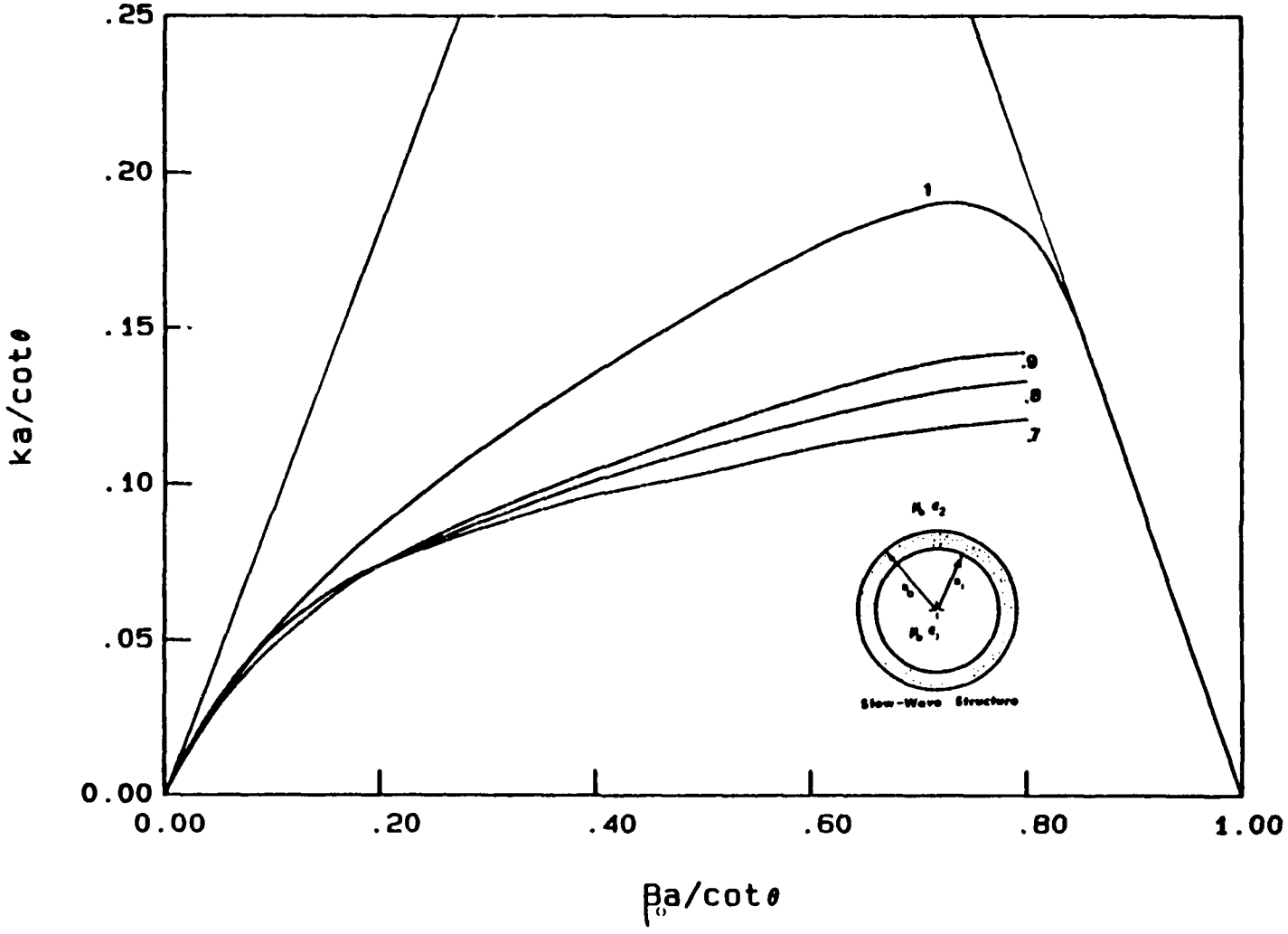

Fig. 2.8. Experimentally derived dispersion characteristics (dot-dashed line) for a contra-wound helix in free space, showing the effect of varying the tape thickness. Values of a_1/a_o = 0.7, 0.8, 0.9 are compared to theoretical results (solid line) in which a_1/a_o = 1. The other geometric parameters are cot θ = 4.4, ξ = π/4.

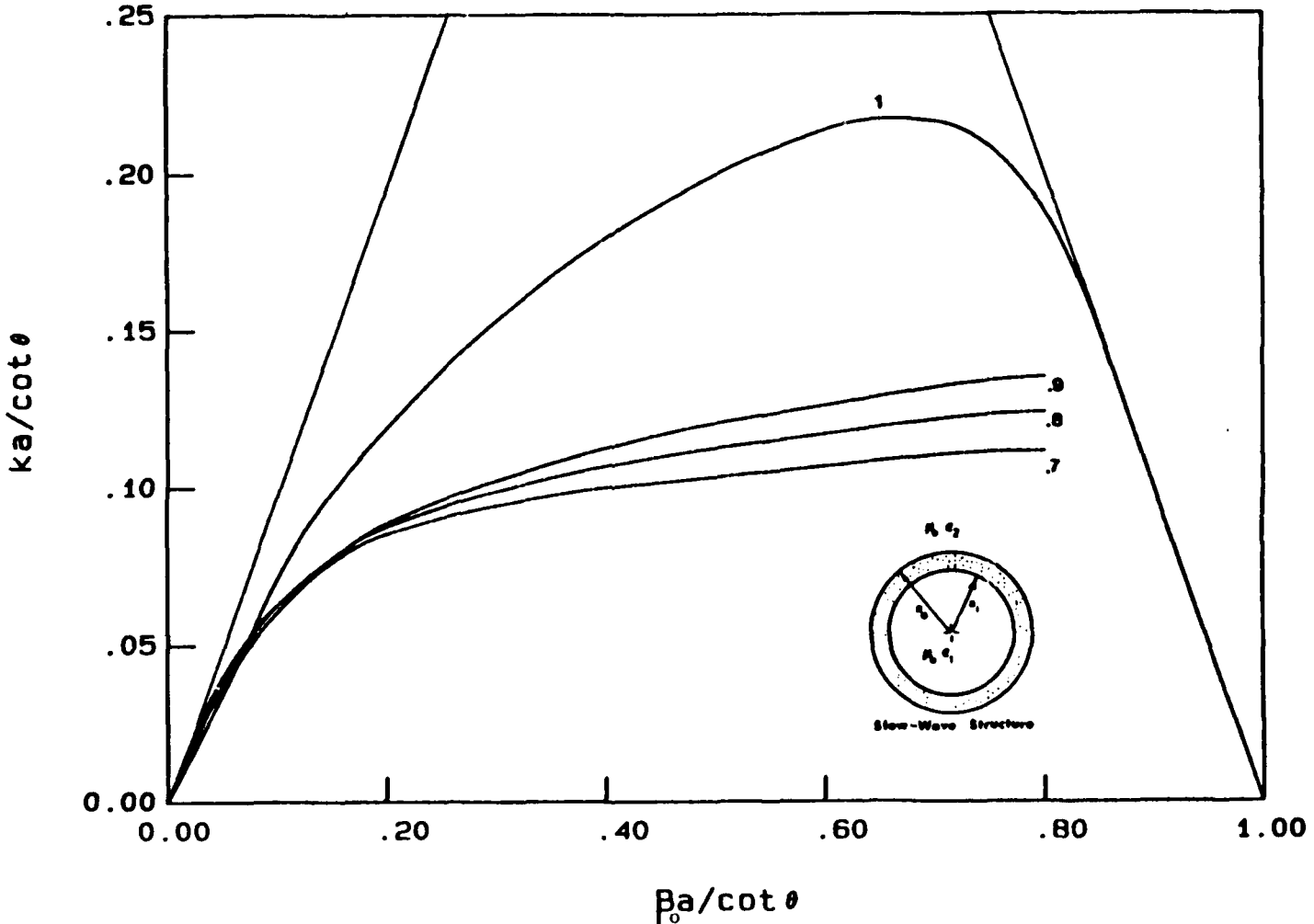

Fig. 2.9. Experimentally derived dispersion characteristics (dot-dashed line) for a contra-wound helix in free space, showing the effect of varying the tape thickness, a_i/a_o = 0.7, 0.8, 0.9, are compared to theoretical results (solid line), in which a_i/a_o = 1. The other geometric parameters are cot θ = 4.4, ξ = 3π/4.

III. ANALYTICAL CONSIDERATIONS OF METAL AND DIELECTRIC LOADING ON THE CONTRAWOUND HELIX

3.1 The Boundary Value Problem

To study the effects of dielectric loading on the dispersion characteristics for the contrawound helix, the dispersion equation developed in Chapter Two must be altered so as to allow for variations in the dielectric properties. As before, the problem is separated into two regions, but each with its own dielectric constant. Figure 3.1 shows schematically that the permeability is still that of free space, μ_o, while the permittivity is arbitrary, ε_1 or ε_2. The field quantities are written as a Fourier decomposition in each region and are then matched across the boundary r = a to express them in terms of the surface current density on the two helix tapes. Finally, the variational method is again employed to obtain a determinantal equation.

If Region 2 is bounded by a conducting sheath at r = b, Fig. 3.2, the problem becomes one in which the contrawound helix feels the effects of an external shield. This effect is handled mathematically simply by reforming the modified cylindrical Bessel function(s) in Region 2 to properly account for this boundary.

3.1.1 The Field Functions

Before writing the Fourier expansions for the field quantities, k and γ must be redefined to correctly account for the dielectric properties in each region. Thus,

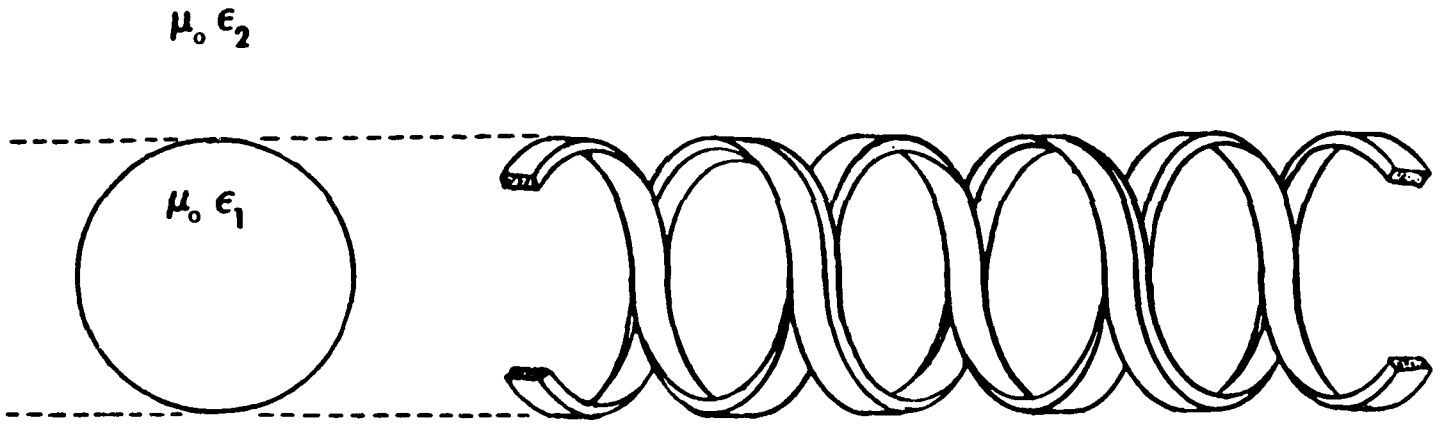

Fig. 3.1. The contrawound helix interposed between two dielectric regions with permittivities ϵ_1 and ϵ_2 and with permeabilities $\mu_1 = \mu_2 = \mu_o$.

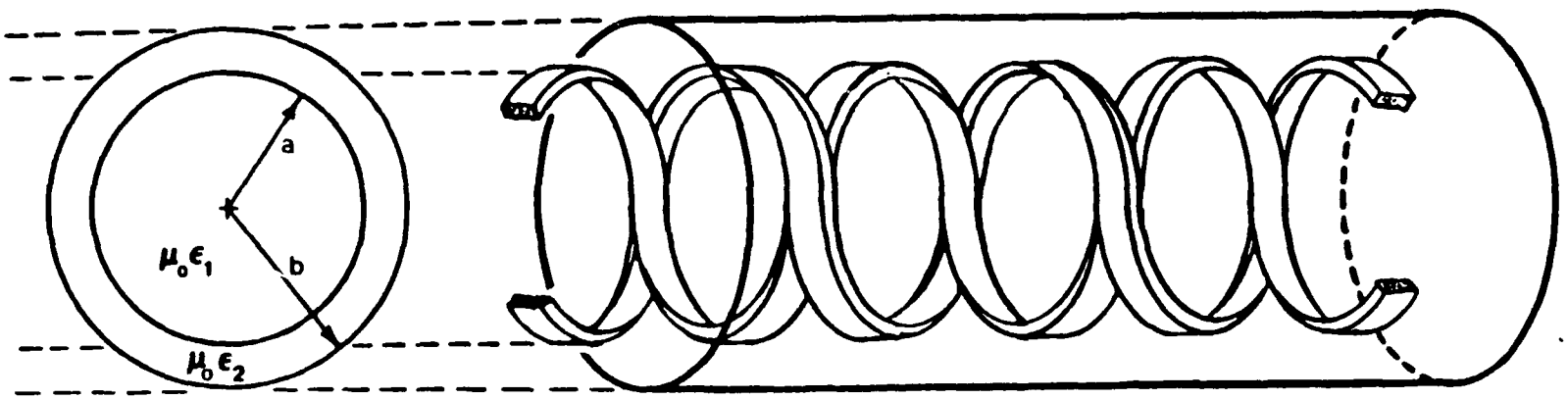

Fig. 3.2. The contrawound helix interposed between two dielectric regions at r = a and bounded by a conducting cylinder at r = b.

$$k_i = \omega\sqrt{\varepsilon_i \mu_o} \qquad i = 1, 2 \tag{3.1}$$

and

$$\left(\gamma_{\ell,n}\right)_i = \left(\beta_{\ell,n}^2 - k_i^2\right)^{1/2} \qquad i = 1, 2 \tag{3.2}$$

where i denotes either Region 1 or Region 2. Furthermore, the intrinsic wave impedance is defined to be

$$\eta_i = \sqrt{\frac{\mu_o}{\varepsilon_i}} \qquad i = 1, 2 \tag{3.3}$$

To facilitate both clarity and understanding, a shorthand notation is adopted in which the ℓ and n dependence of the terms in the Fourier decomposition for the field quantities is assumed:

$$\gamma_i \equiv \left(\gamma_{\ell,n}\right)_i \tag{3.4}$$

$$\beta \equiv \beta_{\ell,n} \tag{3.5}$$

$$F(\gamma_i r) \equiv F_\ell\left[\left(\gamma_{\ell,n}\right)_i r\right], \quad F_\ell = I_\ell, K_\ell, I'_\ell, K'_\ell \tag{3.6}$$

$$\left.\begin{aligned} A &\equiv A_{\ell,n} \\ B &\equiv B_{\ell,n} \\ C &\equiv C_{\ell,n} \\ D &\equiv D_{\ell,n} \end{aligned}\right\} \tag{3.7}$$

Consequently, the Fourier expansions may be written in a form which assumes summation over the two indices ℓ and n whereby

$$\sum = \sum_{\ell,n=-\infty}^{\infty}$$

In this notation, the expressions for E_z, H_z, E_ϕ, and H_ϕ in the two regions are as follows:†

$(0 < r < a)$

$$_1E_z = \sum n_1 \, AI(\gamma_1 r) \, e^{-j\beta z} \, e^{j\ell\phi} \tag{3.8}$$

$$_1E_\phi = \sum \left\{ - \frac{\ell n_1 \beta}{\gamma_1^2 r} AI(\gamma_1 r) - j \frac{k_1}{\gamma_1} CI'(\gamma_1 r) \right\} e^{-j\beta z} \, e^{j\ell\phi} \tag{3.9}$$

$$_1H_z = \sum \frac{C}{n_1} I(\gamma_1 r) \, e^{-j\beta z} \, e^{j\ell\phi} \tag{3.10}$$

$$_1H_\phi = \sum \left\{ j \frac{k_1}{\gamma_1} AI'(\gamma_1 r) - \frac{\ell\beta}{n_1 \gamma_1^2 r} CI(\gamma_1 r) \right\} e^{-j\beta z} \, e^{j\ell\phi} \tag{3.11}$$

$(a < r)$ or $(a < r < b)$

$$_2E_z = \sum n_2 BK_e(\gamma_2 r) \, e^{j\beta z} \, e^{j\ell\phi} \tag{3.12}$$

$$_2E_\phi = \sum \left\{ - \frac{\ell n_2 \beta}{\gamma_2^2 r} BK_e(\gamma_2 r) - j \frac{k_2}{\gamma_2} DK_e'(\gamma_2 r) \right\} e^{-j\beta z} \, e^{j\ell\phi} \tag{3.13}$$

---

† See Appenedix A for more details.

$$ {}_2H_z = \sum \frac{D}{n_2} K_h(\gamma_2 r)\, e^{-j\beta z}\, e^{j\ell\phi} \tag{3.14} $$

$$ {}_2H_\phi = \sum \left\{ j \frac{\kappa_2}{\gamma_2} B K_h'(\gamma_2 r) - \frac{\ell\beta}{n_2 \gamma_2^2 r} D K_h(\gamma_2 r) \right\} e^{-j\beta z}\, e^{j\ell\phi} \tag{3.15} $$

If Region 2 is unbounded, the modified Bessel functions in the last four equations are simply,

$$ \left.\begin{aligned} K_e &= K_\ell \left[\left(\gamma_{\ell,n}\right)_2 r \right] \\ K_e' &= K_\ell' \left[\left(\gamma_{\ell,n}\right)_2 r \right] \\ K_h &= K_\ell \left[\left(\gamma_{\ell,n}\right)_2 r \right] \\ K_h' &= K_\ell' \left[\left(\gamma_{\ell,n}\right)_2 r \right] \end{aligned}\right\} \tag{3.16} $$

If, however, Region 2 is bounded by a perfect conductor at r = b, these same functions take the form (in shorthand notation),

$$ \left.\begin{aligned} K_e &= I(\gamma_2 b)\, K(\gamma_2 r) - K(\gamma_2 b)\, I(\gamma_2 r) \\ K_e' &= I'(\gamma_2 b)\, K'(\gamma_2 r) - K'(\gamma_2 b)\, I'(\gamma_2 r) \\ K_h &= I'(\gamma_2 b)\, K(\gamma_2 r) - K'(\gamma_2 b)\, I(\gamma_2 r) \\ K_h' &= I(\gamma_2 b)\, K'(\gamma_2 r) - K(\gamma_2 b)\, I'(\gamma_2 r) \end{aligned}\right\} \tag{3.17} $$

Applying boundry conditions 2.14 and 2.15 at r = a and proceeding as in Section 2.1.2, the Fourier coefficients for the field components are determined in terms of the surface current density Fourier coefficients. Letting

$$z_J^{\pm} \equiv z_{J\,\ell,n}^{\pm} \tag{3.18}$$

and

$$\phi_J^{\pm} \equiv \phi_{J\,\ell,n}^{\pm} \tag{3.19}$$

the expression for C is found to be

$$C = R(z_J^- + z_J^+) + S(\phi_J^- + \phi_J^+) \tag{3.20}$$

where

$$R = \frac{\eta_1}{\eta_2}\frac{Q}{IN}\left[\left(\gamma_2 a\right)^2 - \left(\gamma_1 a\right)^2\right] \tag{3.21}$$

$$S = \frac{\eta_1}{I} - \frac{\eta_1 Q \ell \beta}{\eta_2 I N \gamma_1^2 a}\left[\left(\gamma_2 a\right)^2 - \left(\gamma_1 a\right)^2\right]$$

$$+ \frac{k_1 I' \gamma_1 a\left(\gamma_2 a\right)^2 \eta_1}{\ell \beta \eta_2 I^3}\left\{\frac{QM}{N}\left[\left(\gamma_2 a\right)^2 - \left(\gamma_1 a\right)^2\right] + Q\right\} \tag{3.22}$$

$$Q = \frac{n_1 n_2 \ell \beta I^2 K_h}{a^3 \gamma_1 \gamma_2 \left[k_2 n_2 \gamma_1 I K_e' - k_1 n_1 \gamma_2 K_h I'\right]} \tag{3.23}$$

$$M = \frac{\ell^2 \beta^2 n_1 I^2 K_h}{(\gamma_2 a)^3 (\gamma_1 a)^3} \left\{ \frac{(\gamma_1 a)^2 - (\gamma_2 a)^2}{k_2 n_2 \gamma_1 I K_e' - k_1 n_1 \gamma_2 K_h I'} \right\} \tag{3.24}$$

and

$$N = \frac{k_1 n_2 \gamma_2 I' K_e - k_2 n_1 \gamma_1 K_h' I}{\gamma_1 \gamma_2 n_2 K_e} - M\left[(\gamma_2 a)^2 - (\gamma_1 a)^2\right] \tag{3.25}$$

Similarly, the expression for A is

$$A = j\left[T(z_J^- + z_J^+) + X(\phi_J^- + \phi_J^+)\right] \tag{3.26}$$

where

$$T = \frac{1}{N} \tag{3.27}$$

and

$$X = -\frac{1}{N}\left\{\frac{\ell\beta}{\gamma_1^2 a} - M\left[\frac{k_1 I' \gamma_1 a (\gamma_2 a)^2}{\ell \beta I^2}\right]\right\} \tag{3.28}$$

In the above equations, the argument of I and I' is $\gamma_1 a$, while K_e, K_e', K_h, and K_h' take the form of Eqs. 3.16 and 3.17 with r = a. Expressions for the Fourier coefficients B and D are determined from the relationships

$$B = A\left(\frac{n_1}{n_2}\frac{I}{K_e}\right) \tag{3.29}$$

and

$$D = \frac{\eta_2}{K_h}\left[\frac{I}{\eta_1} C - (\phi_J^- + \phi_J^+)\right] \tag{3.30}$$

3.1.2 Approximating the Determinantal Equation

As outlined in Section 2.1.5, the solution to the boundary value problem resulting in the determinantal equation can be found by solving four doubly infinite sets of linear homogeneous simultaneous equations, each having the same number of unknowns. However, a more manageable approach is to use the variational method of Section 2.1.6 to obtain an approximation to the determinantal equation.

Since the variational expression for the current problem is the same as that for the contrawound helix in free space, Eq. 2.55 may be used directly. From Eqs. 3.20 and 3.26, the expressions for E_z and E_ϕ at $r = a$ are

$$E_z(r = a) = \sum j\eta_1 I\left[T(z_J^- + z_J^+) + X(\phi_J^- + \phi_J^+)\right] e^{-j\beta z}\, e^{j\ell\phi} \tag{3.31}$$

and

$$E_\phi(r = a) = \sum\left\{-j\,\frac{\ell\eta_1\beta}{\gamma_1^2 a} I\left[T(z_J^- + z_J^+) + X(\phi_J^- + \phi_J^+)\right]\right.$$

$$\left. - j\,\frac{k_1}{\gamma_1} I'\left[R(z_J^- + z_J^+) + S(\phi_J^- + \phi_J^+)\right]\right\} e^{-j\beta z}\, e^{j\ell\phi} \tag{3.32}$$

These expressions are substituted into Eq. 2.55 resulting in Eq. 2.57, with $U_{o,n}$, $Y_{\ell,n}$, and $Z_{\ell,n}$ defined as follows:

$$U_{o,n} = n_1 IT \sin^2\theta \tag{3.33}$$

$$Y_{\ell,n} = n_1 IT \sin^2\theta - \left[\frac{\ell n_1 \beta}{\gamma_1^2 a} IX + \frac{k_1}{\gamma_1} I'S\right] \cos^2\theta + \left[n_1 IX - \frac{\ell n_1 \beta}{\gamma_1^2 a} IT - \frac{k_1}{\gamma_1} I'R\right] \sin\theta \cos\theta \tag{3.34}$$

and

$$Z_{\ell,n} = n_1 IT \sin^2\theta + \left[\frac{\ell n_1 \beta}{\gamma_1^2 a} IX + \frac{k_1}{\gamma_1} I'S\right] \cos^2\theta - \left[n_1 IX - \frac{\ell n_1 \beta}{\gamma_1^2 a} IT - \frac{k_1}{\gamma_1} I'R\right] \sin\theta \cos\theta \tag{3.35}$$

Using the approximation for $\underline{I}_J^-$ given in Eq. 2.62, the determinantal equation is again Eq. 2.71, where $U_{o,o}$, $Y_{\ell,o}$, and $Y_{-\ell,o}$ are determined from Eqs. 3.33 and 3.34.

Similarly, for the single helix interposed between two dielectric regions at r = a and with or without a conducting sheath at r = b, the determinantal equation is found to be the same as Eq. 2.73. As before, U_o, Y_ℓ, and $Y_{-\ell}$ for the single helix are simply $U_{o,o}$, $Y_{\ell,o}$, and $Y_{-\ell,o}$, respectively, but with $U_{o,o}$, $Y_{\ell,o}$, and $Y_{-\ell,o}$ being determined from Eqs.

3.33 and 3.34. The corresponding form of V_o for the two dielectric problem is

$$V_o = -\frac{n_1}{I}\left\{1 + \frac{k_1 I' \gamma_2 n_1 K_h}{\left[k_2 n_2 \gamma_1 I K_e' - k_1 n_1 \gamma_2 I' K_h\right]}\right\}\frac{k_1}{\gamma_1} I' \cos\theta \qquad (3.36)$$

The formulation developed in this section can now be used to explore the effects of dielectric and metal loading.

3.2 Results for Dielectric and Metal Loading

By implementing the formulation of Section 3.1.2, the effects of loading are investigated simultaneously for both the contrawound and single helix.

3.2.1 Dielectric Loading

The dispersion plot in Fig. 3.3 for cot θ = 10 shows how the group velocity and phase velocity are reduced as $\varepsilon_2/\varepsilon_1$ is increased from 1 to 9. This behavior is also present in the experimental work performed by Birdsall and Everhart [4]. They observe that as the distance between a surrounding glass cylinder and the slow-wave structure is reduced, the degree to which the velocities are loaded increases. Their results are reproduced in Fig. 3.4. Inspection of this figure further reveals that the effects of dielectric loading are negligible when the distance between the cylinder and the circuit is increased past a certain point. The reason for this is the fields outside the circuit (Region 2) decrease exponentially and consequently do not penetrate radially a significant distance into Region 2.

Figure 3.5 attempts to correlate the experimental results for loading by a glass cylinder of finite thickness to theoretical predictions for dielectric loading, in which the dielectric of Region 2 extends to infinity. To do so, an equivalent relative permittivity for Region 2 is calculated by volumetrically proportioning the relative permittivity of the glass cylinder.

It is assumed that the fields in Region 2 penetrate to a depth of b/a= 1.21. Consequently, the slow-wave circuit "sees" an effective (two

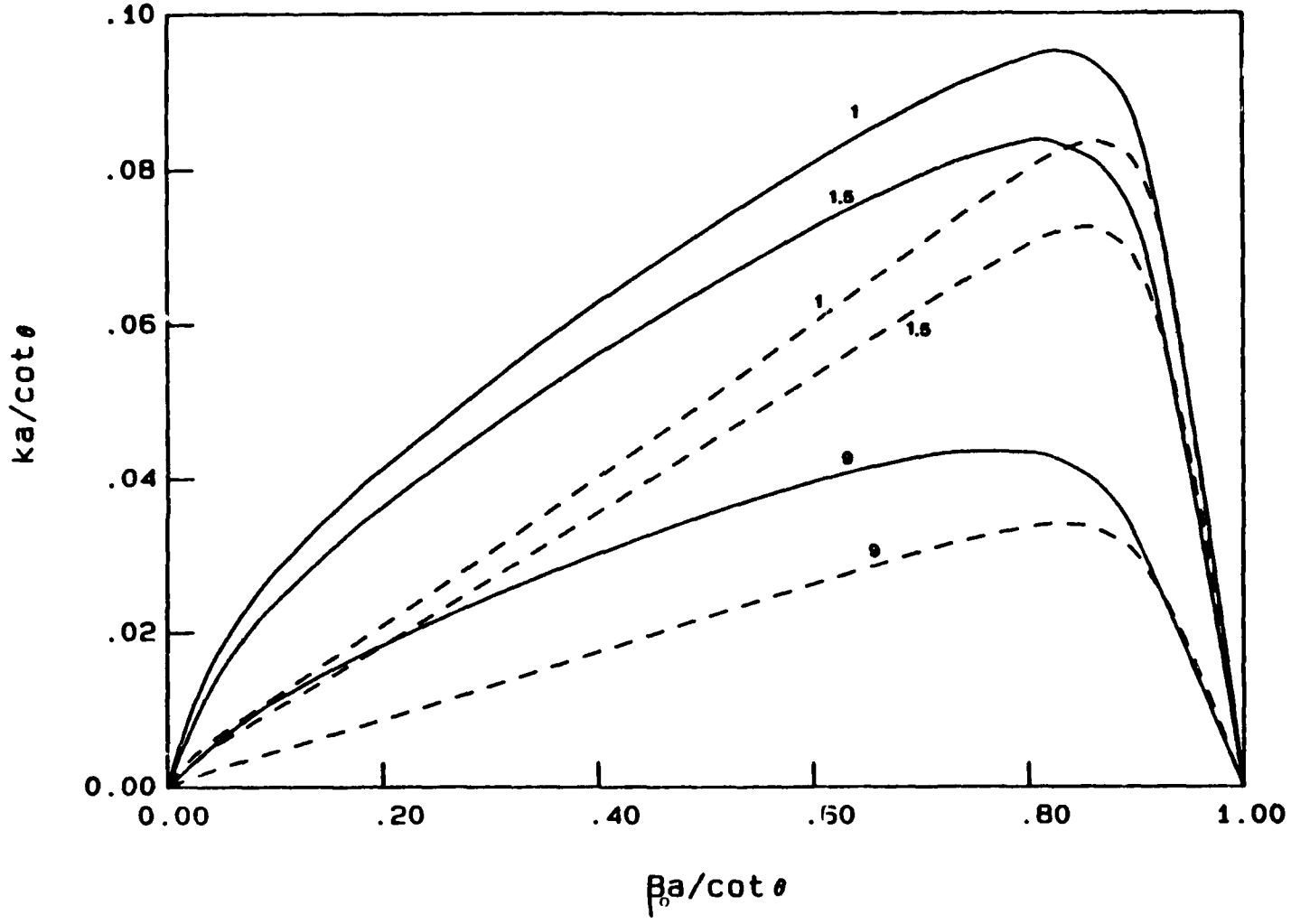

Fig. 3.3. Theoretical dispersion characteristics for a contrawound helix (solid line) and a single helix (dashed line) interposed between two dielectric regions and showing the effect of dielectric loading by the outer region -- region 2 -- such that $\varepsilon_2/\varepsilon_1 = 1, 1.5, 9$ and $k_2/k_1 = 1, 1.225, 3$, correspondingly. cot $\theta = 10$, $\xi = 1$.

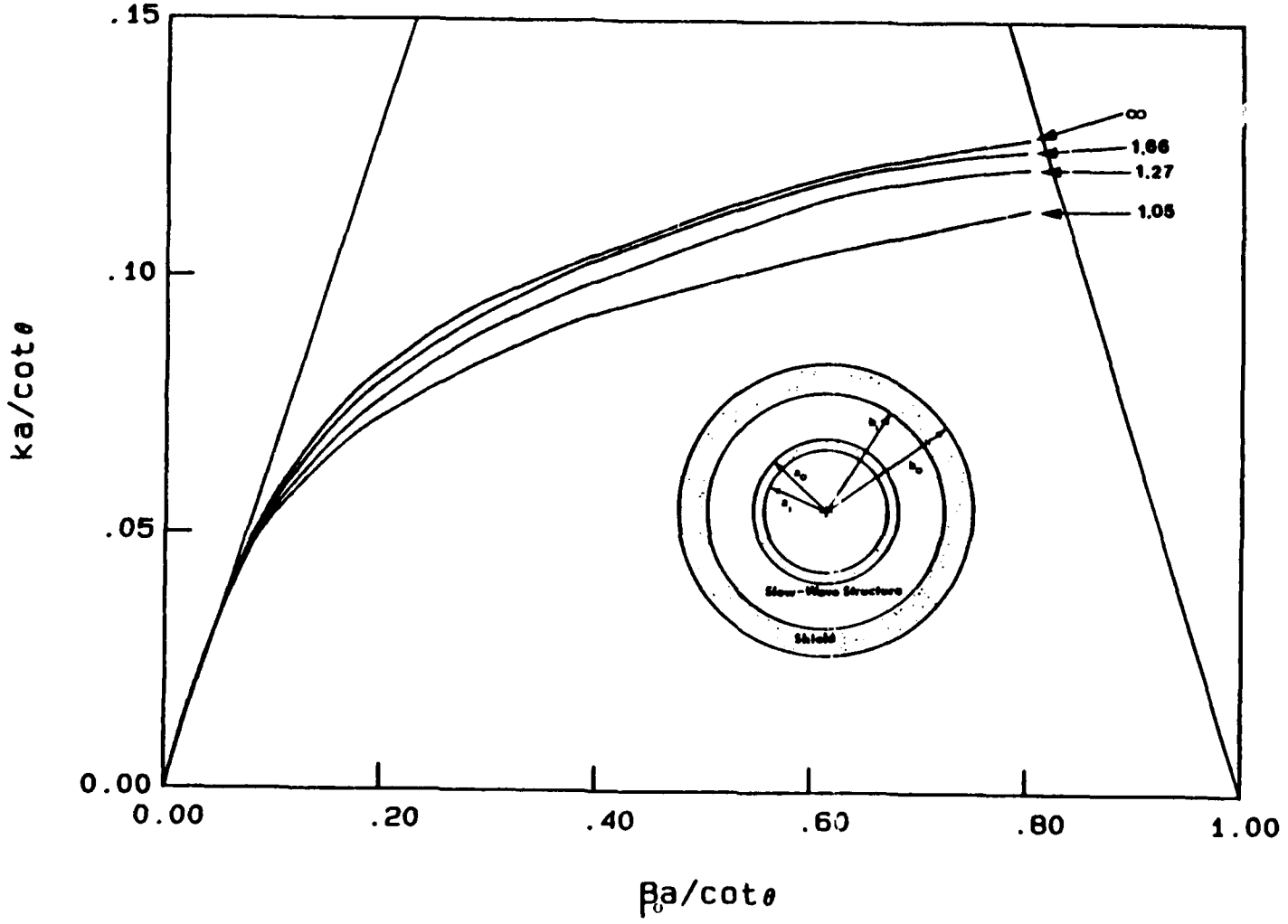

Fig. 3.4. Experimentally derived dispersion characteristics for a contrawound helix (ring-bar variation) of cot θ = 4.4, $\xi = \pi/2$, and a_1/a_o = 0.8 surrounded by a dielectric cylinder at distances of b_1/a_o = 1.05, 1.27, 1.66 and corresponding thicknesses of $(b_o - b_1)/b_1$ = 0.122, 0.132, 0.112. Also shown is the dispersion for the same circuit in free space such that $b_1/a_o = \infty$.

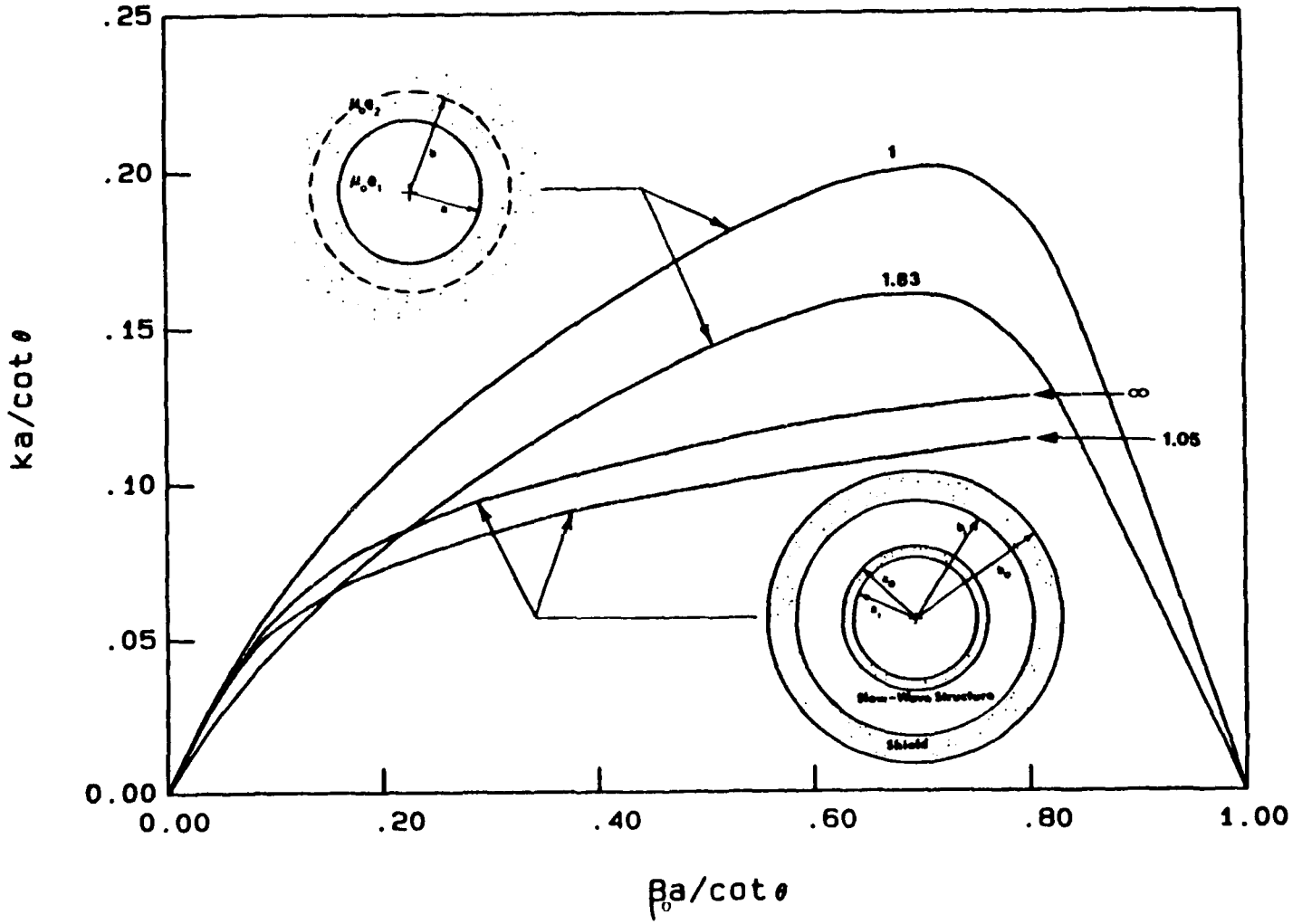

Fig. 3.5. Comparison between theoretically (solid line) and experimentally (dot-dashed line) derived dispersion characteristics showing the effect of dielectric loading. The experimental results are for a contrawound helix (ring-bar variation) of cot θ = 4.4, $\xi = \pi/2$, and a_1/a_0 = 0.8 surrounded by a dielectric cylinder at a distance of b_1/a_0 = 1.05 and with a thickness of $(b_0 - b_1)/b_1$ = 0.122. The theoretical results are for a contrawound helix of cot θ = 4.4, $\xi = \pi/2$, and a_1/a_0 = 1 interposed between two dielectric regions with relative constitutive properties $\varepsilon_2/\varepsilon_1$ = 1.83 and k_2/k_1 = 1.35.

dimensional) volume of

$$\text{vol}_{\text{eff}} = \frac{\pi}{a^2}\left(b^2 - a^2\right) = \pi\left(1.21^2 - 1^2\right)$$

$$\text{vol}_{\text{eff}} = 1.46$$

Comparisons can best be made with the experimental results (Fig. 3.4) for the glass cylinder with dimensions $b_i/a_o = 1.05$ and $(b_o - b_i)/b_i = 0.122$. The ratio b_o/a_o is then 1.178 and the (two dimensional) volume for the cylinder is thus

$$\text{vol}_{\text{gc}} = \frac{\pi}{a_o^2}\left(b_o^2 - b_i^2\right) = \pi\left(1.178^2 - 1.05^2\right)$$

$$\text{vol}_{\text{gc}} = 0.896$$

The relative permittivity of the low loss glass cylinder is assumed to be 3.0, and the equivalent relative permittivity for Region 2 is proportioned as

$$\varepsilon_2 = 3.0\left(\frac{\text{vol}_{\text{gc}}}{\text{vol}_{\text{eff}}}\right) = 3.0\left(\frac{0.896}{1.46}\right)$$

$$\varepsilon_2 = 1.83$$

The theoretical results for $\varepsilon_2 = 1.83$ along with the corresponding experimental results are shown in Fig. 3.5. The deviation between theory and experiment is due to the foreshortened current paths which

result when the two helix tapes are allowed to touch. However, it is clear that the velocity loading is proportionally similar in both cases.

Figures 3.6 and 3.7, like Fig. 3.3, allow $\varepsilon_2/\varepsilon_1$ to vary from 1 to 9, while cot θ is fixed at 5 (Fig. 3.6) and 2.5 (Fig. 3.7). In all three figures, the percentage of dielectric loading relative to no loading is approximately the same.

In Figs. 3.8 and 3.9, $\varepsilon_2/\varepsilon_1$ is fixed at 1.5 and 9, respectively. The overall shape of the dispersion curves changes as cot θ is increased from 2.5 to 10.

3.2.2 Metal Loading

The effects of metal loading are considerably different than the effects of dielectric loading. No longer are there the forbidden regions associated with the open structure. And the general shape of the ω-β diagram changes as the effects of metal loading become stronger.

The dispersion characteristics for a contrawound helix (ξ = 1, cot θ = 10) symmetrically oriented inside a cylindrical conducting sheath are presented in Fig. 3.10. The relative constitutive properties are $k_1/k_2 = 1$, $\mu_1/\mu_2 = 1$, and $\varepsilon_2/\varepsilon_1 = 1$. By varying b/a, the relative distance between the circuit and the cylinder, the aspects of metal loading mentioned above are clearly seen.

The dashed curve, labeled 1, is the dispersion for the nonshielded contrawound helix. The ends of this curve couple into the so-called "velocity of light lines," as this is an open structure. Curve 1A shows the effect of a conducting shield placed radially at a distance of b/a = 2. Instead of coupling into the velocity of light line, curve 1A

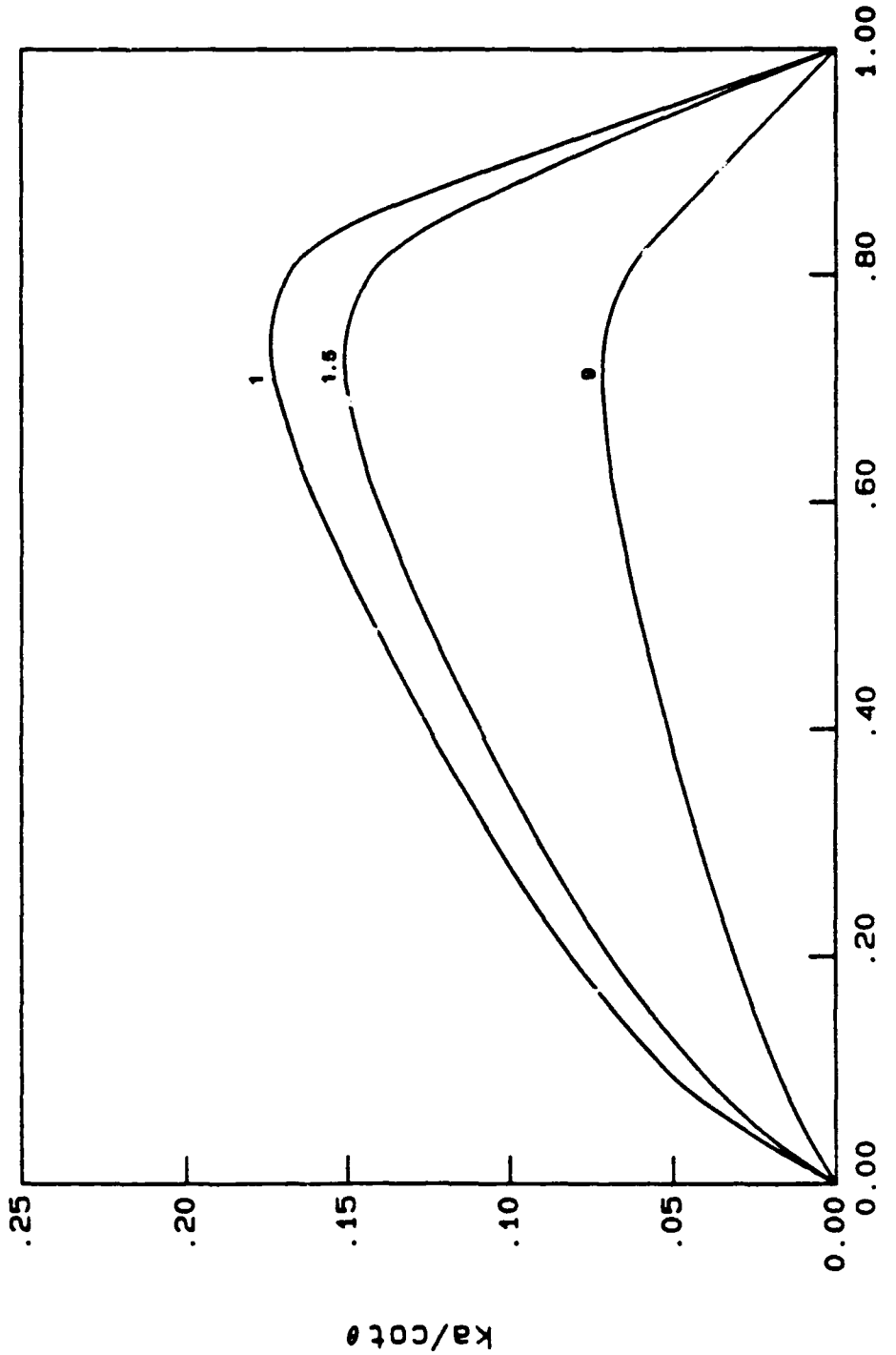

Fig. 3.6. Theoretical dispersion characteristics for a contrawound helix of cot θ = 5 and ξ = 1, interposed between two dielectric regions, showing the effect of dielectric loading: $\varepsilon_2/\varepsilon_1$ = 1, 1.5, 9 and k_2/k_1 = 1, 1.225, 3, correspondingly.

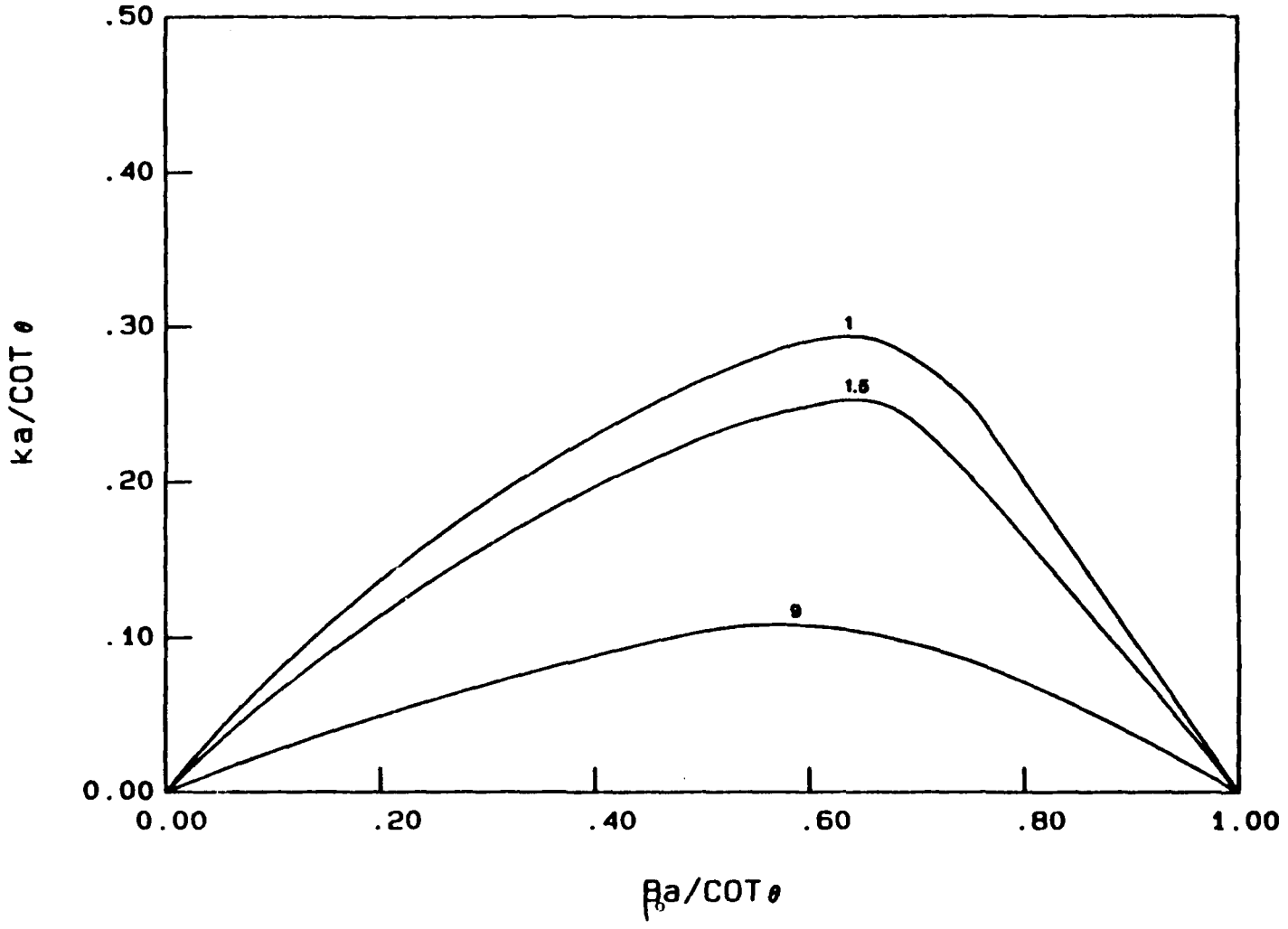

Fig. 3.7. Theoretical dispersion characteristics for a contrawound helix of cot θ = 2.5 and ξ = 1, interposed between two dielectric regions, showing the effect of dielectric loading: $\varepsilon_2/\varepsilon_1$ = 1, 1.5, 9 and k_2/k_1 = 1, 1.225, 3, correspondingly.

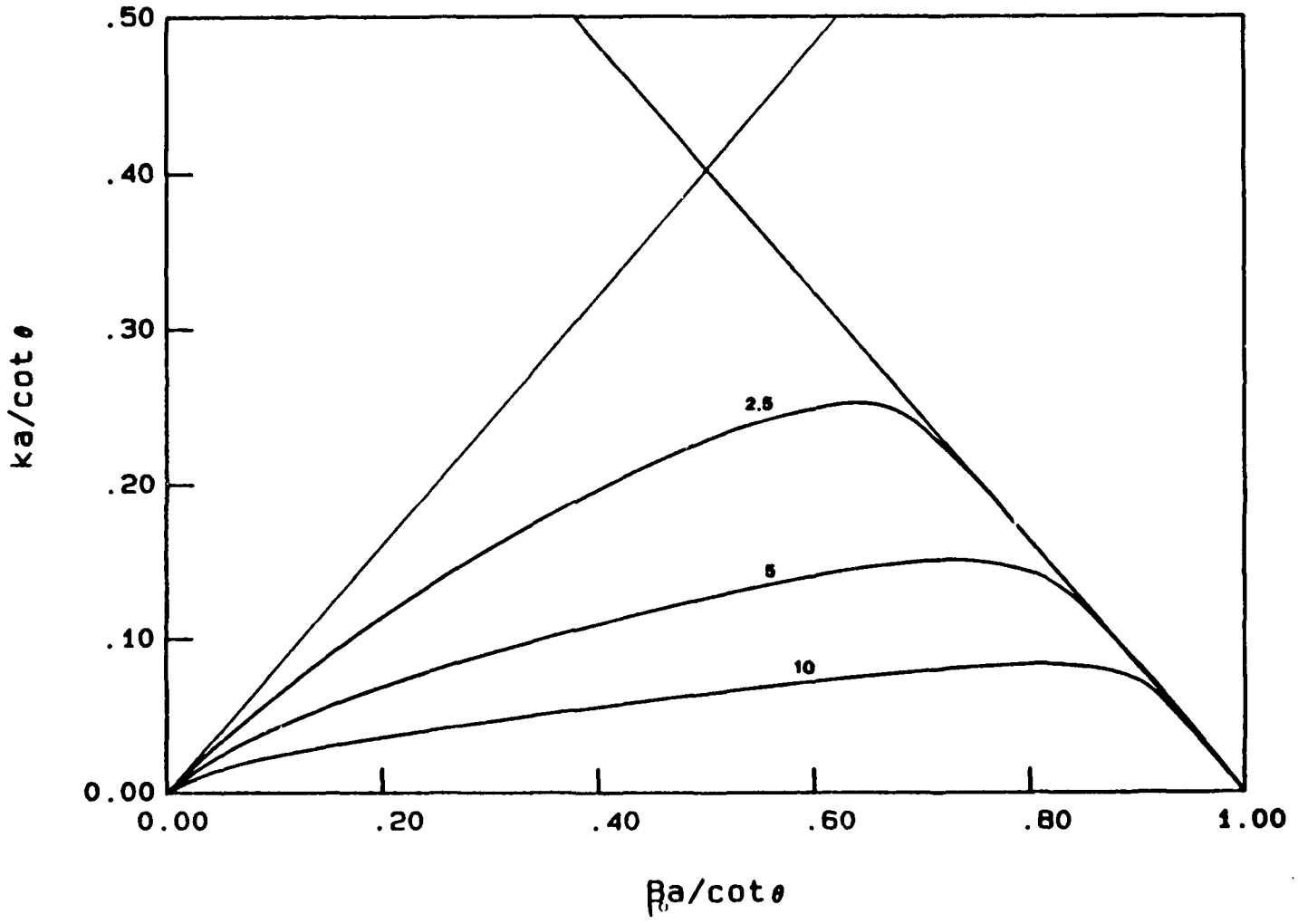

Fig. 3.8. Theoretical dispersion characteristics for a contrawound helix of $\xi = 1$, interposed between two dielectric regions with relative constitutive properties of $\varepsilon_2/\varepsilon_1 = 1.5$ and $k_2/k_1 = 1.225$, showing the effect of varying cot θ: cot θ = 2.5, 5, 10.

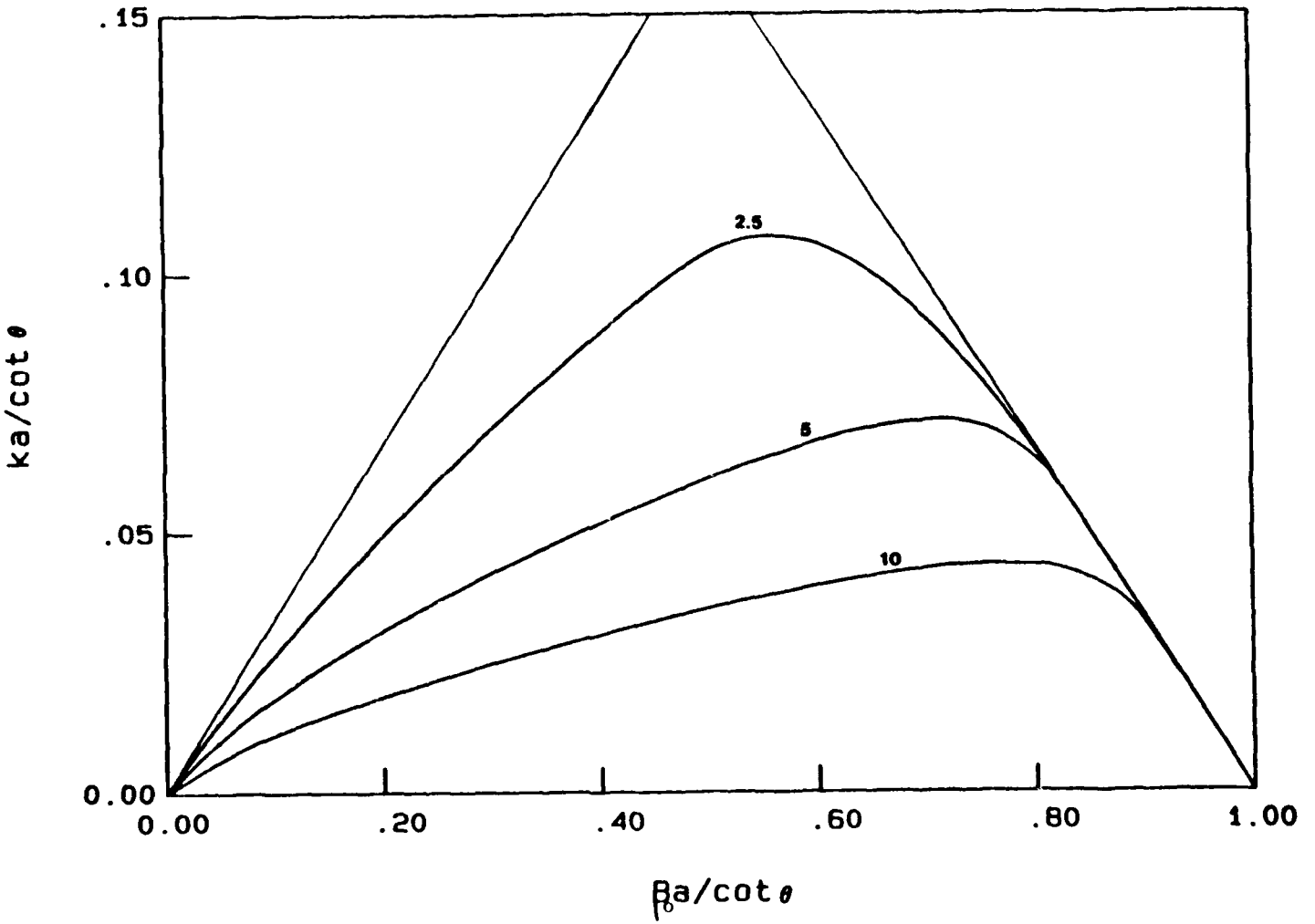

Fig. 3.9. Theoretical dispersion characteristics for a contrawound helix of $\xi = 1$, interposed between two dielectric regions with relative constitutive properties of $\epsilon_2/\epsilon_1 = 9$ and $k_2/k_1 = 3$, showing the effect of varying cot θ: cot θ = 2.5, 5, 10.

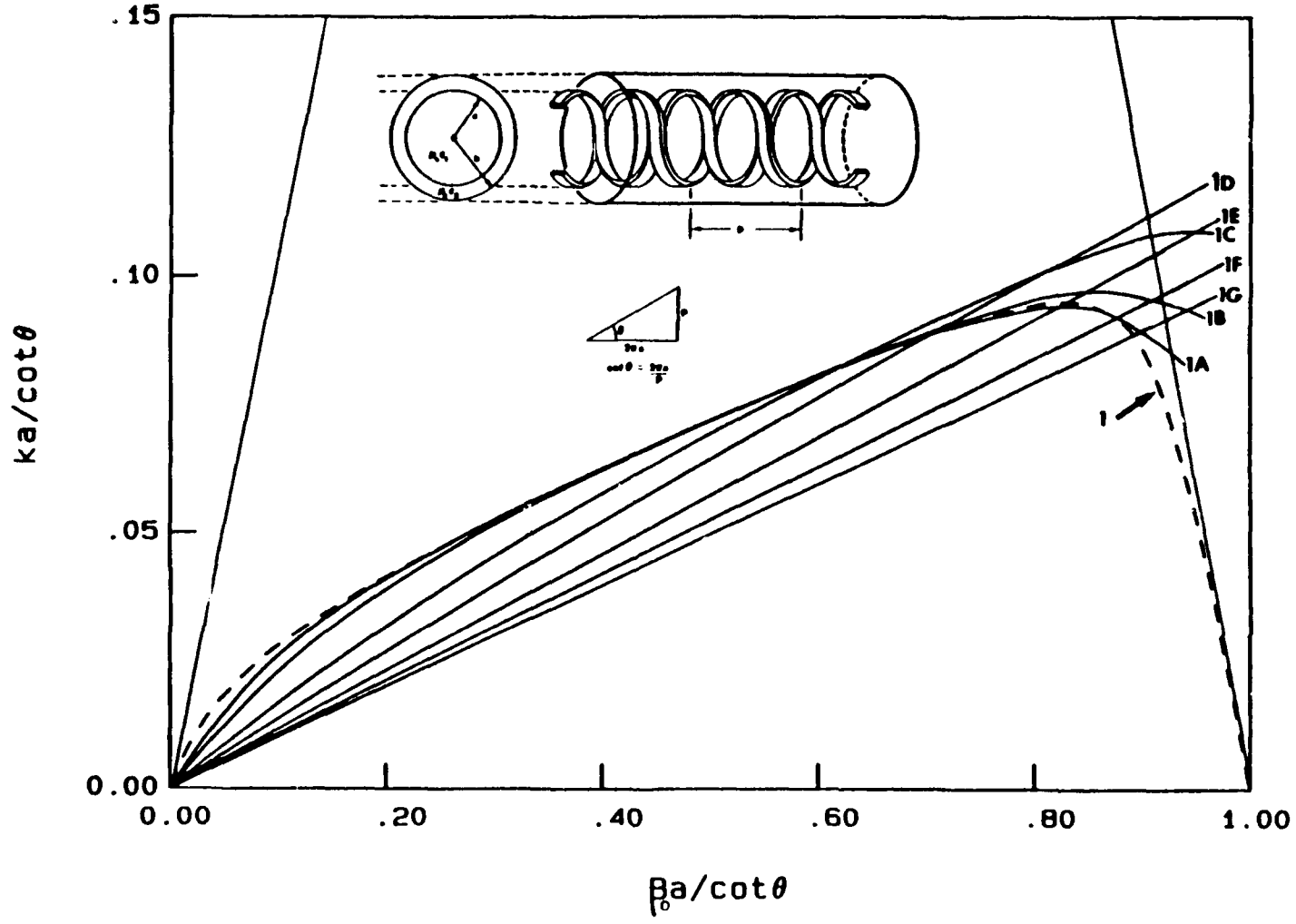

Fig. 3.10. Theoretical dispersion characteristics for a contrawound helix of cot θ = 10 and ξ = 1, symmetrically oriented inside a conducting cylinder, showing the effect of varying b/a. Dashed curve 1: b/a = ∞ (free space); curve 1A: b/a = 2.0; curve 1B: b/a = 1.5; curve 1C: b/a = 1.15; curve 1D: b/a = 1.05; curve 1E: b/a = 1.001; curve 1F: b/a = 1.0001; curve 1G: b/a = 1. The relative constitutive properties are $\varepsilon_2/\varepsilon_1$ and $k_2/k_1 = 1$.

deviates from the nonshielded case at approximately $\beta_o a/\cot\theta = 0.84$ and couples into the coaxial TE_{11} mode. This coaxial mode is formed by the contrawound helix as the inner conductor, and the outer cylinder as the outer conductor. As the outer cylinder is brought closer to the circuit, the cutoff for the coaxial TE_{11} mode moves up in frequency. Consequently,coupling between the fundamental component of the space harmonics and the coaxial TE_{11} mode occurs at higher values of ka (curves 1B and 1C). A point is reached where the shield is close enough to the contrawound helix that coupling no longer occurs -- the TE_{11} mode has moved out of range (curve 1D).

As b/a continues to approach 1, more of the E-field between the circuit and the cylinder is terminated on the cylinder. By this mechanism, the field shape for the traveling wave remains unchanged over a wider range of frequency, thereby reducing the dispersion (curves 1E and 1F). For $b/a = 1$, curve 1G, all of the E-field terminates on the cylinder, resulting in two dispersionless helically traveling waves -- one right handed, the other left handed -- each propagating axially at $p/2\pi a$ times the velocity of light. Whether or not this situation is physically possible is discussed in Chapter Four.

As a comparison, the dispersion for the single helix in free space (nonshielded) is plotted in Fig. 3.11, which repeats Fig. 3.10 with this addition. The dot-dash single helix curve (labeled 2) parallels closely curve 1G. The deviation between the two is shown on an enlarged scale in Figs. 3.12 and 3.13.

The effects of metal loading on the single helix with the same parameters as above are investigated in Fig. 3.14. Like the contrawound

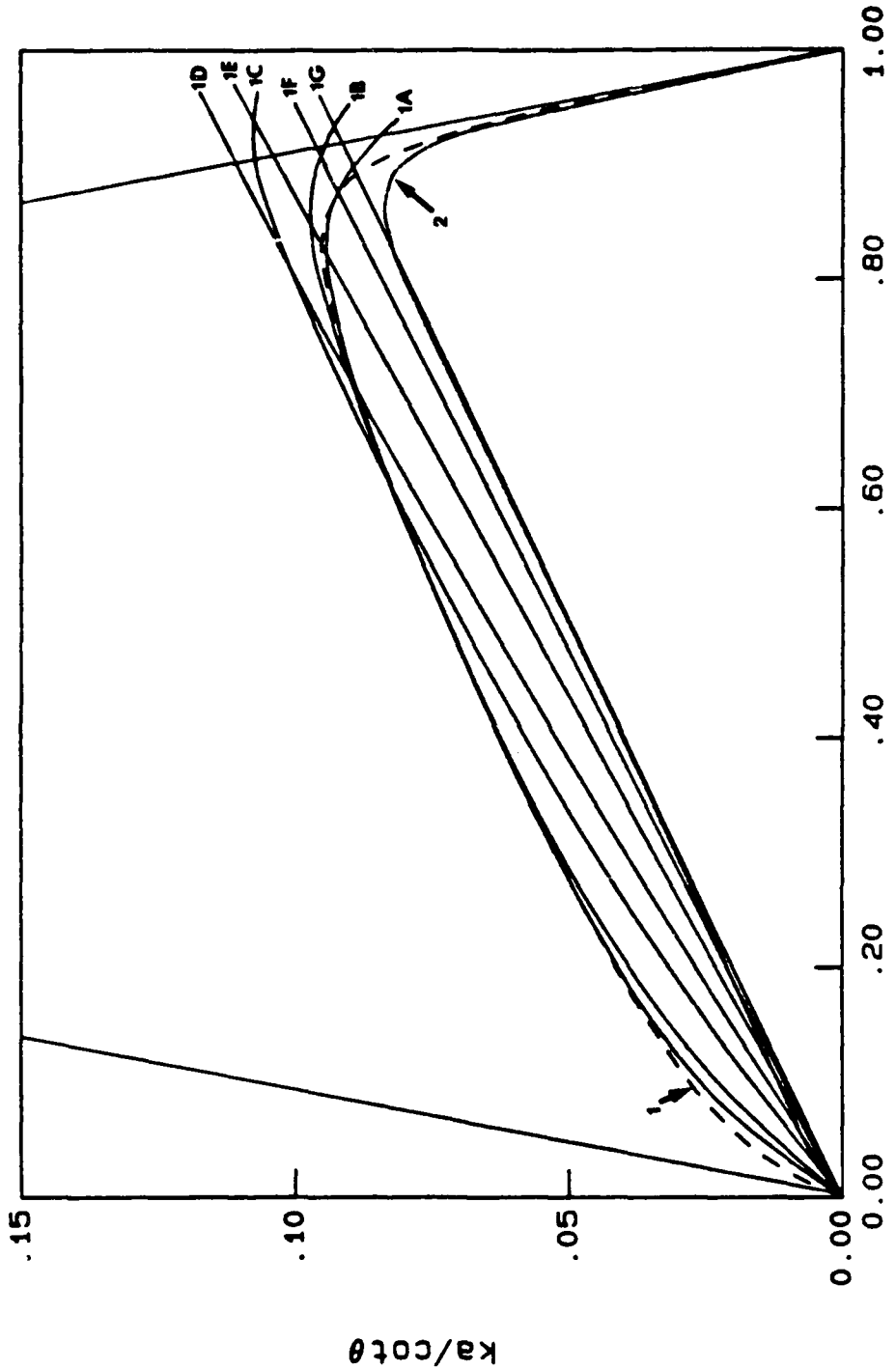

Fig. 3.11. Comparison of Fig. 3.10 with the dispersion for a single helix (cot θ = 10, ξ = 1) in free space (dot-dashed curve 2). Refer to Fig. 3.10 for details.

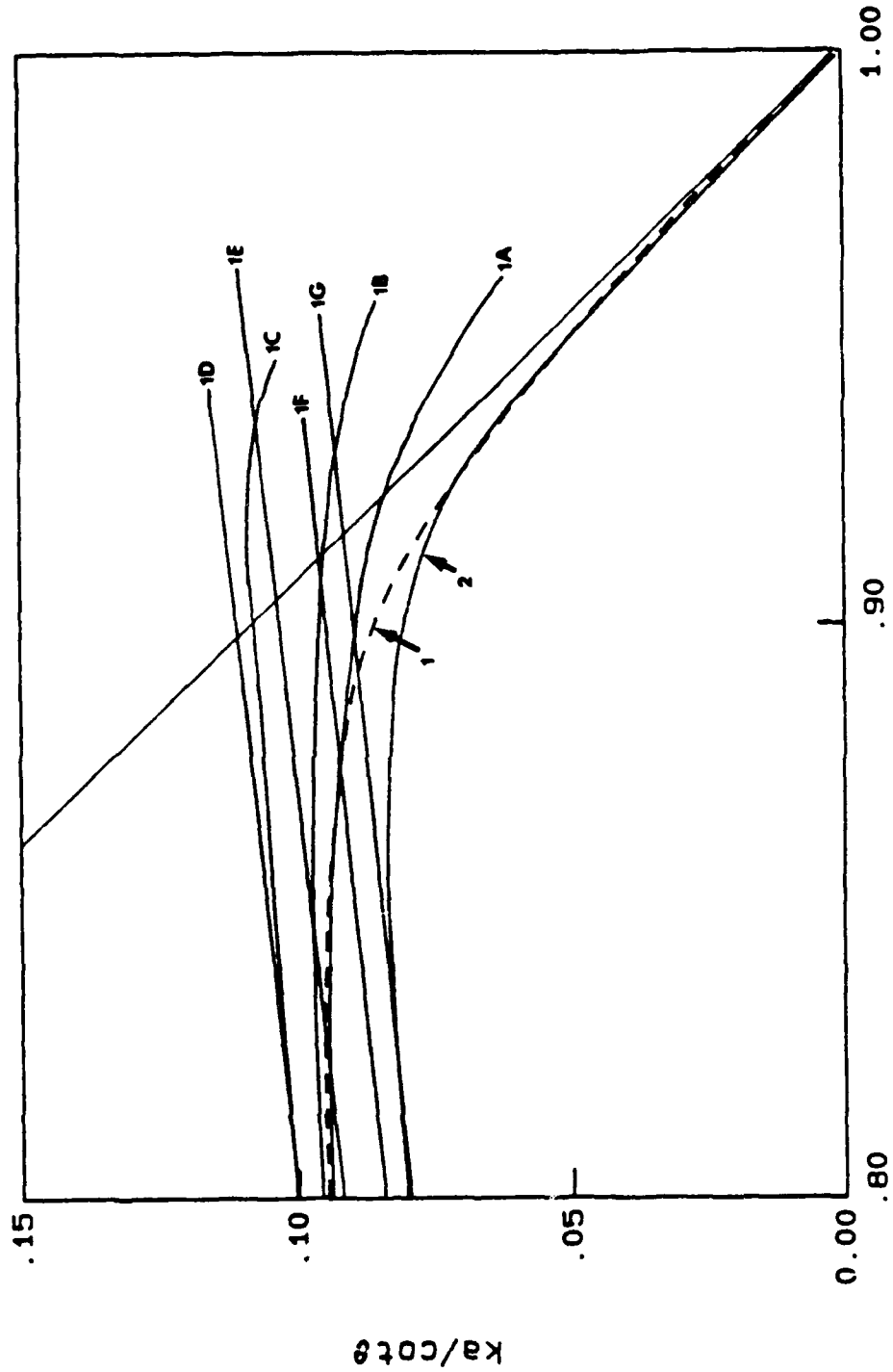

Fig. 3.12. Enlarged portion of Fig. 3.11. Refer to Figs. 3.10 and 3.11 for details.

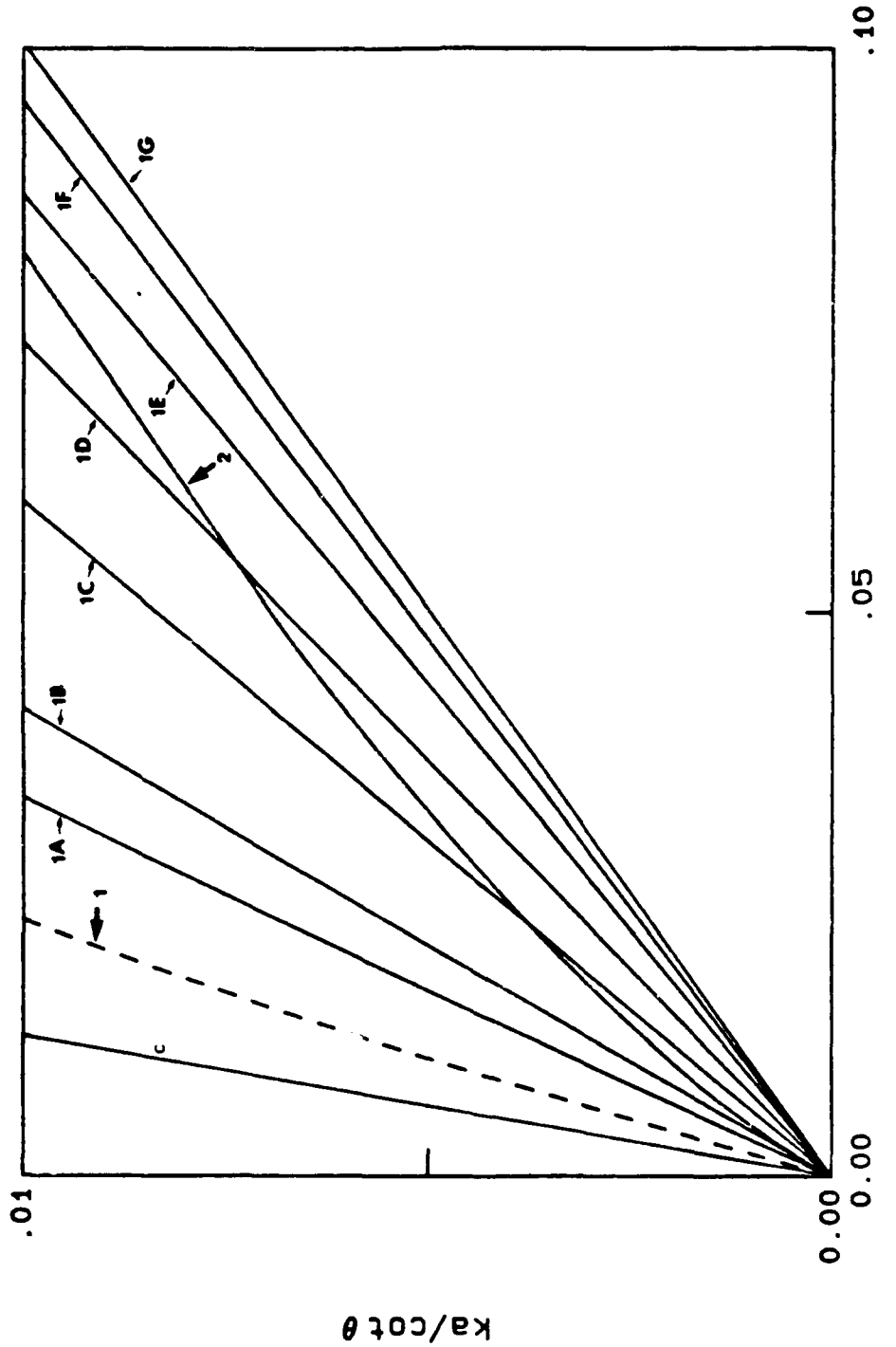

Fig. 3.13. Enlarged portion of Fig. 3.11. Refer to Figs. 3.10 and 3.11 for details.

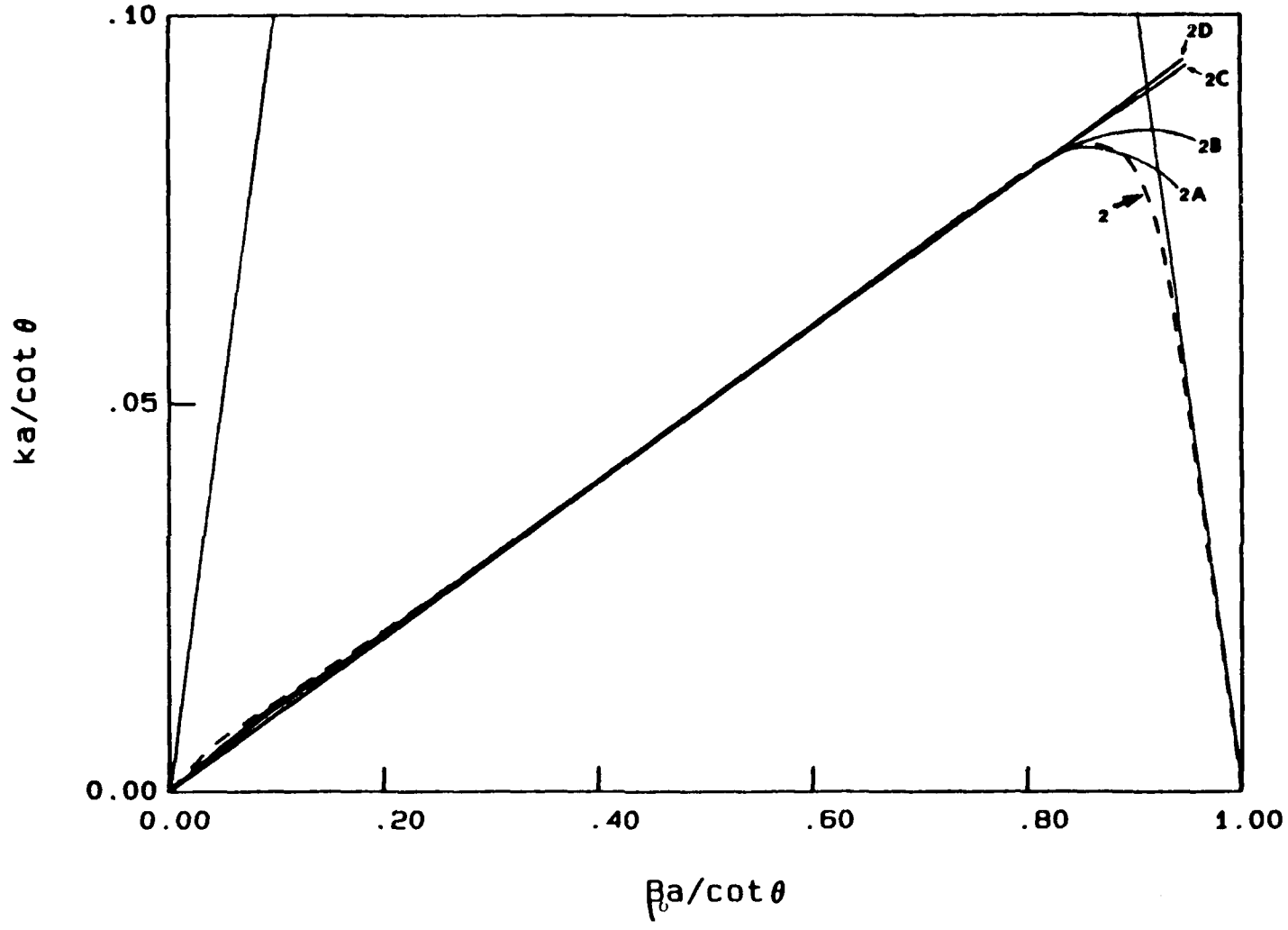

Fig. 3.14. Theoretical dispersion characteristics for a single helix of cot θ = 10 and ξ = 1, symmetrically oriented inside a conducting cylinder, showing the effect of varying b/a. Dashed curve 2: b/a = ∞ (free space); curve 2A: b/a = 2; curve 2B: b/a = 1.5; curve 2C: b/a = 1.1; curve 2D: b/a = 1. The relative constitutive properties are $\varepsilon_2/\varepsilon_1 = 1$ and $k_2/k_1 = 1$.

helix, coupling with the coaxial TE_{11} mode is reduced as b/a approaches 1. And like before, the ideal case of no dispersion is achieved when b/a = 1 (curve 2D). Figure 3.15 shows how the tendency to couple to the velocity of light line is reduced as the distance between the shield and the helix becomes smaller.

The effects of metal loading on a contrawound helix of cot θ = 2.5 are presented in Figs. 3.16 and 3.17.

Experimental analysis performed by Birdsall and Everhart [4] on a ring-bar circuit inside a metal cylinder lends validity to the previous theoretical results. Experimentally derived dispersion curves for two different size cylinders, b/a = 1.33 and b/a = 2.16, are reproduced in Fig. 3.18. Also plotted are the theoretical predictions for the same dimensions. It is clear that as b/a approaches 1, the ω-β curves become less dispersive. Observe also that for values of b/a > 2, the effects of metal loading are minimal. Note again that the deviation between theory and experiment is a consequence of foreshortening the current paths. For the ring-bar geometry, this is equivalent to a large connecting-bar width.

3.2.3 Simultaneous Metal and Dielectric Loading

How the dispersion is affected by the simultaneous loading resulting from a dielectric region interposed between the slow-wave structure and a metal shield can be qualitatively determined by simply superposing the individual effects of dielectric loading and metal loading. However, consideration of accuracy requires the use of the quantitative analysis employed thus far.

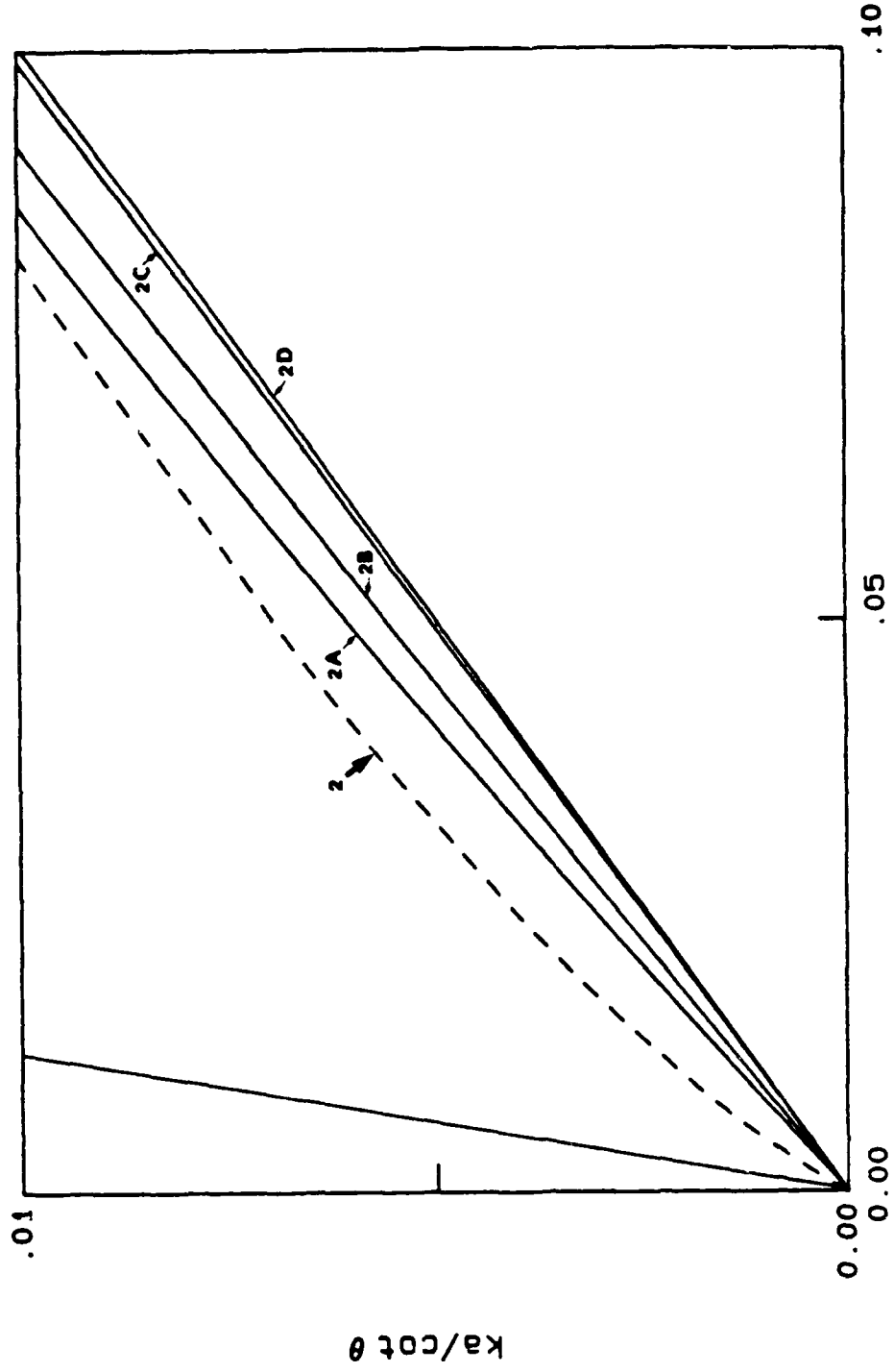

Fig. 3.15. Enlarged portion of Fig. 3.14. Refer to Fig. 3.14 for details.

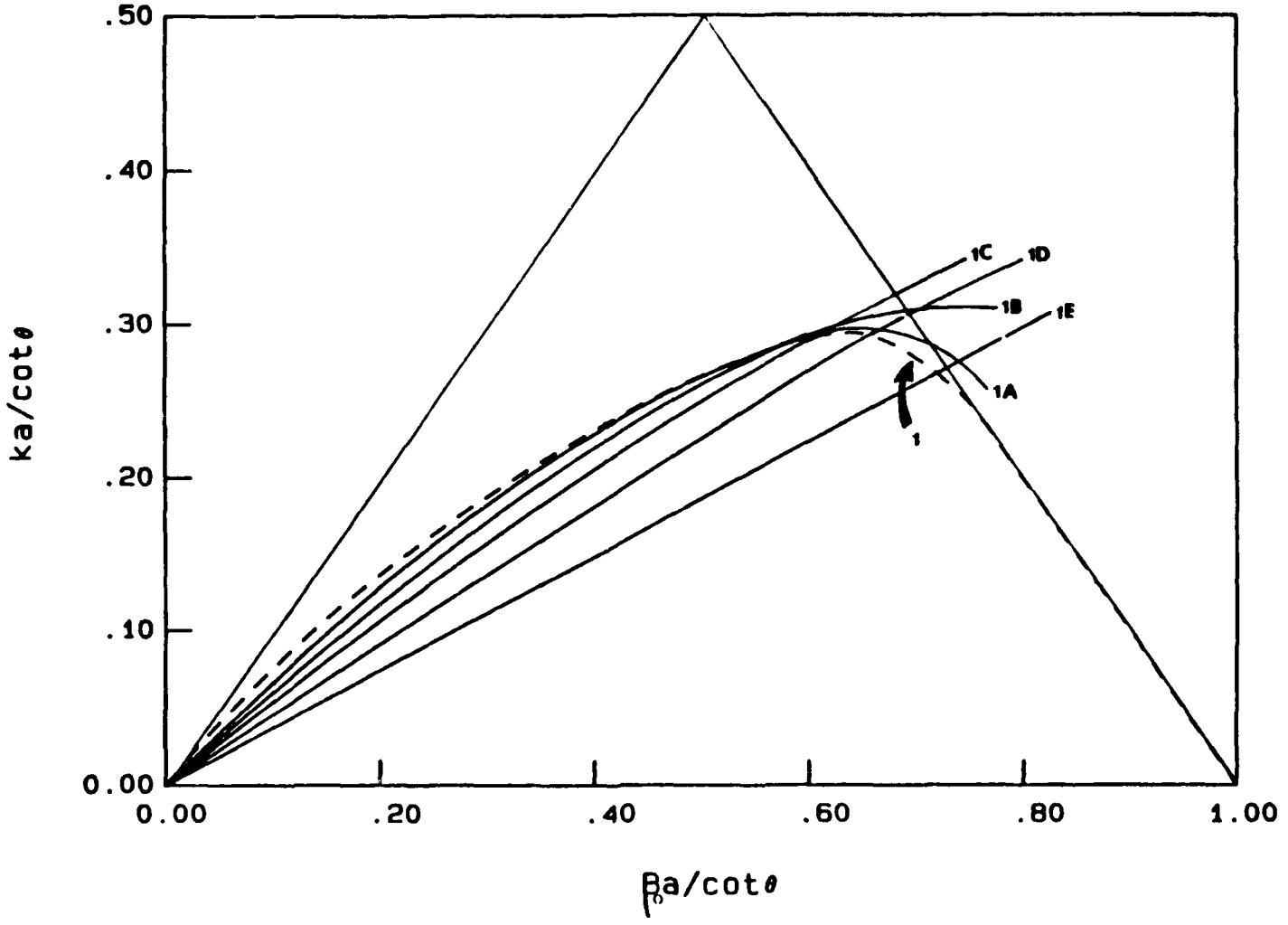

Fig. 3.16. Theoretical dispersion characteristics for a contrawound helix of cot θ= 2.5 and ξ = 1, symmetrically oriented inside a conducting cylinder, showing the effect of varying b/a. Dashed curve 1: b/a = ∞ (free space); curve 1A: b/a = 2; curve 1B: b/a = 1.5; curve 1C: b/a = 1.15; curve 1D: b/a = 1.1; curve 1E: b/a = 1. The relative constitutive properties are $\varepsilon_2/\varepsilon_1 = 1$ and $k_2/k_1 = 1$.

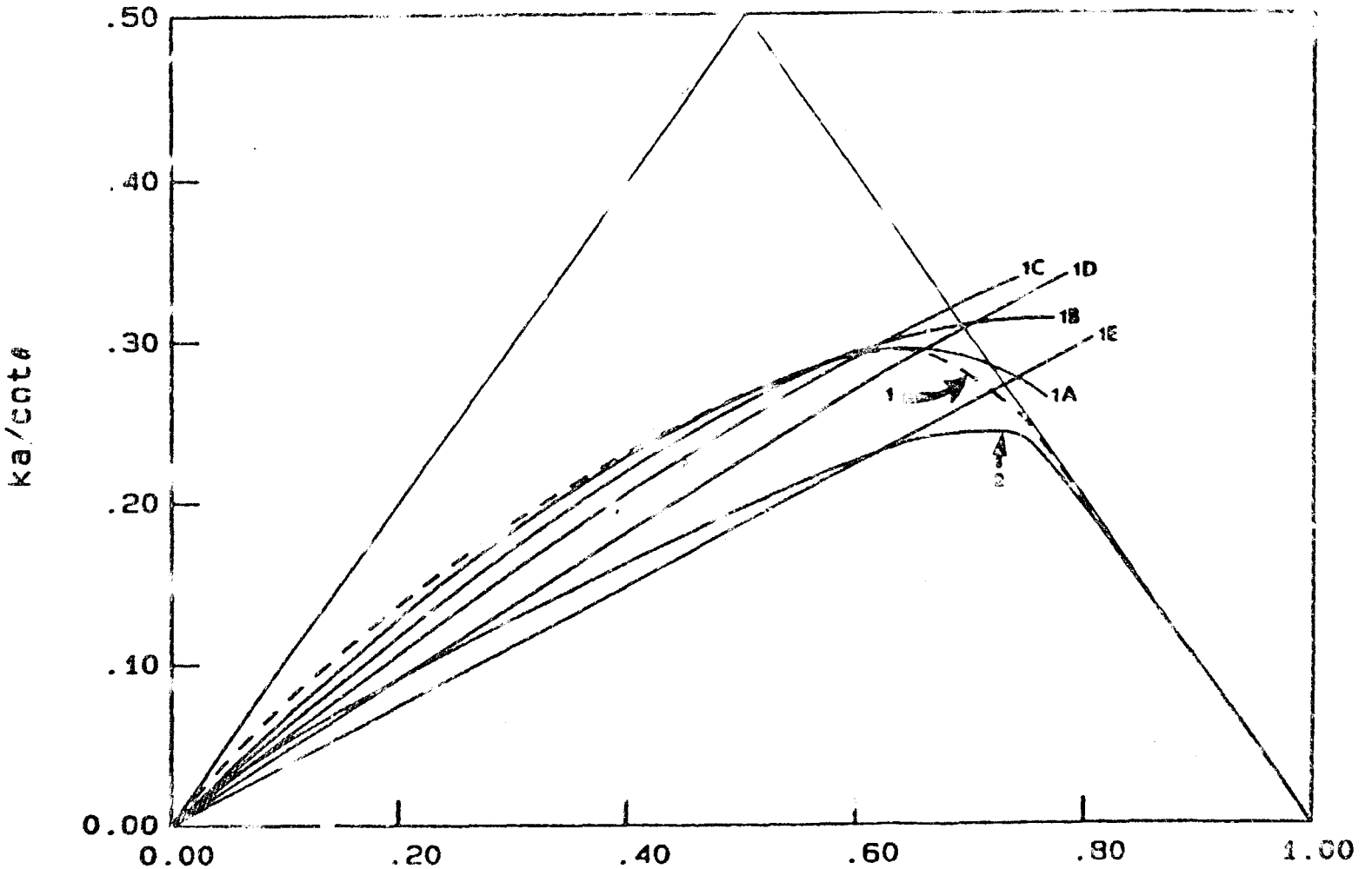

Fig. 3.17. Comparison of Fig. 3.16 with the dispersion for a single helix (cot θ = 2.5, ξ = 1) in free space (dot-dashed curve a). Refer to Fig. 3.16 for details.

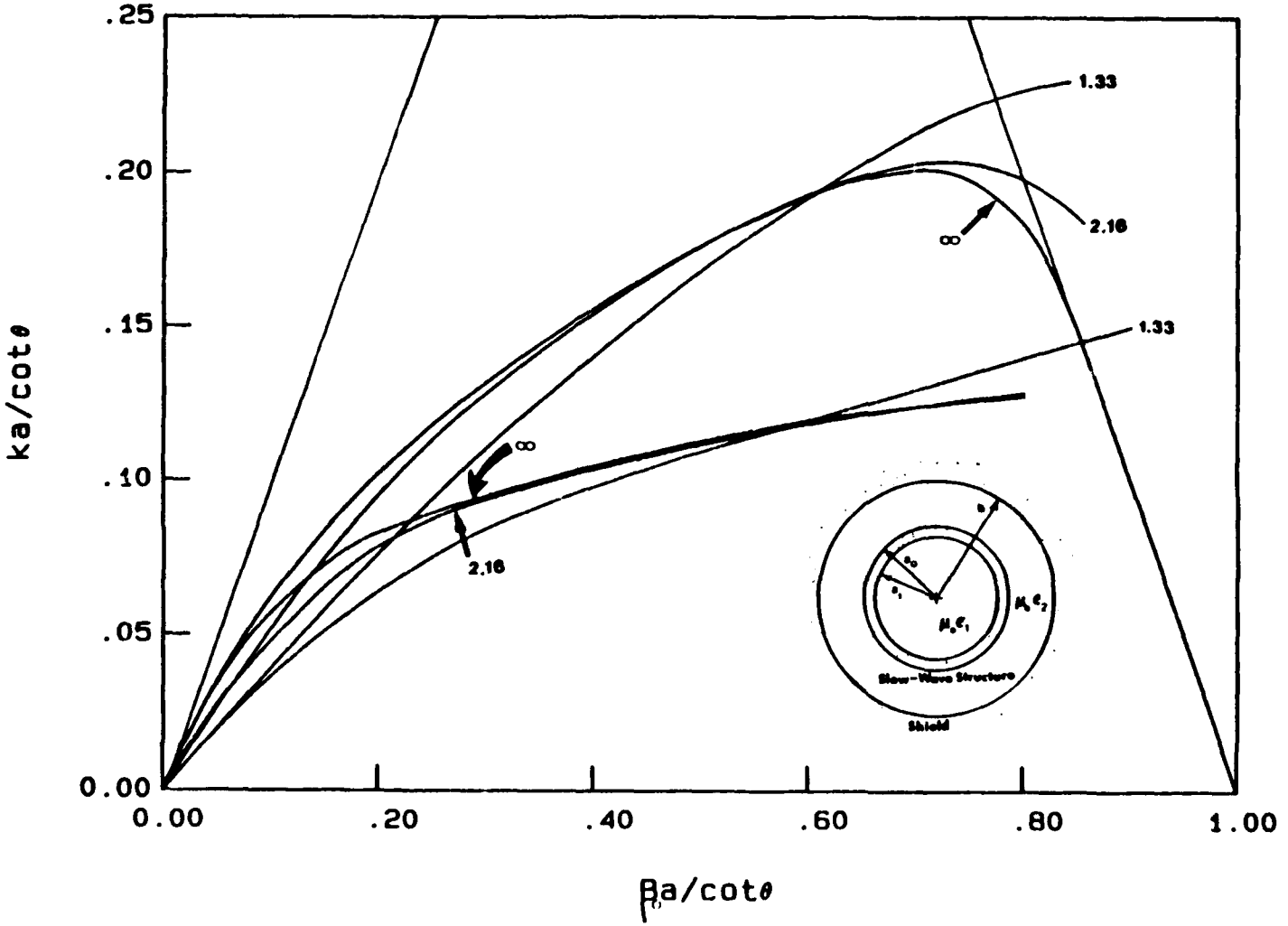

Fig. 3.18. Comparison between theoretically (solid line) and experimentally (dot-dashed line) derived dispersion characteristics for a contrawound helix of cot θ = 4.4 and ξ = $\pi/2$, symmetrically oriented inside a conducting cylinder, showing the effect of metal loading: $b/a_o = \infty$, 1.33, 2.16. The relative constitutive properties $\varepsilon_2/\varepsilon_1 = 1$ and $k_2/k_1 = 1$. In the experiment $a_i/a_o = 0.8$, while $a_i/a_o = 1$ is assumed in the theory.

In Figs. 3.19 and 3.20, the relative constitutive properties are $k_2/k_1 = 1.225$, $\mu_2/\mu_1 = 1$, and $\varepsilon_2/\varepsilon_1 = 1.5$. The ω-β curves for various values of b/a are plotted for the contrawound helix in Fig. 3.19, and for the single helix in Fig. 3.20. In each case, the ω-β curves become ideally nondispersive as b/a approaches 1. Concurrently, the effects of dielectric loading are reduced as the size of Region 2 is decreased. This behavior becomes more pronounced as $\varepsilon_2/\varepsilon_1$ becomes larger.

In Fig. 3.21, the relative permittivity is increased such that $\varepsilon_2/\varepsilon_1 = 9$ and $k_2/k_1 = 3$. The dispersion curves are again plotted for varying values of b/a. These plots are repeated in Fig. 3.22, with the ω-β curves for a single helix ($\varepsilon_2/\varepsilon_1 = 9$ and $\varepsilon_2/\varepsilon_1 = 1$) added for reference.

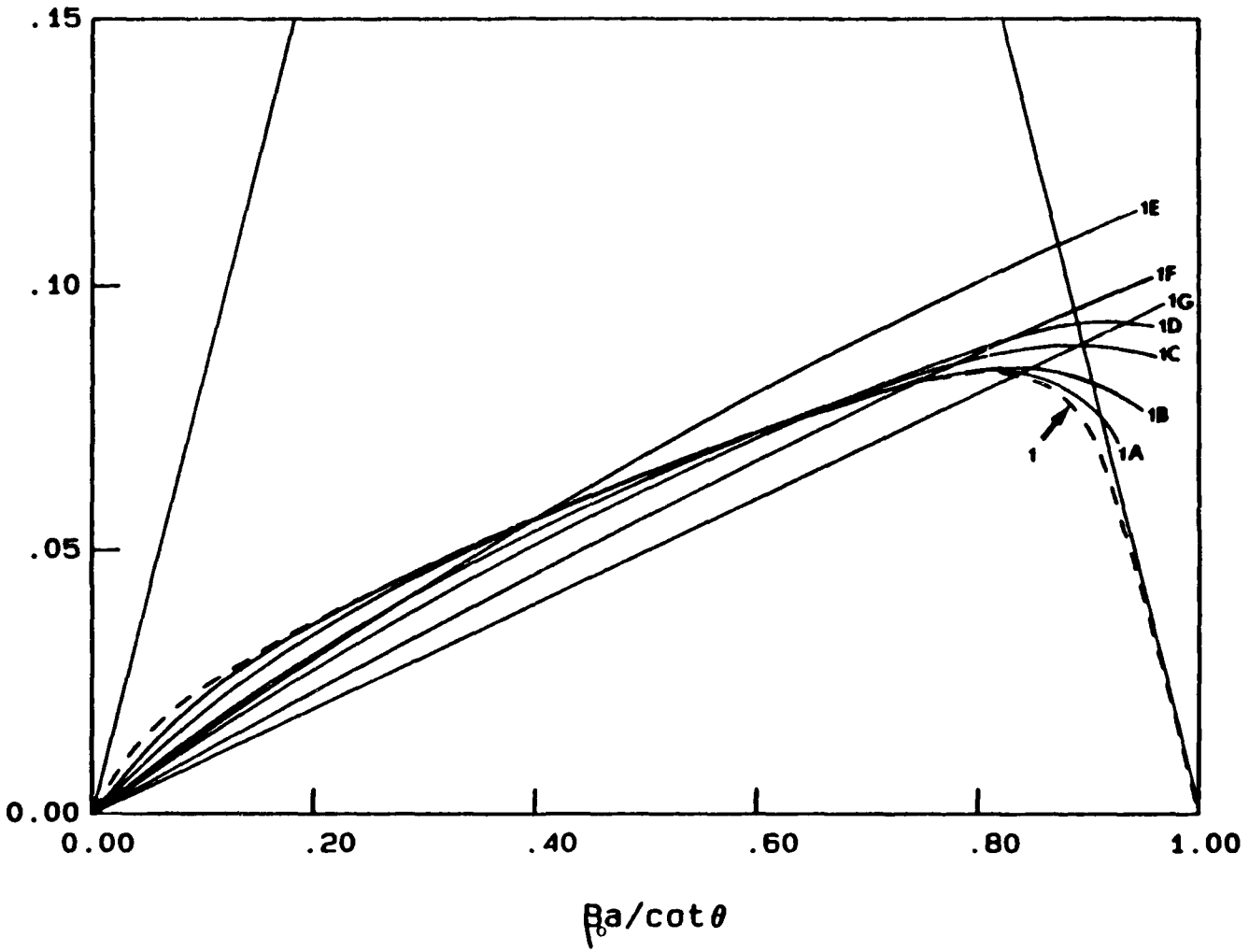

Fig. 3.19. Theoretical dispersion characteristics for a contrawound helix of cot θ = 10 and ξ = 1, interposed between two dielectric regions symmetrially oriented inside a conducting cylinder, showing the effect of varying b/a. The relative constitutive properties are $\varepsilon_2/\varepsilon_1 = 1.5$ and $k_2/k_1 = 1.225$. Dashed curve 1: b/a = ∞; curve 1A: b/a = 2; curve 1B: b/a = 1.5; curve 1C: b/a = 1.25; curve 1D: b/a = 1.15; curve 1E: b/a = 1.1; curve 1F: b/a = 1.05; curve 1G: b/a = 1.

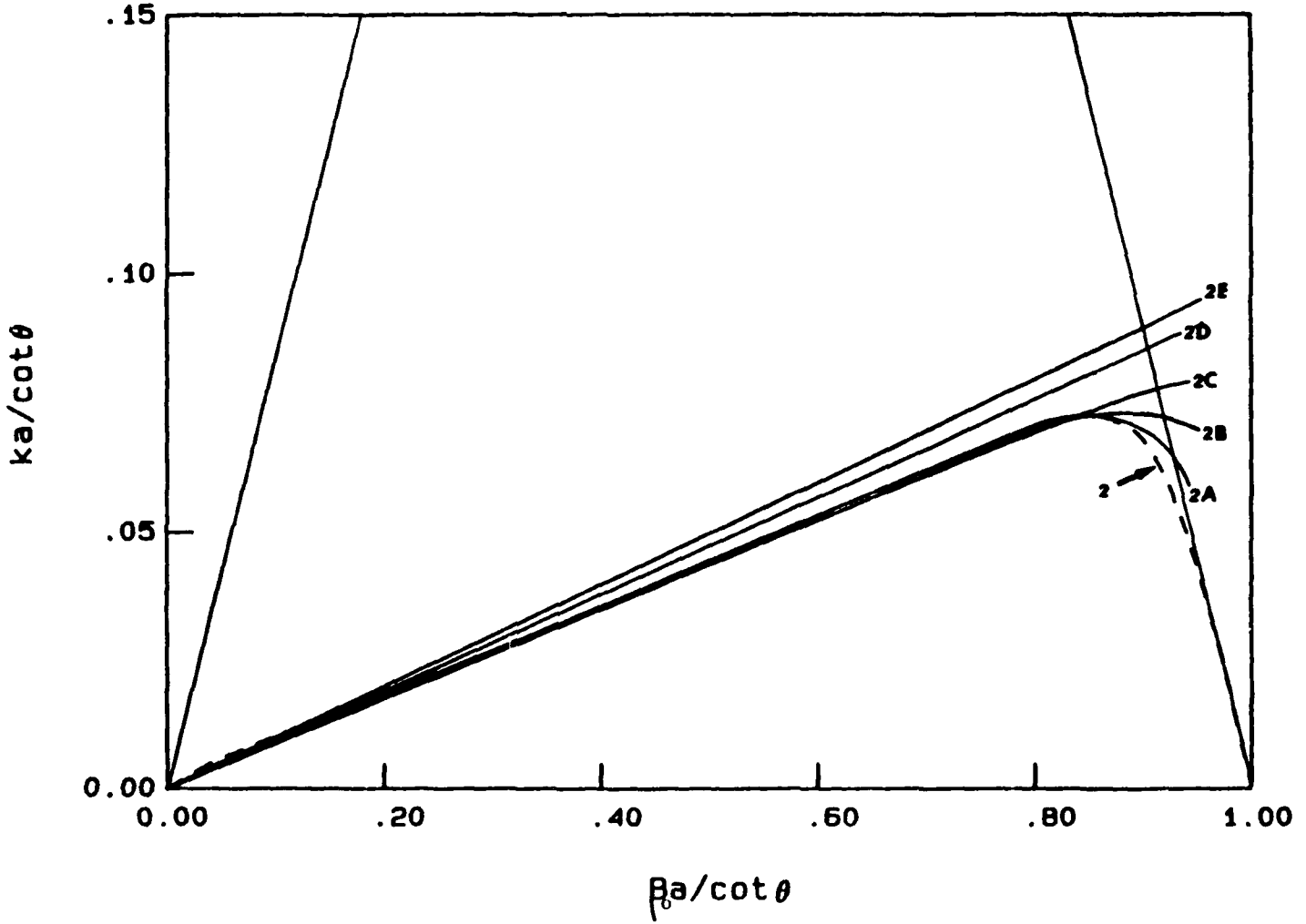

Fig. 3.20. Theoretical dispersion characteristics for a single helix of cot θ = 10 and ξ = 1, interposed between two dielectric regions symmetrically oriented inside a conducting cylinder, showing the effects of varying b/a. The relative constitutive properties are $\varepsilon_2/\varepsilon_1 = 1.5$ and $k_2/k_1 = 1.225$. Dashed curve 2: b/a = ∞; curve 2A: b/a = 2; curve 2B: b/a = 1.5; curve 2C: b/a = 1.1; curve 2D: b/a = 1.00008; curve 2E: b/a = 1.

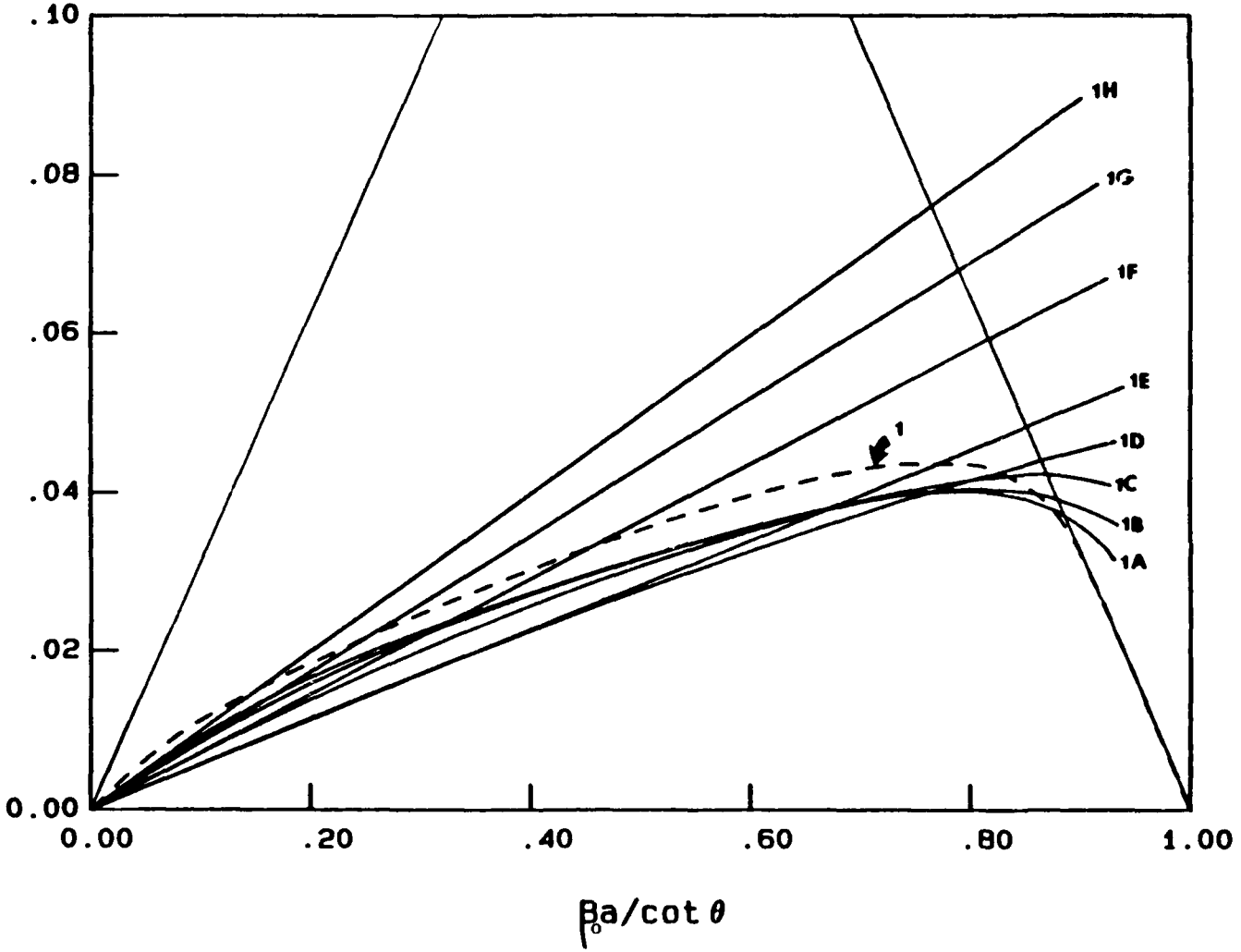

Fig. 3.21. Theoretical dispersion characteristics for a contrawound helix of cot θ = 10 and ξ = 1, interposed between two dielectric regions symmetrically oriented inside a conducting cylinder, showing the effect of varying b/a. The relative constitutive properties are $\varepsilon_2/\varepsilon_1 = 9$ and $k_2/k_1 = 3$. Dashed curve 1: b/a = ∞; curve 1A: b/a = 1.75; curve 1B: b/a = 1.5; curve 1C: b/a = 1.25; curve 1D: b/a = 1.1; curve 1E: b/a = 1.001; curve 1F: b/a = 1.0003; curve 1G: b/a = 1.0001; curve 1H: b/a = 1.

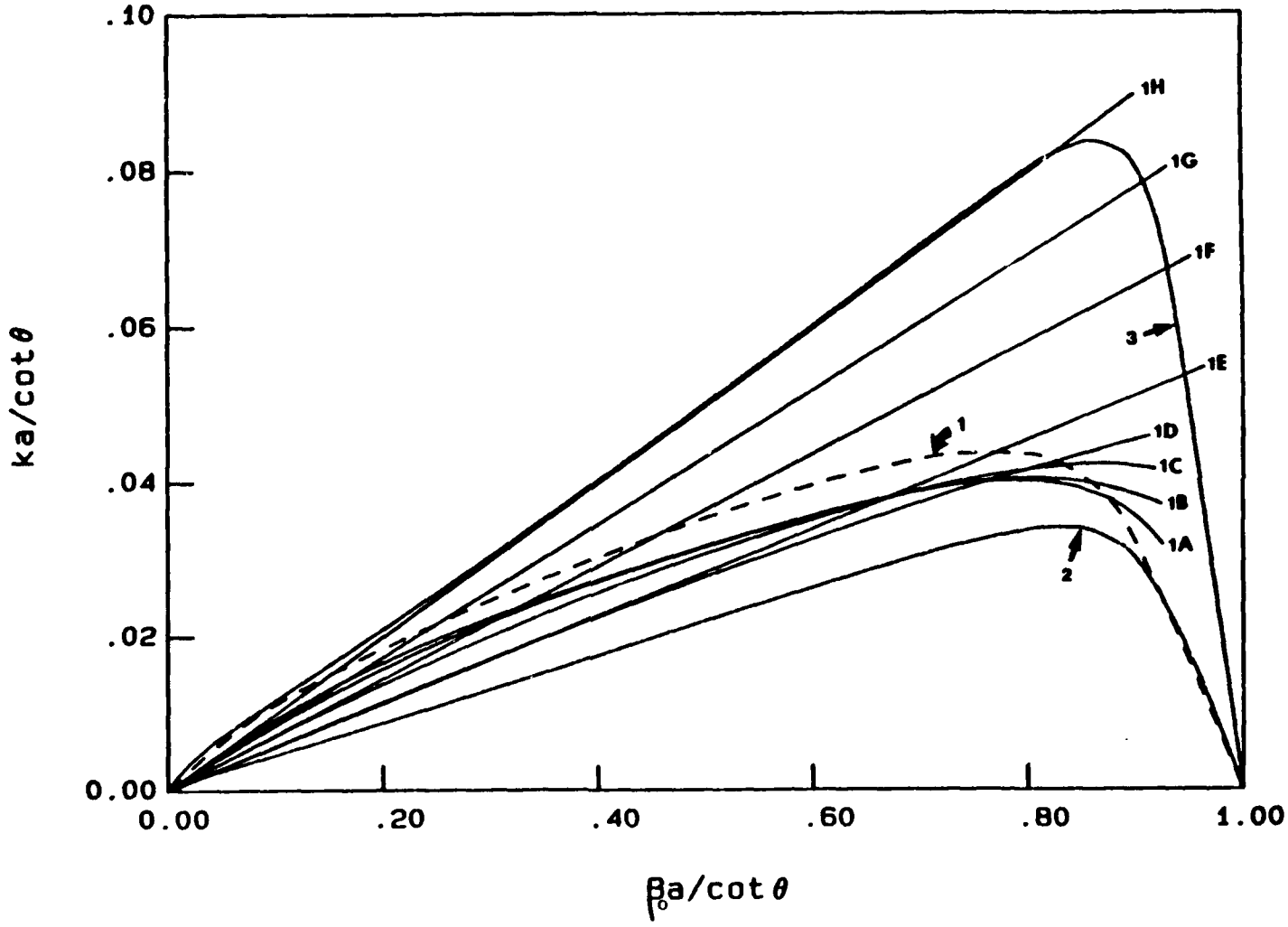

Fig. 3.22. Comparison of Fig. 3.21 with (1) the dispersion for a single helix (dot-dashed curve 2) of cot θ = 10 and ξ = 1 interposed between the two dielectric regions of Fig. 3.21, and (2) the dispersion for a single helix of cot θ = 10 and ξ = 1 in free space (dot-dashed curve 3). In both cases, b/a = ∞. Refer to Fig. 3.21 for other details.

IV. SUMMARY AND CONCLUSIONS

The formulation of Chodorow and Chu [2] for the contrawound helix is expanded to include the effects of dielectric and metal loading. Since wave velocity is inversely proportional to the square root of the dielectric constant whenever a dielectric material is added in the region surrounding the circuit, the wave velocity is decreased. In general, while dielectric loading reduces both the phase velocity and the group velocity, the overall shape of the ω-β diagram remains unchanged. However, this is not the case for metal loading.

As the degree of metal loading is increased, the dispersion is effectively reduced for both the single helix as well as the contrawound helix. The mechanism whereby this is accomplished is provided for by the outer conducting cylinder. This cylinder allows the propagating mode to retain in detail its particular shape by providing an alternative termination for the electric fields. Consequently, the field pattern for this mode tends to change only in scale as the frequency is varied. This effect is increased as the cylinder is brought closer to the circuit, thereby reducing the dispersion. Unfortunately, the reduced dispersion is offset by an accompanying decrease in the circuit interaction impedance. An inductive coupling of the helix currents to the metal cylinder and the flow of current in the circumferential direction in the cylinder results in an increase of the excess stored energy in E_r between the circuit and the cylinder, energy which is useless for interaction with electron beams.

In the limit, the effects of metal loading would be greatest if the slow-wave structure and the outer cylinder were allowed to touch. The theory would not break down in this situation provided the currents could be maintained along their helical path. If this could be accomplished, the field shape for the slow-wave mode would be "perfectly" maintained independent of the frequency, and the phase velocity and group velocity would become $p/2\pi a$ times the velocity of light -- ideally nondispersive. Unfortunately, if contact were to be made between the circuit and the cylinder, the slow-wave mode would be shorted out such that only circular cylindrical waveguide modes could exist.

APPENDIX A

THE FOURIER DECOMPOSITION OF THE E AND H FIELDS

For a homogeneous source-free region, the vector nature of an arbitrary electromagnetic field can be expressed as the sum of TE and TM fields, and in the case of circular cylindrical geometry, these may be defined as being transverse with respect to the axial coordinate. For regular boundaries such as that for a circular waveguide, the TE and TM portions of the fields uncouple, giving separate solutions. However, for open structures such as the single helix, contrawound helix, and ring-bar circuits, the skew boundary conditions necessitate both the TE and TM aspects of the fields to be simultaneously present.

The E_z and H_z field expressions for the free space problem shown in Fig. 2.1 are

$$\left.\begin{matrix} {}_1E_z(r,\phi,z) \\ {}_2E_z(r,\phi,z) \end{matrix}\right\} = \sum_{\ell,n=-\infty}^{\infty} \left\{\begin{matrix} A_{\ell,n}I_\ell(\gamma_{\ell,n}r) \\ B_{\ell,n}K_\ell(\gamma_{\ell,n}r) \end{matrix}\right\} e^{-j\beta_{\ell,n}z}\, e^{j\ell\phi} \qquad \left\{\begin{matrix} 0 < r < a & \text{(A.1)} \\ a < r & \text{(A.2)} \end{matrix}\right.$$

and

$$\left.\begin{matrix} {}_1H_z(r,\phi,z) \\ {}_2H_z(r,\phi,z) \end{matrix}\right\} = \sum_{\ell,n=-\infty}^{\infty} \left\{\begin{matrix} C_{\ell,n}I_\ell(\gamma_{\ell,n}r) \\ D_{\ell,n}K_\ell(\gamma_{\ell,n}r) \end{matrix}\right\} e^{-j\beta_{\ell,n}z}\, e^{j\ell\phi} \qquad \left\{\begin{matrix} 0 < r < a & \text{(A.3)} \\ a < r & \text{(A.4)} \end{matrix}\right.$$

and from these expressions and Maxwell's equations, the other field

components take the form in Region 1:

$(0 < r < a)$

$$ {}_1E_\phi(r,z,\phi) = \sum_{\ell,n=-\infty}^{\infty} \left[- \frac{\ell\beta_{\ell,n} r}{\left(\gamma_{\ell,n} r\right)^2} A_{\ell,n} I_\ell(\gamma_{\ell,n} r) - \frac{j\omega\mu}{\gamma_{\ell,n}} C_{\ell,n} I'_\ell(\gamma_{\ell,n} r) \right] e^{-j\beta_{\ell,n} z} e^{j\ell\phi} \qquad (A.5) $$

$$ {}_1E_r(r,z,\phi) = \sum_{\ell,n=-\infty}^{\infty} \left[\frac{j\beta_{\ell,n}}{\gamma_{\ell,n}} A_{\ell,n} I'_\ell(\gamma_{\ell,n} r) - \frac{\ell\omega\mu r}{\left(\gamma_{\ell,n} r\right)^2} C_{\ell,n} I_\ell(\gamma_{\ell,n} r) \right] e^{-j\beta_{\ell,n} z} e^{j\ell\phi} \qquad (A.6) $$

$$ {}_1H_\phi(r,z,\phi) = \sum_{\ell,n=-\infty}^{\infty} \left[\frac{j\omega\varepsilon}{\gamma_{\ell,n}} A_{\ell,n} I'_\ell(\gamma_{\ell,n} r) - \frac{\ell\beta_{\ell,n} r}{\left(\gamma_{\ell,n} r\right)^2} C_{\ell,n} I_\ell(\gamma_{\ell,n} r) \right] e^{-j\beta_{\ell,n} z} e^{j\ell\phi} \qquad (A.7) $$

$$ {}_1H_r(r,z,\phi) = \sum_{\ell,n=-\infty}^{\infty} \left[\frac{\ell\omega\varepsilon r}{\left(\gamma_{\ell,n} r\right)^2} A_{\ell,n} I_\ell(\gamma_{\ell,n} r) + \frac{j\beta_{\ell,n}}{\gamma_{\ell,n}} C_{\ell,n} I'(\gamma_{\ell,n} r) \right] e^{-j\beta_{\ell,n} z} e^{j\ell\phi} \qquad (A.8) $$

and in Region 2,

(a < r)

$$2E_\phi(r,z,\phi) = \sum_{\ell,n=-\infty}^{\infty} \left[\frac{\ell\beta_{\ell,n} r}{\left(\gamma_{\ell,n} r\right)^2} B_{\ell,n} K_\ell(\gamma_{\ell,n} r) - \frac{j\omega\mu}{\gamma_{\ell,n}} D_{\ell,n} K'_\ell(\gamma_{\ell,n} r) \right] e^{-j\beta_{\ell,n} z} e^{j\ell\phi} \qquad (A.9)$$

$$2E_r(r,\phi,z) = \sum_{\ell,n=-\infty}^{\infty} \left[\frac{j\beta_{\ell,n}}{\gamma_{\ell,n}} B_{\ell,n} K'_\ell(\gamma_{\ell,n} r) - \frac{\ell\omega\mu r}{\left(\gamma_{\ell,n} r\right)^2} D_{\ell,n} K_\ell(\gamma_{\ell,n} r) \right] e^{-j\beta_{\ell,n} z} e^{j\ell\phi} \qquad (A.10)$$

$$2H_\phi(r,\phi,z) = \sum_{\ell,n=-\infty}^{\infty} \left[\frac{j\omega\epsilon}{\gamma_{\ell,n}} B_{\ell,n} K'(\gamma_{\ell,n} r) - \frac{\ell\beta_{\ell,n} r}{\left(\gamma_{\ell,n} r\right)^2} D_{\ell,n} K_\ell(\gamma_{\ell,n} r) \right] e^{-j\beta_{\ell,n} z} e^{j\ell\phi} \qquad (A.11)$$

$$2H_r(r,\phi,z) = \sum_{\ell,n=-\infty}^{\infty} \left[\frac{\ell\omega\epsilon r}{\left(\gamma_{\ell,n} r\right)^2} B_{\ell,n} K_\ell(\gamma_{\ell,n} r) + \frac{j\beta_{\ell,n}}{\gamma_{\ell,n}} C_{\ell,n} K'(\gamma_{\ell,n} r) \right] e^{-j\beta_{\ell,n} z} e^{j\ell\phi} \qquad (A.12)$$

In the above equations, the four sets of Fourier coefficients $A_{\ell,n}$, $B_{\ell,n}$, $C_{\ell,n}$, and $D_{\ell,n}$ are the result of the TE and TM fields in the two regions, as summarized in Table A.1.

By expressing the Fourier coefficients for the fields in terms of the Fourier coefficients for the surface current densities on the two helix tapes, the field expansions for the contrawound helix take the form:

$$\left.\begin{matrix} {}_1E_z(r,\phi,z) \\ \\ {}_2E_z(r,\phi,z) \end{matrix}\right\} = -j \sum_{\ell,n=-\infty}^{\infty} \frac{\gamma_{\ell,n}a}{ka}\left[(\gamma_{\ell,n}a)\left(z_{J^-_{\ell,n}} + z_{J^+_{\ell,n}}\right) - \frac{\ell\beta_{\ell,n}a}{\gamma_{\ell,n}a}\left(\phi_{J^+_{\ell,n}} + \phi_{J^-_{\ell,n}}\right)\right]$$

$$\left\{\begin{matrix} K_\ell(\gamma_{\ell,n}a)I_\ell(\gamma_{\ell,n}r) \\ \\ I_\ell(\gamma_{\ell,n}a)K_\ell(\gamma_{\ell,n}r) \end{matrix}\right\} e^{-j\beta_{\ell,n}z}\, e^{j\ell\phi} \qquad \left\{\begin{matrix} 0 < r < a \quad (A.13) \\ \\ a < r \quad (A.14) \end{matrix}\right.$$

Table. A.1. TE and TM Fourier coefficients used in conjunction with the formulation of Appendix A.

	REGION	
	1 (0<r<a)	2 (a<r)
TM ⇨	$A_{\ell,n}$	$B_{\ell,n}$
TE ⇨	$C_{\ell,n}$	$D_{\ell,n}$

$$\left.\begin{matrix} {}_1E_\phi(r,\phi,z) \\ \\ {}_2E_\phi(r,\phi,z) \end{matrix}\right\} = -j \sum_{\ell,n=-\infty}^{\infty} \left[\frac{\ell\beta_{\ell,n}a}{ka} \left\{ \left(z_{J^-_{\ell,n}} + z_{J^+_{\ell,n}} \right) - \frac{\ell\beta_{\ell,n}a}{\left(\gamma_{\ell,n}a\right)^2} \left(\phi_{J^-_{\ell,n}} + \phi_{J^+_{\ell,n}} \right) \right\} \right.$$

$$\left. * \frac{a}{r} \left\{ \begin{matrix} K_\ell(\gamma_{\ell,n}a) I_\ell(\gamma_{\ell,n}r) \\ \\ I'_\ell(\gamma_{\ell,n}a) K_\ell(\gamma_{\ell,n}r) \end{matrix} \right\} - ka\left(\phi_{J^-_{\ell,n}} + \phi_{J^+_{\ell,n}} \right) \left\{ \begin{matrix} K'_\ell(\gamma_{\ell,n}a) I'_\ell(\gamma_{\ell,n}r) \\ \\ I'_\ell(\gamma_{\ell,n}a) K'_\ell(\gamma_{\ell,n}r) \end{matrix} \right\} \right]$$

$$* e^{-j\beta_{\ell,n}z} e^{j\ell\phi} \quad \begin{cases} 0 < r < a & \text{(A.15)} \\ \\ 0 < r & \text{(A.16)} \end{cases}$$

$$\left.\begin{matrix} {}_1E_r(r,\phi,z) \\ \\ {}_2E_r(r,\phi,z) \end{matrix}\right\} = \sum_{\ell,n=-\infty}^{\infty} \left[\frac{\ell ka}{\gamma_{\ell,n}a} \left(\phi_{J^-_{\ell,n}} + \phi_{J^+_{\ell,n}} \right) \frac{a}{r} \left\{ \begin{matrix} K'_\ell(\gamma_{\ell,n}a) I_\ell(\gamma_{\ell,n}r) \\ \\ I'_\ell(\gamma_{\ell,n}a) K_\ell(\gamma_{\ell,n}r) \end{matrix} \right\} \right.$$

$$- \frac{\beta_{\ell,n}a}{ka} \left\{ (\gamma_{\ell,n}a) \left(z_{J^-_{\ell,n}} + z_{J^+_{\ell,n}} \right) - \frac{\ell\beta_{\ell,n}a}{\gamma_{\ell,n}a} \left(\phi_{J^-_{\ell,n}} + \phi_{J^+_{\ell,n}} \right) \right\}$$

$$\left. \left\{ \begin{matrix} K_\ell(\gamma_{\ell,n}a) I_\ell(\gamma_{\ell,n}r) \\ \\ I_\ell(\gamma_{\ell,n}a) K_\ell(\gamma_{\ell,n}r) \end{matrix} \right\} \right] e^{-j\beta_{\ell,n}z} e^{j\ell\phi} \quad \begin{cases} 0 < r < a & \text{(A.17)} \\ \\ 0 < r & \text{(A.18)} \end{cases}$$

$$\left.\begin{matrix} {}_1H_z(r,\phi,z) \\ \\ {}_2H_z(r,\phi,z) \end{matrix}\right\} = -\sum_{\ell,n=-\infty}^{\infty} \gamma_{\ell,n} a \left(\phi J^-_{\ell,n} + \phi J^+_{\ell,n}\right)$$

$$* \begin{cases} K'_\ell(\gamma_{\ell,n}a) I_\ell(\gamma_{\ell,n}r) \\ \\ I'_\ell(\gamma_{\ell,n}a) K_\ell(\gamma_{\ell,n}r) \end{cases} e^{-j\beta_{\ell,n}z}\, e^{j\ell\phi} \qquad \begin{cases} 0 < r < a & \text{(A.19)} \\ \\ a < r & \text{(A.20)} \end{cases}$$

$$\left.\begin{matrix} {}_1H_\phi(r,\phi,z) \\ \\ {}_2H_\phi(r,\phi,z) \end{matrix}\right\} = \sum_{\ell,n=-\infty}^{\infty} \left[\frac{\ell\beta_{\ell,n}}{\gamma_{\ell,n}a} \left(\phi J^-_{\ell,n} + \phi J^+_{\ell,n}\right) \frac{a}{r} \begin{cases} K'_\ell(\gamma_{\ell,n}a) I_\ell(\gamma_{\ell,n}r) \\ \\ I'_\ell(\gamma_{\ell,n}a) K_\ell(\gamma_{\ell,n}r) \end{cases} \right.$$

$$\left. - \left\{ \gamma_{\ell,n} a \left(z J^-_{\ell,n} + z J^+_{\ell,n}\right) - \frac{\ell\beta_{\ell,n}a}{\gamma_{\ell,n}a} \left(\phi J^-_{\ell,n} + \phi J^+_{\ell,n}\right) \right\} \right.$$

$$\left. * \begin{cases} K_\ell(\gamma_{\ell,n}a) I'_\ell(\gamma_{\ell,n}r) \\ \\ I_\ell(\gamma_{\ell,n}a) K'_\ell(\gamma_{\ell,n}r) \end{cases} \right] e^{-j\beta_{\ell,n}z}\, e^{j\ell\phi} \qquad \begin{cases} 0 < r < a & \text{(A.21)} \\ \\ a < r & \text{(A.22)} \end{cases}$$

$$\left.\begin{matrix} {}_1H_r(r,\phi,z) \\ \\ {}_2H_r(r,\phi,z) \end{matrix}\right\} = j \sum_{\ell,n=-\infty}^{\infty} \left[\beta_{\ell,n} a \left(\phi_J^- + \phi_J^+ \right) \left\{ \begin{matrix} K_\ell'(\gamma_{\ell,n} a) I_\ell'(\gamma_{\ell,n} r) \\ \\ I_\ell'(\gamma_{\ell,n} a) K_\ell'(\gamma_{\ell,n} r) \end{matrix} \right\} \right.$$

$$- \ell \left\{ \left(z_{J\ell,n}^- + z_{J\ell,n}^+ \right) - \frac{\ell \beta_{\ell,n} a}{\left(\gamma_{\ell,n} a\right)^2} \left(\phi_{J\ell,n}^- + \phi_{J\ell,n}^+ \right) \right\}$$

$$\left. * \frac{a}{r} \left\{ \begin{matrix} K_\ell(\gamma_{\ell,n} a) I_\ell(\gamma_{\ell,n} r) \\ \\ I_\ell(\gamma_{\ell,n} a) K_\ell(\gamma_{\ell,n} r) \end{matrix} \right\} \right] e^{-j\beta_{\ell,n} z} \, e^{j\ell\phi} \left\{ \begin{matrix} 0 < r < a & \text{(A.23)} \\ \\ a < r & \text{(A.24)} \end{matrix} \right.$$

Considered next is the situation in which Regions 1 and 2 are allowed to have individually distinct dielectric properties, as illustrated in Figs. 3.1 or 3.2. The intrinsic wave impedance is given by

$$\eta_i = \sqrt{\frac{\mu_o}{\epsilon_i}} \qquad i = 1, 2 \qquad \text{(A.25)}$$

where i denotes either Region 1 or Region 2. Similarly, the radial propagation constant is defined to be

$$\left(\gamma_{\ell,n}\right)_i = \left(\beta_{\ell,n}^2 - k_i^2\right)^{1/2} \qquad i = 1, 2 \qquad \text{(A.26)}$$

For convenience, a shorthand notation is adopted whereby the ℓ and n dependence is assumed, In this notation,

$$ {}_1E_r = \sum \left\{ \frac{j n_1 \beta}{\gamma_1} AI'(\gamma_1 r) - \frac{\ell k_1}{\gamma_1^2 r} CI(\gamma_1 r) \right\} e^{-j\beta z} e^{j\ell\phi} \qquad (A.33) $$

$$ {}_1H_z = \sum \frac{C}{n_1} I(\gamma_1 r) e^{-j\beta z} e^{j\ell\phi} \qquad (A.34) $$

$$ {}_1H_\phi = \sum \left\{ j \frac{k_1}{\gamma_1} AI'(\gamma_1 r) - \frac{\ell\beta}{\gamma_1 \gamma_1^2 r} CI(\gamma_1 r) \right\} e^{-j\beta z} e^{j\ell\phi} \qquad (A.35) $$

$$ {}_1H_r = \sum \left\{ \frac{\ell k_1}{\gamma_1^2 r} AI(\gamma_1 r) + \frac{j\beta}{n_1 \gamma_1} CI'(\gamma_1 r) \right\} e^{-j\beta z} e^{j\ell\phi} \qquad (A.36) $$

and in Region 2,

(a < r) or (a < r < b)

$$ {}_2E_z = \sum n_2 BK_e(\gamma_2 r) e^{-j\beta z} e^{j\ell\phi} \qquad (A.37) $$

$$ {}_2E_\phi = \sum \left\{ - \frac{\ell n_2 \beta}{\gamma_2^2 r} BK_e(\gamma_2 r) - \frac{j k_2}{\gamma_2 r} DK_e'(\gamma_2 r) \right\} e^{-j\beta z} e^{j\ell\phi} \qquad (A.38) $$

$$ {}_2E_r = \sum \left\{ \frac{j n_2 \beta}{\gamma_2} BK_e'(\gamma_2 r) - \frac{\ell k_2}{\gamma_2^2 r} DK_e(\gamma_2 r) \right\} e^{-j\beta z} e^{j\ell\phi} \qquad (A.39) $$

$$ {}_2H_z = \sum \frac{D}{n_2} K_h(\gamma_2 r) e^{-j\beta z} e^{j\ell\phi} \qquad (A.40) $$

$$ {}_2H_\phi = \sum \left\{ j \frac{k_2}{\gamma_2} BK_h'(\gamma_2 r) - \frac{\ell\beta}{n_2 \gamma_2^2 r} DK_h(\gamma_2 r) \right\} e^{-j\beta z} e^{j\ell\phi} \qquad (A.41) $$

$$\gamma_i = \left(\gamma_{\ell,n}\right)_i \tag{A.27}$$

$$\beta = \beta_{\ell,n} \tag{A.28}$$

$$F(\gamma_i r) = F_\ell\left[\left(\gamma_{\ell,n}\right)_i r\right], \quad F_\ell = I_\ell,\ K_\ell,\ I'_\ell,\ K'_\ell \tag{A.29}$$

and

$$\left.\begin{aligned} A &= A_{\ell,n} \\ B &= B_{\ell,n} \\ C &= C_{\ell,n} \\ D &= D_{\ell,n} \end{aligned}\right\} \tag{A.30}$$

Keeping in mind that the Fourier expansion of the E and H field components is over the double summation $\sum_{\ell,n=-\infty}^{\infty}$, the shorthand form of these field components becomes in Region 1,

$(0 < r < a)$

$$_1E_z = \sum n_1 AI(\gamma_1 r)\, e^{-j\beta z}\, e^{j\ell\phi} \tag{A.31}$$

$$_1E_\phi = \sum\left\{\frac{\ell n_1 \beta}{\gamma_1^2 r}\, AI(\gamma_1 r) - \frac{jk_1}{\gamma_1}\, CI'(\gamma_1 r)\right\} e^{-j\beta z}\, e^{j\ell\phi} \tag{A.32}$$

$$\sum_{\ell,n} A_{\ell,n}\, e^{j\ell\phi}\, e^{j\ell\pi}\, e^{-j\beta_n z}\, e^{-j\beta_n p/2} = e^{-j\beta_o p/2} \sum_{\ell,n} A_{\ell,n}\, e^{j\ell\phi}\, e^{-j\beta_n z} \tag{B.20}$$

The necessary and sufficient condition for this equation to be satisfied is

$$e^{j\ell\pi}\, e^{-j\beta_n p/2}\, e^{j\beta_o p/2} = 1 = e^{-j2\pi u} \tag{B.21}$$

where u is an integer. Application of Eq. B.17 to Eq. B.21 implies that

$$\ell - n = 2u \tag{B.22}$$

or

$$n = 2u + \ell \tag{B.23}$$

At this point, one may pursue the analysis from two different perspectives. The first considers the problem redefined in terms of a pseudo-period $L = p/2$. The double summation over ℓ and n is restricted as a consequence of Eq. B.22 so that if ℓ is even, n is even, and if ℓ is odd, n is odd. This then implies a coupling between ϕ and z, as would be expected, and which is necessary for the orthogonality integral to be evaluated over $p/2$ rather than the usual full period p.

The second and more familiar scenario maintains orthogonality over the entire period p, but redefines the propagation characteristics for the space harmonics. Substituting Eq. B.23 for n in the expression for β_n given in Eq. B.17 and noting u is allowed to vary over the entire

$$\beta_n = \beta_o + \frac{2\pi n}{p} \tag{B.17}$$

The result is that the propagation constant for the nth order space harmonic is defined by Eq. B.17.

When step-turn periodicity (also called screw symmetry) is present, as is the case for the contrawound helix, Floquet's theorem provides the expression,

$$E\left(\phi + \pi,\ z + \frac{p}{2}\right) = e^{-j\beta_o p/2}\, E(\phi,\ z) \tag{B.18}$$

Like Eq. B.11, the above equation states that the electric field evaluated at ϕ and z (written $E(\phi, z)$) and propagated a distance $p/2$ (written $e^{-j\beta_o p/2}$) is identical to the electric field evaluated at the position $\phi = \phi + \pi$ and $z = z + p/2$. The fact that the fields at these two positions are inverted from one another is automatically accounted for by $\phi = \phi + \pi$.

By writing the Fourier expansion for the z component of the E field at the position $\phi = \phi + \pi$ and $z = z + p/2$,

$$E_z\left(r,\ \phi + \pi,\ z + \frac{p}{2}\right)_{r \le a} = \sum_{\ell,n=-\infty}^{\infty} A_{\ell,n}\, \frac{I_\ell(\gamma_n r)}{I_\ell(\gamma_n a)}\, e^{j\ell\phi}\, e^{j\ell\pi}\, e^{-j\beta_n z}\, e^{-j\beta_n p/2} \tag{B.19}$$

and substituting this along with Eq. B.12 into Eq. B.18 at $r = a$, one obtains the following equation:

(written $e^{-j\beta_o p}$), is identical to the same functional form for the E fields evaluated instead at $z = z + p$ (written $E(z + p)$).

For a periodic slow wave structure with circular cylindrical geometry of radius "a," the electric field can be decomposed into a Fourier series. Consequently, $E(z)$ is written as

$$E_z(r, \phi, z) = \sum_{\ell,n=-\infty}^{\infty} A_{\ell,n} \frac{I_\ell(\gamma_n r)}{I_\ell(\gamma_n a)} e^{j\ell\phi} e^{-j\beta_n z} \qquad (B.12)$$
$$r \leq a$$

where $A_{\ell,n}$ is the amplitude factor and

$$\beta_n^2 = \gamma_n^2 + k^2 \qquad (k = \omega/c) \qquad (B.13)$$

The Fourier decomposition of $E_z(r, \phi, z + p)$ is similarly given by

$$E_z(r, \phi, z + p) = \sum_{\ell,n=-\infty}^{\infty} A_{\ell,n} \frac{I_\ell(\gamma_n r)}{I_\ell(\gamma_n a)} e^{j\ell\phi} e^{-j\beta_n z} e^{-j\beta_n p} \qquad (B.14)$$
$$r \leq a$$

Letting $r = a$ and substituting Eqs. B.12 and B.14 into Eq. B.11 yields

$$\sum_{\ell,n} A_{\ell,n} e^{j\ell\phi} e^{-j\beta_n z} e^{-j\beta_n p} = e^{-j\beta_o p} \sum_{\ell,n} A_{\ell,n} e^{j\ell\phi} e^{-j\beta_n z} \qquad (B.15)$$

For Eq. B.15 to be true implies that

$$e^{-j\beta_n p} e^{j\beta_o p} = 1 = e^{-j2\pi n} \qquad (B.16)$$

further implying that

> For a given mode of propagation and at a given frequency, the wave functions at two points on a transmission system, separated by one period, differ by a complex constant.

The application of Floquet's theorem to periodic slow wave structures allows one to determine the propagation characteristic of the space harmonics.

For a lossless periodic transmission system, the E fields are given the form,

$$E(z) = \tilde{E}(z)\, e^{-j\beta_o z} \tag{B.8}$$

which corresponds to Eq. B.7 with $\Gamma = -j\beta_o$; and for $z = z + p$, Eq. B.8 becomes

$$E(z + p) = \tilde{E}(z + p)\, e^{-j\beta_o z}\, e^{-j\beta_o p} \tag{B.9}$$

From Floquet's theorem, it is necessary that $\tilde{E}(z + p) = \tilde{E}(z)$, as seen in Eq. B.6. Thus, Eq. B.9 can be expressed as

$$E(z + p) = \tilde{E}(z)\, e^{-j\beta_o z}\, e^{-j\beta_o p} \tag{B.10}$$

which is obviously

$$E(z + p) = E(z)\, e^{-j\beta_o p} \tag{B.11}$$

The above equation simply states that the functional form for the E fields, evaluated at z (written E(z)) and propagated a distance p

A useful corollary to Floquet's theorem is obtained in the following manner. Let k take the form,

$$k = e^{np\Gamma} \tag{B.3}$$

If $\Phi(x)$ is defined as

$$\Phi(x) = e^{-\Gamma x}\, y(x) \tag{B.4}$$

then

$$\Phi(x + np) = e^{-np\Gamma}\, e^{-\Gamma x}\, y(x + np) \tag{B.5}$$

Applying Eq. B.2 to the above equation gives

$$\Phi(x + np) = e^{-np\Gamma}\, e^{-\Gamma x} \left[e^{np\Gamma}\, y(x) \right] = e^{-\Gamma x}\, y(x) = \Phi(x) \tag{B.6}$$

so that Floquet's theorem states that one can always find a solution to Mathieu's equation of the form,

$$y(x) = e^{\Gamma x}\, \Phi(x) \tag{B.7}$$

where $\Phi(x)$ is periodic with period p.

It should be apparent from Eq. B.7 that the functions y(x) can represent wave functions. In light of this, Floquet's theorem becomes a statement about periodic translational symmetry. For a periodic transmission system, Floquet's theorem may be stated as follows:

APPENDIX B

FLOQUET'S THEOREM AND STEP-TURN PERIODICITY

Floquet's theorem results from a consideration of the second order linear differential equation,

$$y'' + \left[a + b \cos\left(\frac{2\pi x}{p}\right)\right] y = 0 \qquad (B.1)$$

where a and b are real constants. Known as Mathieu's equation, Eq. B.1 occurs in problems of wave motion with elliptical boundaries, the simplest example being the vibrations of an elliptical drum head. Although the equation can be solved by the usual power series method (method of Frobenius), such a solution is not valid when $x = np$, "n" being an integer. Other methods are then employed to arrive at the more general solution and, of particular interest, solutions which are periodic in x, i.e., $y(x) = y(x + np)$, where n is an integer and p is the period. However, such periodicity is obtained only when the constant "a" is allowed certain values. If "a" differs from these allowed values, then the solution is no longer periodic. Instead, it takes the form

$$y(x + np) = ky(x) \qquad (B.2)$$

k being a (complex) constant. Equation B.2 is the statement of Floquet's theorem and, though not performed here, it is a simple matter to prove this theorem using linear algebra [6, 7].

Finally, the Fourier coefficients B and D can be expressed in terms of ${}^{\phi}J^{\pm}$ and ${}^{z}j^{\pm}$ through the relationships

$$B = A\left(\frac{\eta_1}{\eta_2}\frac{I}{K_e}\right) \tag{A.58}$$

and

$$D = \frac{\eta_2}{K_h}\left[\frac{I}{\eta_1}C - ({}^{\phi}J^{-} + {}^{\phi}J^{+})\right] \tag{A.59}$$

At $r = a$, E_z and E_ϕ in terms of the surface current density are

$$E_z(r = a) = \sum j\eta_1 I\left[T({}^{z}J^{-} + {}^{z}J^{+}) + X({}^{\phi}J^{-} + {}^{\phi}J^{+})\right] e^{-j\beta z}\, e^{j\ell\phi} \tag{A.60}$$

$$E_\phi(r = a) = \sum \left\{-j\frac{\ell\eta_1\beta}{\gamma_1^2 a} I\left[T({}^{z}J^{-} + {}^{z}J^{+}) + X({}^{\phi}J^{-} + {}^{\phi}J^{+})\right]\right.$$

$$\left. -j\frac{k_1}{\gamma_1} I'\left[R({}^{z}J^{-} + {}^{z}J^{+}) + S({}^{\phi}J^{-} + {}^{\phi}J^{+})\right]\right\} e^{-j\beta z}\, e^{j\ell\phi} \tag{A.61}$$

If $\eta_1 = \eta_2$, Eqs. A.60 and A.61 reduce to Eqs. A.13 (A.14) and A.15 (A.16) for $r = a$, respectively.

and

$$I' = I'_{\ell}\left[\left(\gamma_{\ell,n}\right)_1 a\right] \tag{A.55}$$

This is also true for K_e, K'_e, K_h, and K'_h, such that

$$\left.\begin{aligned} K_e &= K_{\ell}\left[\left(\gamma_{\ell,n}\right)_2 a\right] \\ K'_e &= K'_{\ell}\left[\left(\gamma_{\ell,n}\right)_2 a\right] \\ K_h &= K_{\ell}\left[\left(\gamma_{\ell,n}\right)_2 a\right] \\ K'_h &= K'_{\ell}\left[\left(\gamma_{\ell,n}\right)_2 a\right] \end{aligned}\right\} \tag{A.56}$$

A conducting sheath placed at r = b in Region 2 (Fig. 3.2) effects only the last four equations. These become (in shorthand notation)

$$\left.\begin{aligned} K_e &= I(\gamma_2 b)\, K(\gamma_2 a) - K(\gamma_2 b)\, I(\gamma_2 a) \\ K'_e &= I'(\gamma_2 b)\, K'(\gamma_2 a) - K'(\gamma_2 b)\, I'(\gamma_2 a) \\ K_h &= I'(\gamma_2 b)\, K(\gamma_2 a) - K'(\gamma_2 b)\, I(\gamma_2 a) \\ K'_h &= I(\gamma_2 b)\, K'(\gamma_2 a) - K(\gamma_2 b)\, I'(\gamma_2 a) \end{aligned}\right\} \tag{A.57}$$

$$Q = \frac{n_1 n_2 \ell\beta I^2 K_h}{a^3 \gamma_1 \gamma_2 \left[k_2 n_2 \gamma_1 I K_e' - k_1 n_1 \gamma_2 K_h I'\right]} \tag{A.48}$$

$$M = \frac{\ell^2 \beta^2 n_1 I^2 K_h}{(\gamma_2 a)^3 (\gamma_1 a)^3} \left\{ \frac{(\gamma_1 a)^2 - (\gamma_2 a)^2}{k_2 n_2 \gamma_1 I K_e' - k_1 n_1 \gamma_2 K_h I'} \right\} \tag{A.49}$$

and

$$N = \frac{k_1 n_2 \gamma_2 I' K_e - k_2 n_1 \gamma_1 K_h' I}{\gamma_1 \gamma_2 n_2 K_e} - M\left[(\gamma_2 a)^2 - (\gamma_1 a)^2\right] \tag{A.50}$$

The expression for A is

$$A = j\left[T(z_J^- + z_J^+) + X(\phi_J^- + \phi_J^+)\right] \tag{A.51}$$

where

$$T = \frac{1}{N} \tag{A.52}$$

and

$$X = -\frac{1}{N}\left\{\frac{\ell\beta}{\gamma_1^2 a} - M\left[\frac{k_1 I' \gamma_1 a (\gamma_2 a)^2}{\ell\beta I^2}\right]\right\} \tag{A.53}$$

In the above equations, the argument of the modified Bessel functions I and I' is $\gamma_1 a$, i.e.,

$$I = I_\ell\left[(\gamma_{\ell,n})_1 a\right] \tag{A.54}$$

$$ {}_2H_r = \sum \left\{ \frac{\ell k_2}{\gamma_{2r}^2} BK_h(\gamma_2 r) + \frac{j\beta}{n_2 \gamma_2} DK_h'(\gamma_2 r) \right\} e^{-j\beta z} e^{j\ell\phi} \qquad (A.42) $$

where K_e, K_e', K_h, and K_h' have the functional form given in either Eqs. 3.16 or Eq. 3.17. As before, the Fourier coefficients A, B, C, and D are a consequence of the TE and TM fields, as outlined in Table A.1.

Next, the Fourier coefficients A and C can be written in terms of the z and ϕ components of the surface current density on the two helices. Letting

$$ z_J^{\pm} = z_{J\ell,n}^{\pm} \qquad (A.43) $$

and

$$ \phi_J^{\pm} = \phi_{J\ell,n}^{\pm} \qquad (A.44) $$

the expression for C is

$$ C = R(z_J^- + z_J^+) + S(\phi_J^- + \phi_J^+) \qquad (A.45) $$

where

$$ R = \frac{\eta_1}{\eta_2} \frac{Q}{IN} \left[(\gamma_2 a)^2 - (\gamma_1 a)^2 \right] \qquad (A.46) $$

$$ S = \frac{\eta_1}{I} - \frac{\eta_1}{\eta_2} \frac{Q}{IN} \frac{\ell\beta}{\gamma_1^2 a} \left[(\gamma_2 a)^2 - (\gamma_1 a)^2 \right] $$

$$ + \frac{k_1 I' \gamma_1 a (\gamma_2 a)^2 \eta_1}{\ell\beta \eta_2 I^3} \left\{ \frac{QM}{N} \left[(\gamma_2 a)^2 - (\gamma_1 a)^2 \right] + Q \right\} \qquad (A.47) $$

since $\underline{E} = 0$ at $r = \infty$, and from No. 2,

$$\int_{\text{helix tapes}} \underline{E}^* \cdot \underline{s} \cdot \underline{E}\, ds = \int_{\text{helix tapes}} \underline{E}^* \cdot \hat{n} \times \nabla \times \underline{E}\, ds = 0 \qquad (C.9)$$

since $\hat{n} \times \nabla \times \underline{E} = 0$ on the helix tapes. Similarly, applying No. 3 to the infinite planes at $z = 0$ and $z = p$ gives

$$\int_{\substack{\text{planes:}\\ z=0,\ z=p}} \underline{E}^* \cdot \underline{s} \cdot \underline{E}\, ds = \int_0^\infty r\, dr \int_0^{2\pi} d\phi \left[\underline{E}^*(z = 0) \cdot \underline{s}(z = 0) \cdot \underline{E}(z = 0) + e^{j\beta_o p}\, \underline{E}^*(z = 0) \cdot \underline{s}(z = p) \cdot e^{-j\beta_o p}\, \underline{E}(z = 0) \right]$$

$$= \int_0^\infty r\, dr \int_0^{2\pi} d\phi\, \underline{E}^*(z = 0) \left[\underline{s}(z = 0) + \underline{s}(z = p) \right] \underline{E}(z = 0) = 0 \qquad (C.10)$$

since $\underline{s}(z = p) = -\underline{s}(z = 0)$ on account of a reversal in the direction of $\hat{n}$. Considered together, Eqs. C.8 through C.10 imply that

$$\int_S \underline{E}^* \cdot s \cdot \underline{E}\, ds = 0 \qquad (C.11)$$

and Eq. C.1 reduces to

$$L = \int_V \left[(\nabla \times \underline{E}^*) \cdot (\nabla \times \underline{E}) - k^2 \underline{E}^* \cdot \underline{E} \right] dv \qquad (C.12)$$

By application of the vector Green's theorem to Eq. C.12, L is transformed to

to be satisfied requires that

$$\nabla \times \nabla \times \underline{E} = k^2 \underline{E} \qquad \text{in } V \tag{C.6}$$

$$\hat{n} \times \nabla \times \underline{E} = \underline{s} \cdot \underline{E} \qquad \text{on } S \tag{C.7}$$

Thus, $\underline{E}$ must satisfy the vector wave equation in Eq. C.6 and the boundary condition in Eq. C.7, as expected.

Next, for the boundary value problem consisting of the contrawound helix in free space, V is taken to be an infinitely large circular cylinder having infinite radius and finite length of one helix pitch p. The surface S enclosing V consists of the two infinite planes $z = 0$ and $z = p$; one cylindrical surface at $r = \infty$, $0 \leq z \leq p$; and the metallic surface of the helix tapes at $r = a$.

The physical nature of the problem is such that $\underline{E}$ must:

1. Vanish at $r = \infty$.
2. Have no tangential component on the metallic surface of the helix tapes.
3. Satisfy Floquet's for a periodic structure, i.e.,

$$\underline{E}(z = p) = e^{-j\beta_o p} \underline{E}(z = 0)$$

Using these conditions, the surface integral in Eq. C.1 can be shown to be zero. From No. 1,

$$\int_{r=\infty} \underline{E}^* \cdot \underline{s} \cdot \underline{E} \, ds = 0 \tag{C.8}$$

$$\delta L = \int_V (\nabla \times \delta \underline{E})^* \cdot (\nabla \times \underline{E})\, dv + \int_V (\nabla \times \underline{E})^* \cdot (\nabla \times \delta \underline{E})\, dv$$

$$- k^2 \int_V \delta \underline{E}^* \cdot \underline{E}\, dv - k^2 \int_V \underline{E}^* \cdot \delta \underline{E}\, dv$$

$$+ \int_S \delta \underline{E}^* \cdot \underline{s} \cdot \underline{E}\, ds + \int_S \underline{E}^* \cdot \underline{s} \cdot \delta \underline{E}\, ds \qquad (C.2)$$

or since

$$\int_S \underline{E}^* \cdot \underline{s} \cdot \delta \underline{E}\, ds = \int_S \delta \underline{E} \cdot \underline{s} \cdot \underline{E}^*\, ds \qquad (C.3)$$

Eq. C.2 is written as

$$\delta L = \int_V \left[(\nabla \times \delta \underline{E})^* \cdot (\nabla \times \underline{E}) - k^2 \delta \underline{E}^* \cdot \underline{E} \right] dv + \int_S \delta \underline{E}^* \cdot \underline{s} \cdot \underline{E}\, ds + c.c. \qquad (C.4)$$

Note that the unexpressed terms in Eq. C.4 are extraneous for the following discussion.

By means of the vector Green's theorem, δL can be transformed to the form,

$$\delta L = \int_V \delta \underline{E}^* \cdot (\nabla \times \nabla \times \underline{E} - k^2 \underline{E})\, dv$$

$$- \int_S \delta \underline{E}^* \cdot (\hat{n} \times \nabla \times \underline{E} - \underline{s} \cdot \underline{E})\, ds + c.c. \qquad (C.5)$$

Because the first variation of L is zero and $\delta \underline{E}^*$ is an <u>arbitrary</u> variation, each integral in Eq. C.5 is individually zero. For this condition

APPENDIX C

DERIVATION OF THE LAGRANGIAN USED IN CONJUNCTION WITH THE VARIATIONAL METHOD OF SOLUTION†

To employ the method of calculus of variations (the variational method), it is necessary to determine the correct form of the Lagrangian for the problem. One begins with the general form of the Lagrangian for Maxwell's equations:

$$L = \int_V \left[(\nabla \times \underline{E})^* \cdot (\nabla \times \underline{E}) - k^2 \underline{E}^* \cdot \underline{E} \right] dv + \int_S \underline{E}^* \cdot \underline{s} \cdot \underline{E} \, ds \qquad (C.1)$$

In Eq. C.1, S is the surface enclosing the volume V under consideration. The most general boundary condition on S is represented by $\underline{s}$ such that $\hat{n} \times \nabla \times \underline{E} = \underline{s} \cdot \underline{E}$. Conditions 2.14 and 2.15 (noting $\hat{n} \times \nabla \times \underline{E} = -j\omega\mu \hat{n} \times H$) are then a specialized case of $\underline{s} \cdot \underline{E}$. It should be pointed out that $\underline{s}$ is Hermitian and that the relationshi $\underline{s} \cdot \underline{E} = \underline{E} \cdot \underline{s}^*$ is valid for any arbitarary vector $\underline{E}$.

The Lagrangian must be constrained to match the boundary value problem. Consequently, the first variation of L,

$$\delta L = 0$$

is performed giving

---

† See also reference 2, pp. 47-51.

$$\beta_{\ell,n} = \beta_o + \frac{2\pi}{p}(\ell + 3n) \tag{B.29}$$

The single helix is invariant under the differential step-turn symmetry,

$$E\left(r, \phi + \frac{2\pi}{p}\Delta z, z + \Delta z\right) = e^{-j\beta_o \Delta z} E(r, \phi, z) \tag{B.30}$$

The coupling expression for ℓ and n (equivalent to Eq. B.22 in the case of 180° step-turn symmetry) is found to be

$$\ell - n = \frac{2p}{\Delta z} u \tag{B.31}$$

Though u, like ℓ and n, is allowed to vary over the entire range of integers, Eq. B.31 is true for all values of Δz only if $u = 0$. Therefore, $\ell = n$ such that the Fourier decomposition of E_z for the single helix needs to be summed over only one index.

range of integers, one can define $\beta_{\ell,u}$ to be

$$\beta_{\ell,u} = \beta_o + \frac{2\pi}{p} (\ell + 2u) \tag{B.24}$$

or, since u and n are dummy indices,

$$\beta_{\ell,n} = \beta_o + \frac{2\pi}{p} (\ell + 2n) \tag{B.25}$$

The Fourier expansion for E_z is then rewritten as

$$E_z(r, \phi, z) = \sum_{\ell,n} A_{\ell,n} \frac{I_\ell(\gamma_{\ell,n} r)}{I_\ell(\gamma_{\ell,n} a)} e^{-j\beta_{\ell,n} z} e^{j\ell\phi} \tag{B.26}$$

in which $\beta_{\ell,n}$ is given by Eq. B.25 and $\gamma_{\ell,n}$ is defined by

$$\gamma^2_{\ell,n} = \beta^2_{\ell,n} - k^2 \tag{B.27}$$

Thus, coupling between ϕ and z occurs through the propagation constant for the ℓ,n^{th} order space harmonic.

It becomes apparent that if step-turn symmetry is present in a given problem, then coupling exists between ϕ and z through the propagation constant $\beta_{\ell,n}$. For example, the 120° step-turn symmetry

$$E\left(r, \phi + \frac{2\pi}{3}, z + \frac{p}{3}\right) = e^{-j\beta_o p/3} E(r, \phi, z) \tag{B.28}$$

results in $\beta_{\ell,n}$ being given by

$$L = \int_{V_1} \underline{E}_1^* \cdot (\nabla \times \nabla \times \underline{E}_1 - k^2 \underline{E}_1)\, dv$$

$$+ \int_{V_2} \underline{E}_2^* \cdot (\nabla \times \nabla \times \underline{E}_2 - k^2 \underline{E}_2)\, dv$$

$$- \int_S \underline{E}^* \cdot \hat{n} \times \nabla \times \underline{E}\, ds$$

$$- \int_{\substack{r=a, \\ \text{excluding tapes}}} \underline{E}^* \cdot (\hat{n}_1 \times \nabla \times \underline{E}_1 + \hat{n}_2 \times \nabla \times \underline{E}_2)\, ds \qquad (C.13)$$

where the subscripts 1 and 2 denote quantities for $r \leq a$ and $r \geq a$, respectively. The first three integrals in the above equation are zero because of Eqs. C.6 and C.11, and the fourth can be extended over the entire surface $r = a$ because of Eq. C.9. With these simplifications, the Lagrangian is restricted to an integral over the surface $r = a$. Let I denote the Lagrangian, now properly constrained to fit the boundary value problem. Thus, from Eq. C.13,

$$I = - \int_{r=a} \underline{E}^* \cdot (\hat{n}_1 \times \nabla \times \underline{E}_1 + \hat{n}_2 \times \nabla \times \underline{E}_2)\, ds \qquad (C.14)$$

$$= j\omega\mu \int_{r=a} \underline{E}^* \cdot \hat{n}_1 \times (\underline{H}_1 - \underline{H}_2)\, ds \qquad (C.15)$$

in which the relation $-j\omega\mu\underline{H} = \nabla \times \underline{E}$ is employed and noting $\hat{n}_1 = -\hat{n}_2$.†

† To facilitate understanding, the problem has been limited to the case of $\mu_1 = \mu_2 = \mu$

By expressing $\underline{H}_1 - \underline{H}_2$ in terms of surface current densities, one obtains the variational integral

$$I = j\omega\mu \int_0^p dz \int_0^{2\pi} a\, d\phi \left\{ E_\phi^*(r = a) \left[{}^{\phi}J^- + {}^{\phi}J^+ \right] + E_2^*(r = a) \left[{}^{z}J^- + {}^{z}J^+ \right] \right\} \tag{C.16}$$

The exact solution to the boundary value problem will have $I = 0$. This is because the integrand of I vanishes everywhere; $E_\phi(r = a)$ and $E_z(r = a)$ vanish on the helices, while ${}^{\phi}J^{\pm}$ and ${}^{z}J^{\pm}$ vanish off the helices. However, the converse statement is not true, and to obtain the exact solution, one must solve the variational equation

$$\delta I = 0 \tag{C.17}$$

Nevertheless, one can get an approximate solution by simply solving the equation $I = 0$.

The physical interpretation of I is very simple; I is the complex power which might be generated or absorbed by the cylindrical surface $r = a$. It is, therefore, certainly reasonable that I should be zero.

The case of a contrawound helix separating two dielectric regions at $r = a$ and bounded by a perfectly conducting cylinder at $r = b$ is analyzed in much the same fashion. The resulting variational integral is again C.16, which is not surprising based on the physical interpretation of I.

APPENDIX D

RELATIONSHIPS BETWEEN THE COEFFICIENTS OF THE FOURIER DECOMPOSITION OF THE SURFACE CURRENT DENSITIES FOR THE SYMMETRICAL MODE

The symmetrical relationships between the parallel and perpendicular components of the surface current densities are

$$\underline{I}_{J}^{+}(a, \phi, z) = \underline{I}_{J}^{-}(a, -\phi, z) \tag{2.40a}$$

$$\underline{\perp}_{J}^{+}(a, \phi, z) = \underline{\perp}_{J}^{-}(a, -\phi, z) \tag{2.40b}$$

the superscripts "-" and "+" representing the right-handed and left-handed helices, respectively. With the Fourier decomposition of each surface current density component given as

$$\underline{I}_{J}^{\pm}(a, \phi, z) = \sum_{\ell,n=-\infty}^{\infty} I_{J_{\ell,n}}^{\pm} e^{-j\beta_{\ell,n}z} e^{j\ell\phi} \tag{2.41a}$$

$$\underline{\perp}_{J}^{\pm}(a, \phi, z) = \sum_{\ell,n=-\infty}^{\infty} \perp_{J_{\ell,n}}^{\pm} e^{-j\beta_{\ell,n}z} e^{j\ell\phi} \tag{2.41b}$$

one can determine a relationship between the two sets of coefficients $I_{J_{\ell,n}}^{+}$ and $I_{J_{\ell,n}}^{-}$, as well as the two sets of coefficients $\perp_{J_{\ell,n}}^{+}$ and $\perp_{J_{\ell,n}}^{-}$.

Since the propagation constant for the ℓ,n^{th} order space harmonic is defined as

$$\beta_{\ell,n} = \beta_o + \frac{2\pi}{p}\,[\ell + 2n] \tag{2.12}$$

it is observed here that

$$\beta_{-\ell,n+\ell} = \beta_o + \frac{2\pi}{p}\,[-\ell + 2(n + \ell)] = \beta_{\ell,n} \tag{2.43a}$$

and that

$$\beta_{\ell,n-\ell} = \beta_o + \frac{2\pi}{p}\,[\ell + 2(n - \ell)] = \beta_{-\ell,n} \tag{2.43b}$$

Next, Eq. 2.40a can be written in terms of the Fourier expansion given in Eq. 2.41a:

$$\sum_{\ell,n} I_{J^+_{\ell,n}}\, e^{-j\beta_{\ell,n}z}\, e^{j\ell\phi} = \sum_{\ell,n} I_{J^-_{\ell,n}}\, e^{-j\beta_{\ell,n}z}\, e^{j\ell(-\phi)} \tag{D.1}$$

Letting $\ell = -\ell$ and $n = n + \ell$ for the right-hand side (RHS) of Eq. D.1 gives

$$\sum_{\ell,n} I_{J^+_{\ell,n}}\, e^{-j\beta_{\ell,n}z}\, e^{j\ell\phi} = \sum_{\ell,n} I_{J^-_{-\ell,n+\ell}}\, e^{-j\beta_{-\ell,n+\ell}z}\, e^{j\ell\phi} \tag{D.2}$$

Note that the RHS still sums over the same range as the left-hand side (LHS) as a consequence of ℓ and n spanning the entire set of integers. Substituting $\beta_{\ell,n}$ for $\beta_{-\ell,n+\ell}$ (Eq. 2.43a) in the above equation finally gives the result,

$$\sum_{\ell,n} I_{J^+_{\ell,n}}\, e^{-j\beta_{\ell,n}z}\, e^{j\ell\phi} = \sum I_{J^-_{-\ell,n+\ell}}\, e^{-j\beta_{\ell,n}z}\, e^{j\ell\phi} \tag{D.3}$$

From orthogonality, the only way the LHS can equal the RHS is if the coefficients are equal term by term. Thus,

$$I_{J^+_{\ell,n}} = I_{J^-_{-\ell,n+\ell}} \tag{2.44a}$$

Referring again to Eq. D.1, one could just as easily make the substitution $\ell = -\ell$ and $n = n + \ell$ for the LHS to produce the relation,

$$I_{J^+_{-\ell,n+\ell}} = I_{J^-_{\ell,n}} \tag{2.44b}$$

Similar relationships hold true for the perpendicular components. Namely, that

$$\perp_{J^+_{\ell,n}} = \perp_{J^-_{-\ell,n+\ell}} \tag{D.4}$$

and

$$\perp_{J^+_{-\ell,n+\ell}} = \perp_{J^-_{\ell,n}} \tag{D.5}$$

Furthermore, using the relationships in Eqs. 2.38 and 2.39, it is a simple matter to show that

$$\phi_{J^+_{\ell,n}} = -\phi_{J^-_{-\ell,n+\ell}} \tag{D.6}$$

The expression for H_z as given in Eq. 2.34 is rewritten here as

$$H_z = \sum_{\ell,n=-\infty}^{\infty} {}^{z}H_{\ell,n} \begin{Bmatrix} I'_\ell(\gamma_{\ell,n}a)\, K_\ell(\gamma_{\ell,n}r) \\ \\ K'_\ell(\gamma_{\ell,n}a)\, I_\ell(\gamma_{\ell,n}r) \end{Bmatrix} e^{-j\beta_{\ell,n}z}\, e^{j\ell\phi} \qquad \begin{cases} r \geq a \\ \\ r \leq a \end{cases} \tag{D.7}$$

$${}^{z}H_{\ell,n} = -(\gamma_{\ell,n}a)\left({}^{\phi}J^{-}_{\ell,n} + {}^{\phi}J^{+}_{\ell,n}\right) \tag{D.8}$$

By substituting Eq. D.6 into Eq. D.8, one finds that

$${}^{z}H_{\ell,n} = -(\gamma_{\ell,n}a)\left({}^{\phi}J^{-}_{\ell,n} - {}^{\phi}J^{-}_{-\ell,n+\ell}\right) = 0 \qquad \text{for } \ell = 0 \tag{D.9}$$

Equation D.9 shows that the fundamental component of any wave field operating in the symmetrical mode is a pure TM field; the TE parts of the fundamental component arising from the two helices cancel each other. In other words, the symmetrical solution has *no* H_z component with $\ell = 0$. This is rigorously true because no approximation is involved.

APPENDIX E

NUMERICAL CONSIDERATIONS

The numerical solutions to the determinantal equations are obtained with a Hewlett Packard 1000 minicomputer.

Because of numerical limitations and because the series in Eqs. 2.71 and 2.73 converge slowly, these equations are reformed to provide rapid convergence [8, 9]. Equation 2.71 is transformed to

$$2U_{o,o} + L_{o,o} \sin\theta \frac{2}{\xi^2}\left[\Lambda_3(o) - \Lambda_3(\xi)\right] + \sum_{\ell=1}^{\infty} \alpha_\ell^2 \left(Y_{\ell,o} + Y_{-\ell,o} - L_{o,o}\frac{\sin\theta}{\ell}\right) = 0 \qquad (E.1)$$

where

$$L_{o,o} = \left(\gamma_{o,o}a\right)^2 \sin^2\theta - (ka)^2\cos^2\theta \qquad (E.2)$$

and

$$\Lambda_3(\xi) \equiv \sum_{\ell=1}^{\infty} \frac{\cos(\ell\xi)}{\ell^3} = 1.2002 + \frac{1}{2}\xi^2\log(\xi) - \frac{3}{4}\xi^2 - \frac{1}{288}\xi^4 - \ldots. \qquad (E.3a)$$

$$\Lambda_3(o) = \sum_{\ell=1}^{\infty} \frac{1}{\ell^3} = 1.2002 \qquad (E.3b)$$

In Eq. E.1, the series

$$\sum_{\ell=1}^{\infty} \alpha_\ell^2 L_{o,o} \frac{\sin\theta}{\ell} \tag{E.4}$$

is chosen because it converges at about the same rate as the series

$$\sum_{\ell=1}^{\infty} \alpha_\ell^2 \left(Y_{\ell,o} + Y_{-\ell,o}\right) \tag{E.5}$$

The term $L_{o,o}$ is reasoned by examining the quantity $(Y_{\ell,o} + Y_{-\ell,o})$ for $\ell = 0$. From the physical considerations, the expression

$$2Y_{o,o} > \left(Y_{\ell,o} + Y_{-\ell,o}\right) \tag{E.6}$$

is guaranteed for all ℓ. Thus, $L_{o,o}$ is a consequence of

$$L_{o,o} = 2Y_{o,o} = 2\left[\left(\gamma_{o,o}a\right)^2 K_o\left(\gamma_{o,o}a\right) I_o\left(\gamma_{o,o}a \sin^2\theta\right) + (ka)^2 K_o'\left(\gamma_{o,o}a\right) I_o'\left(\gamma_{o,o}a\right) \cos^2\theta\right] \tag{E.7}$$

Equation E.2 results from making the approximations that $K_oI_o = 1/2$ and $K_o'I_o' = -1/2$, for $\gamma_{o,o}a = O(1)$.

The series E.4 summed by manipulating α_ℓ^2/ℓ into a suitable form using the definition for α_ℓ given in Eq. 2.69. This form is as follows:

$$\frac{\alpha_\ell^2}{\ell} = \frac{4}{\ell^3\xi^2}\sin^2(\ell\xi/2) = \frac{4}{\ell^3\xi^2}\left[\frac{1}{2} + \left(\frac{1}{2} - \cos^2(\ell\xi/2)\right)\right] = \frac{2}{\xi^2}\left[\frac{1}{\ell^3} - \frac{\cos(\ell\xi)}{\ell^3}\right]$$

or

$$\sum_{\ell=1}^{\infty} \frac{\alpha_\ell^2}{\ell} = \frac{2}{\xi^2}\left[\Lambda_3(o) - \Lambda_3(\xi)\right] \tag{E.8}$$

where Λ_3 is defined by Eq. E.3.

Using the same reasoning, Eq. 2.73 is transformed to

$$U_o + V_o + L_o \sin\theta \frac{2}{\xi^2}\left[\Lambda_3(o) - \Lambda_3(\xi)\right] + \sum_{\ell=1}^{\infty} \alpha_\ell^2 \left(Y_\ell + Y_{-\ell} - L_o \frac{\sin\theta}{\ell}\right) = 0 \tag{E.9}$$

where

$$L_o = \left(\gamma_o a\right)^2 \sin^2\theta - (ka)^2 \cos\theta \tag{E.10}$$

Equations E.1 (resp. Eq. E.9) is solved numerically to obtain ka as a function of $\beta_{o,o}a$ (resp. $\beta_o a$) for the contrawound helix (resp. single helix) in free space. For the two dielectric problem of Chapter Three, $L_{o,o}$ (resp. L_o) is scaled by the factor

$$\frac{\eta_1}{I_\ell}$$

in which the argument of the modified Bessel function is $\gamma_{\ell,o}a$ (resp. $\gamma_\ell a$).

To further facilitate numerical calculation, a numerical device is employed which extrapolates an infinite series to its true sum, using a

finite number of approximations. For example, if f_i represents a partial sum of Eq. E.1,

$$f_i = 2U_{o,o} + L_{o,o} \sin\theta \frac{2}{\xi^2}\left[\Lambda_3(o) - \Lambda(\zeta)\right] + \sum_{\ell=1}^{i} \alpha_\ell^2 \left(Y_{\ell,o} + Y_{-\ell,o} - L_{o,o}\frac{\sin\theta}{\ell}\right) \qquad (E.11)$$

then the true value of the infinite sum is approximated by the following extrapolation:

$$f_\infty = f_{i+2} - \frac{\left(f_{i+2} - f_{i+1}\right)^2}{\left(f_{i+2} - 2f_{i+1} + f_i\right)} \qquad (E.12)$$

Known as Aitken's δ^2 process [11], this extrapolation may be used to accelerate the convergence of linear iterations provided

$$\left(f_\infty - f_{i+1}\right) = C_i\left(f_\infty - f_i\right) \qquad |C_i| < 1 \qquad (E.13)$$

The physical considerations again ensure that condition E.13 is satisfied for the determinantal equations E.1 and E.9.

REFERENCES

[1] R. Kompfner, "The Invention of the Traveling-Wave Tube," from a lecture series at the University of California at Berkeley, published by San Francisco Press, 1963.

[2] M. Chodorow and E. L. Chu, "Cross-Wound Twin Helices for Traveling-Wave Tubes," TR-No. 249, Microwave Laboratory, Stanford University, Stanford, California, 1954.

[3] W. R. Ayers and R. T. Kirstein, "Theoretical and Experimental Characteristics of Connected-Ring Structures for Use in High-Power Traveling-Wave Tubes," TR-No. 358, Microwave Laboratory, Stanford University, Stanford, California, 1957.

[4] C. K. Birdsall and T. E. Everhart, "Modified Contrawound Helix Circuits for High-Power Traveling-Wave Tubes," Technical Memorandum No. 400, Hughes Aircraft Company, 1955.

[5] J. E. Nevins, Jr., "Investigations and Application of the Contrawound Helix," TR-No. 232-1, Microwave Laboratory, Stanford University, Stanford, California, 1956.

[6] J. Mathews and R. L. Walker, Mathematical Methods of Physics, W. A. Benjamin, Inc., Menlo Park, California, 1970, pp. 198-200.

[7] D. C. Stinson, Intermediate Mathematics of Electromagnetics, Prentice-Hall, Inc., Englewood Cliffs, New Jersey, 1976, pp. 24-27.

[8] R. W. Hamming, Numerical Methods for Scientists and Engineers, McGraw-Hill Book Company, New York, 1962, pp. 41-56, 93-94.

[9] A. D. Wheelon, Tables of Summable Series and Integrals Involving Bessel Functions, Holden-Day, Inc., San Francisco, California, 1968.

[10] M. Abramowitz and I. A. Stegun, Handbook of Mathematical Functions, National Bureau of Standards, Washington, DC, 1965.

[11] A. Ralston and P. Rabinowitz, A First Course in Numerical Analysis, McGraw-Hill Book Company, New York, 1978, p. 358.

MISSION
of
Rome Air Development Center

RADC plans and executes research, development, test and selected acquisition programs in support of Command, Control, Communications and Intelligence (C^3I) activities. Technical and engineering support within areas of competence is provided to ESD Program Offices (POs) and other ESD elements to perform effective acquisition of C^3I systems. The areas of technical competence include communications, command and control, battle management information processing, surveillance sensors, intelligence data collection and handling, solid state sciences, electromagnetics, and propagation, and electronic reliability/maintainability and compatibility.

END
FILMED
4-89
DTIC